FRICTION FACTOR DATA FOR FLAT PLATE TESTS OF SMOOTH AND HONEYCOMB SURFACES

A Thesis

by

TAE WOONG HA

Submitted to the Office of Graduate studies of
Texas A&M University
in partial fulfillment of the requirements for the degree of

MASTER OF SCIENCE

MAY 1989

Major Subject: Mechanical Engineering

ABSTRACT

Friction Factor Data for Flat Plate Tests
of Smooth And Honeycomb Surfaces. (May 1989)
Tae Woong Ha, B.S., Han Yang University in Korea
Chair of Advisory Committee: Dr. Dara Childs

Friction factors for honeycomb surfaces are measured with a flat plate tester. The flat plate test apparatus is described and a method is discussed for determining the friction factor experimentally. The friction factor model is developed for the flat plate test based on the Fanno Line Flow. The comparisons of the friction factor are plotted for smooth surface and six-honeycomb surfaces with three-clearances, 6.9 bar to 17.9 bar range of inlet pressure, and 5,000 to 100,000 range of the Reynolds number. The optimum geometries for the maximum friction factor are found as a function of cell width to cell depth and cell width to clearance ratios.

DEDICATION

To My Wife, Kung Suk Ha

TABLE OF CONTENTS

Page

LIST OF FIGURES

Figure Page

Appendix A

Figure Page

NOMENCLATURE

A	=	Cross-sectional area (L^2)
A_w	=	Surface area (L^2)
b	=	Honeycomb cell width (L), illustrated in fig. 1
d	=	Honeycomb cell depth (L), illustrated in fig. 1
D_h	=	Hydraulic diameter (L)
f	=	Fanning friction factor
g_c	=	Acceleration of gravity (L/t^2)
H	=	Minimum clearance of a test section (L), illustrated in fig. 3
M_a	=	Mach number
m	=	Mass (M)
$\dot{m}$	=	Mass flow rate (M/t)
P	=	Static pressure (F/L^2)
P_t	=	Stagnation pressure at the entrance of a test section (F/L^2)
P_o	=	Static pressure at the exit of a test section (F/L^2)
R	=	Gas constant
T	=	Fluid temperature (T)
T_t	=	Stagnation temperature at the entrance of a test section (T)
T_o	=	Fluid temperature at the exit of a test section (T)
U	=	Fluid velocity in axial direction (L/t)
W	=	Width of a test section (L), illustrated in fig. 3
γ	=	Ratio of specific heats for air
μ	=	Fluid viscosity (Ft/L^2)

ρ = Fluid density (M/L^3)

τ_w = Wall shear stress (F/L^2)

CHAPTER I

INTRODUCTION

The accurate determination of the leakage and rotordynamic coefficients of a labyrinth seal requires that the surface friction factor of the rotor and stator material be known. Various kinds of intentionally roughened surfaces were tested by Childs and Kim(1985), Nelson(1984), and Childs and Kim(1986) and used in liquid and gas seal designs.

In recent years, comparisons of smooth rotor annular seal test data for honeycomb, labyrinth, and smooth stators were presented by Childs et al.(1988), showing that the honeycomb seal had the best sealing(minimum leakage) performance and the best rotordynamic stability for prerotated fluid entering the seal. An example of damping improvement is provided by Childs and Moyer(1985) on the HPOTP(High Pressure Oxygen Turbopump) of the SSME(Space Shuttle Main Engine) where a change of the turbine interstage seal from a stepped- labyrinth, tooth-on-rotor configuration to a smooth-rotor, honeycomb-stator configuration eliminated serious synchronous and subsynchronous vibration problems.

The honeycomb is a structure of rows of hexagonal cells. Since multiple small cells of honeycomb create a more diffcult flow path in seal assemblies thereby reducing leakage, it is used for seal-surface materials and also used for flow straighteners, radio frequency shielding, shock absorbers, and so forth. Figure 1 shows the honeycomb cell pattern.

Since Moody(1944) demonstrated that the friction factor for pipe flow is based on two dimensionless quantities, the relative roughness of the surface and the

---

Journal model: *ASME Journal of Tribology.*

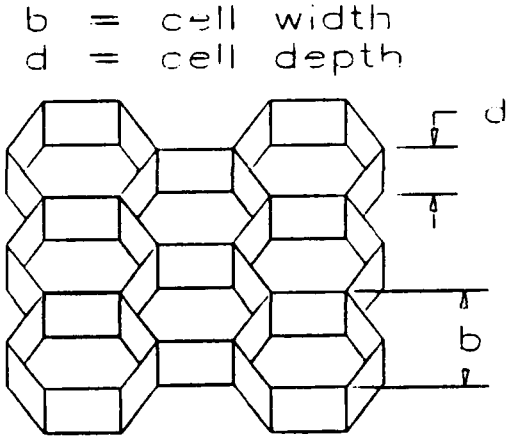

Figure 1. Honeycomb cell pattern.

Reynolds number, extensive literature for friction factors have been published. The effect of friction on the flow of compressible fluids in pipes of uniform cross-sectional area was investigated analytically by Grashof(1875) and Zeuner(1900), who arrived at a relationship between velocity and friction factor for perfect gases. Stodola(1927) showed that the curves of Fanno permit a general graphical treatment for any law of friction. Frössel(1938) presented the first extensive measurements of friction factors for the flow of air through a smooth tube with velocities above and below the speed of sound. Keenan(1939) presented experimental data on commercial pipe for the flow of water and for the flow of steam at subsonic velocities. Stocker, Cox, and Holle(1977) provided leakage data for various honeycomb seals with a two-dimensional static seal test rig. To the author's knowledge, for the friction factor of the honeycomb seals, Elrod(1988) has presented the only prior test data with a smooth rotor and honeycomb stators, which is given in part in his paper. The experimental data for honeycomb seals presented by both Stocker, Cox, and Holle, and Elrod are taken from only one honeycomb surface, and it is difficult to separate the friction factor for the honeycomb surface from their experimental data. Therefore, more improved data for honeycomb surfaces are needed.

The purpose of this report is to present the air flow friction factor data for honeycomb surfaces (i.e., 1.57 mm, 0.79 mm and 0.51 mm in cell width, 3.81 mm and 2.29 mm in cell depth) with a flat plate tester. The flat plate tester is designed to measure pressure drops, flowrate, and temperature for the flow passing through two honeycomb surfaces which have the same surface roughnesses. The friction factor data to be presented are given as a function of the Reynolds number, cover the range 5,000 to 100,000. The flow is subsonic. Reynolds number is defined by

$$R_e = \frac{\rho(2H)\,U}{\mu} \tag{1}$$

where ρ is the density of air, μ is the viscosity of air, and H is the minimum clearance of a test section. The test is conducted with 5 inlet pressures of 6.9bar, 9.7bar, 12.4bar, 15.2bar, and 17.9bar, respectively and 3 clearances between honeycombs which are 0.25mm, 0.38mm and 0.51mm. These clearance values are representative of actual seals used in the turbomachinary. The following questions will be answered:

1) Does the effect of the friction factor depend on inlet pressure?
2) Does the effect of the friction factor depend on Reynolds number?
3) Does the effect of the friction factor depend on honeycomb cell width?
4) Does the effect of the friction factor depend on honeycomb cell depth?
5) Does the effect of the friction factor depend on clearance between honeycomb seals?

In chapter II, the test apparatus, Flat-Plate-Tester, designed to meet the above requirements, is described and chapter III explains the procedure of a test. Chapter IV shows the friction factor model for a one dimensional, steady, adiabatic flow of a perfect gas through a constant area duct. Experimental data in chapter V and appendix A, B, and C are presented which depend on inlet pressure, Reynolds number, honeycomb cell width and depth, and clearance between honeycomb surfaces.

CHAPTER II

TEST APPARATUS

The flat plate test system is designed to measure flowrate, temperature and pressure gradient through the flat plate test specimen under the various test parameters. Figure 2 shows the schematic friction factor measurement system.

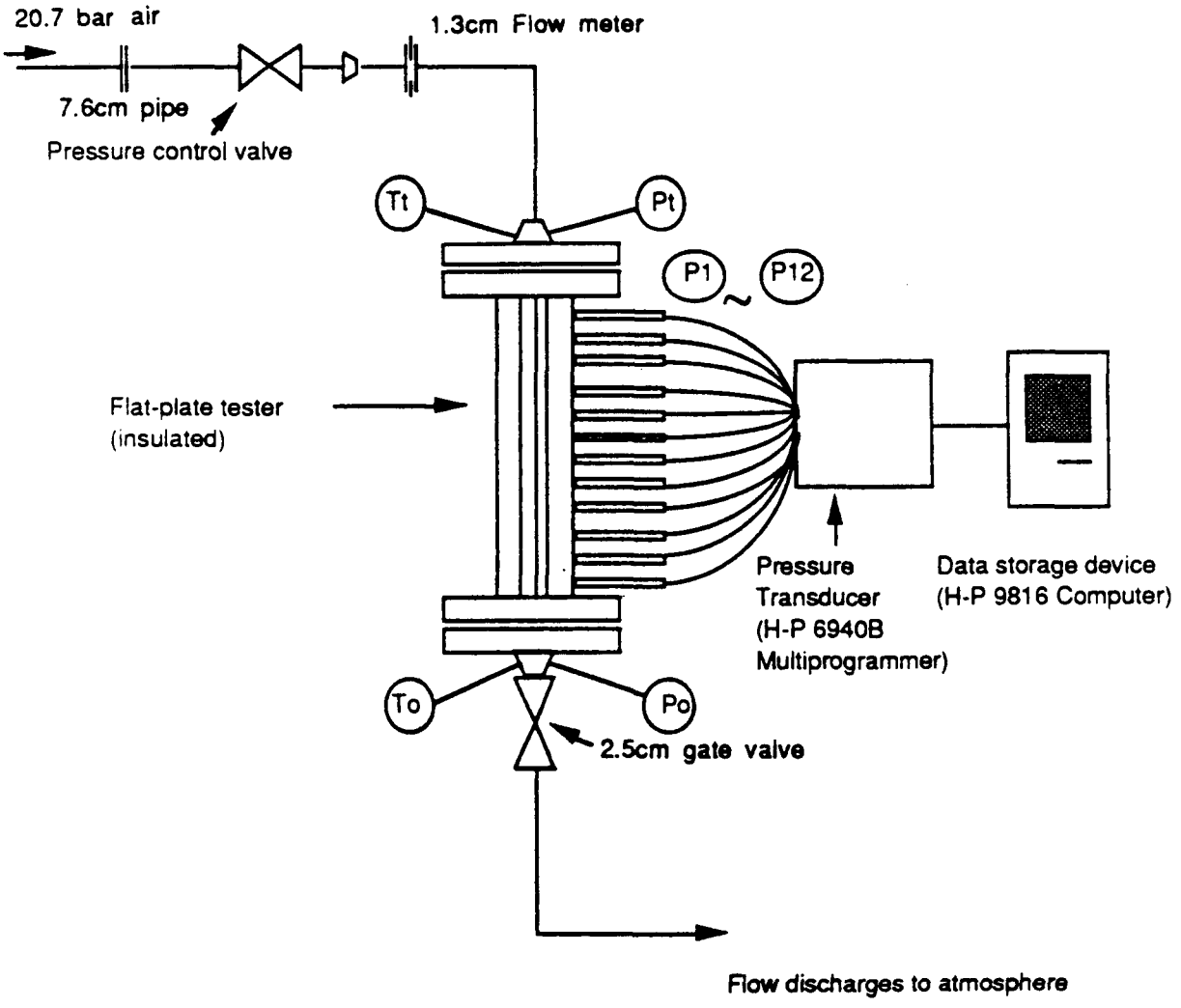

Figure 2. Friction factor measurement system schematic.

The flat plate tester consists of a test block, a spacer, and a honeycomb test specimen, as shown in figure 3, and designed to permit the installation of various honeycomb test specimens. To prevent side leakage, a 3 mm diameter O-ring is positioned along the spacers. A 1.3 cm wide by 15.2 cm long precision stainless steel shim stock is used for the spacer.

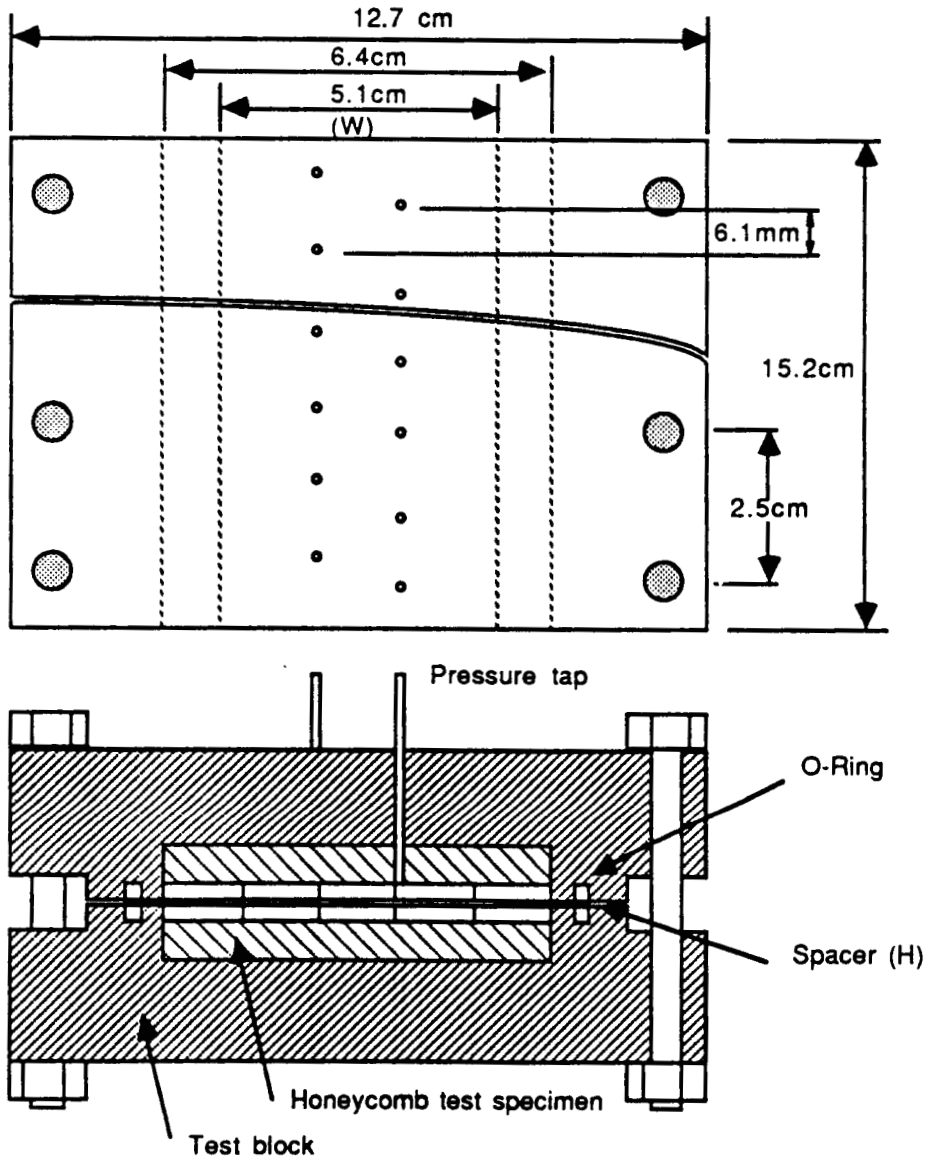

Figure 3. Flat plate tester assembly.

The honeycomb test specimen of figure 4 is made by attaching a honeycomb plate, made of Hastelloy "x", a Kentucky Metals Inc. product, to a precision-ground stock base plate with a 0.24 mm thickness structual adhesive film. The orignal design of the honeycomb test specimen was 6.4 cm wide by 15.2 cm long, but this resulted in too low Reynolds number range. Therefore, the length of the honeycomb test specimen was shortened to 7.6 cm to get a high enough Reynolds number range.

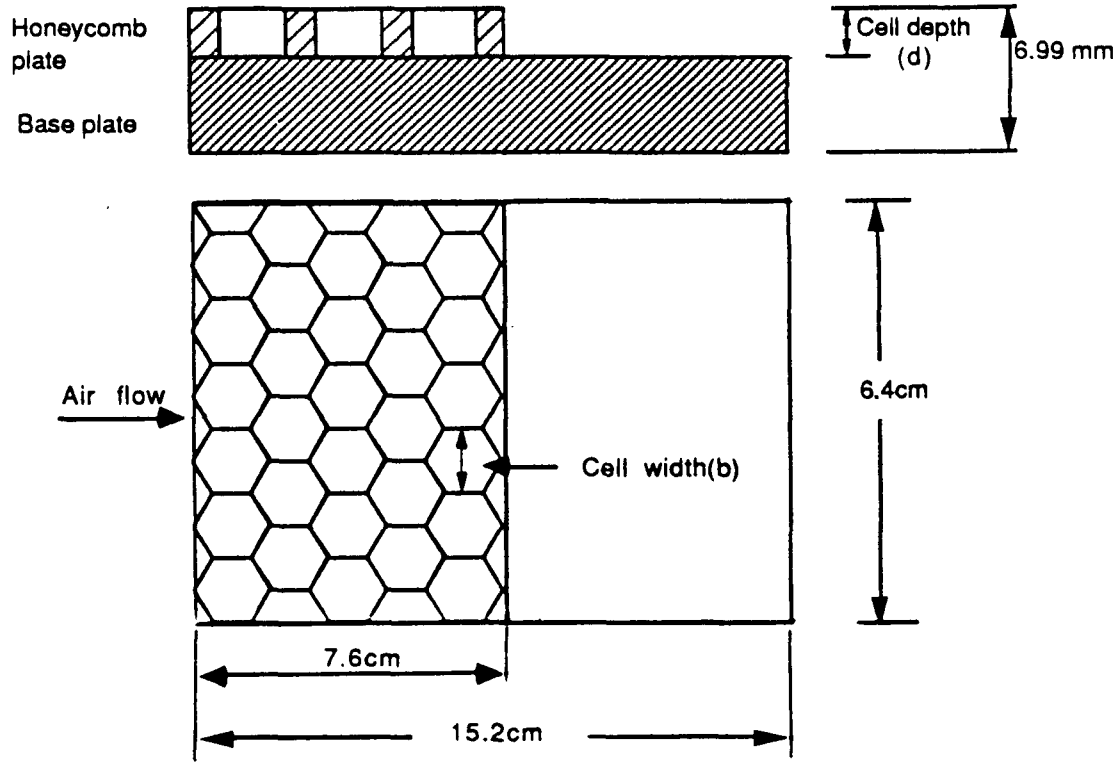

Figure 4. Honeycomb test specimen.

Air at 20.7 bar whose dewpoint is approximately $-40°C$ is supplied through a 7.6 cm diameter steel pipe for this system from the compressor. Figure 5 shows the air flow path detail.

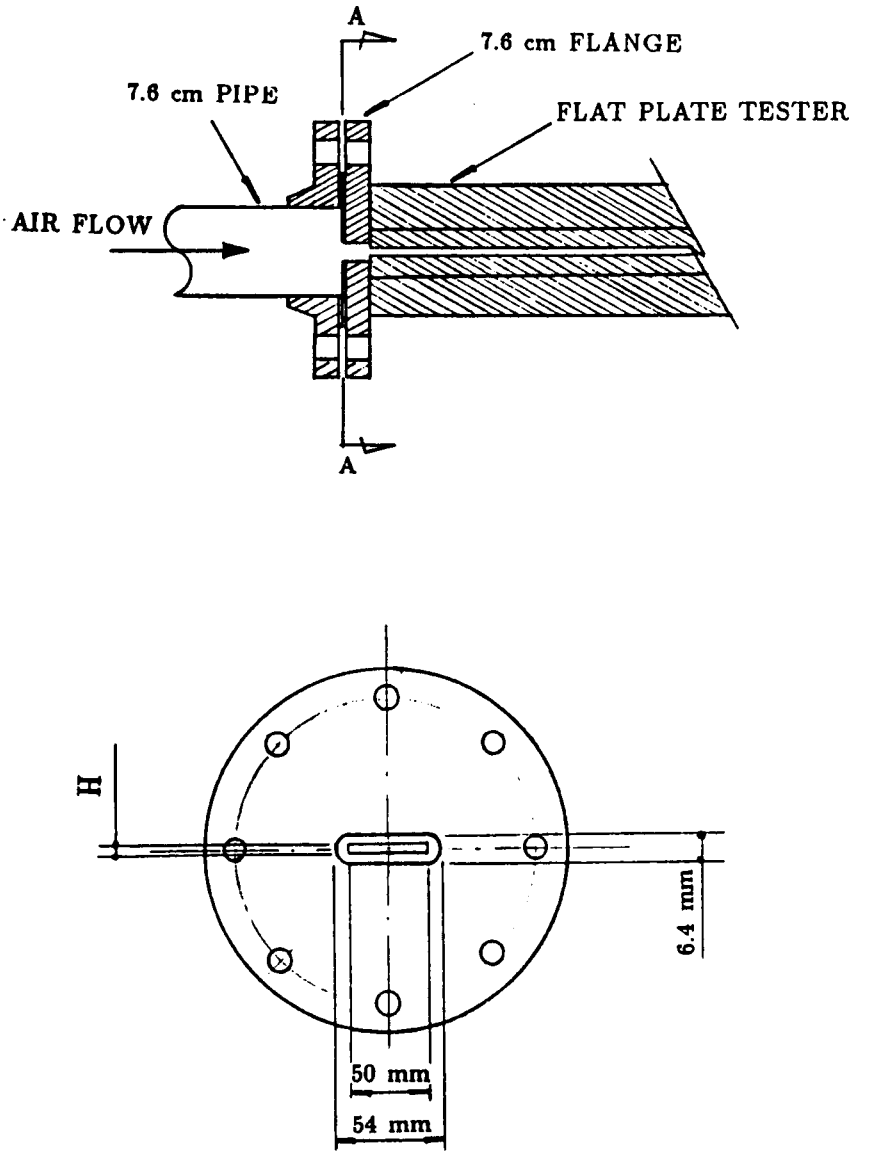

Figure 5. Air flow path detail.

The pressure control valve is positioned upstream of the test section to control inlet pressure, and a 2.5 cm gate valve is also equiped downstream to control back pressure. The flowrate through the test section is measured by a 1.3 cm turbine flow meter, located in the piping upstream of the test section. Resolution of the flow meter is $5X10^{-5}$ (m^3/min). Pressure and temperature upstream and downstream of the flow meter are measured for mass flow rate determination.

For measurement of the pressure gradient through the honeycomb test specimen, as shown in figure 3, one side of a 7.6 cm long honeycomb test specimen has twelve 1.6 mm pressure taps, equally distributed, drilled along the length of the test specimen, flush with the surface of the base plate. These pressures, as well as all others, are measured with a 0 to 20.7 bar scanivalve differential-type pressure transducer through a 48 port, remotely-controlled, scanivalve model J scanner. Transducer resolution is 0.96 kpa.

For measurement of the temperature upstream and downstream of the flow meter and the entrance and exit of the test section, a 1.59 mm diameter thermocouple with an iron-constantan stainless steel 304 sheath, is used. Resolution of temperature measurement is $1°K$.

CHAPTER III

TEST METHOD AND DATA ACQUISITION

At the start of each day's testing, pressure and flowmeter systems are calibrated. The total system, from transducer to computer, is calibrated for each of these variables. An air-operated dead-weight pressure tester is used for pressure system calibration, and flowmeter system calibration is achieved with an internal precision quartz clock which simulates a known flowrate. To check against possible leakage from the test section, a soap-and-water solution is applied at each connection. The test block is insulated with "styrofoam" to achieve adiabatic conditions.

A typical test begins by setting the test menu of five inlet pressures and five Reynolds numbers. The control valve upstream of the test section is used to give the desired inlet pressure. The exit(back) pressure is controlled to meet the desired Reynolds number requirement with a downstream gate valve. When steady flow condition is reached, readings are taken of all pressures, temperatures, and flowrate at definite intervals of time. Data acquisition is directed from a Hewlett-Packard 9816(16-bit) computer with disk driver and 9.8 megabyte hard disk. The computer controls an HP 6940B multiprogrammer with a 12-bit A/D converter board which acquires test data from the instruments.

For each test case (i.e., one particular honeycomb cell width and cell depth, clearance, inlet pressure and Reynolds number), the test is performed three times and test data is averaged to be recorded. This test sequence was followed for a smooth plate, and honeycomb test specimens with three cell widths, two cell depths, and 3 clearances. Table 1 shows the list of a smooth and honeycomb test specimens.

Table 1. List of a smooth and honeycomb test specimens

Test no.	Cell width	Cell depth	Clearance
1	smooth	-	0.25 mm
2	smooth	-	0.38 mm
3	smooth	-	0.51 mm
4	1.57 mm	2.29 mm	0.25 mm
5	1.57 mm	2.29 mm	0.38 mm
6	1.57 mm	2.29 mm	0.51 mm
7	1.57 mm	3.81 mm	0.25 mm
8	1.57 mm	3.81 mm	0.38 mm
9	1.57 mm	3.81 mm	0.51 mm
10	0.79 mm	2.29 mm	0.25 mm
11	0.79 mm	2.29 mm	0.38 mm
12	0.79 mm	2.29 mm	0.51 mm
13	0.79 mm	3.81 mm	0.25 mm
14	0.79 mm	3.81 mm	0.38 mm
15	0.79 mm	3.81 mm	0.51 mm
16	0.51 mm	2.29 mm	0.25 mm
17	0.51 mm	2.29 mm	0.38 mm
18	0.51 mm	2.29 mm	0.51 mm
19	0.51 mm	3.81 mm	0.25 mm
20	0.51 mm	3.81 mm	0.38 mm
21	0.51 mm	3.81 mm	0.51 mm

CHAPTER IV

A FLAT PLATE FRICTION FACTOR MODEL FOR AIR CHANNEL FLOW

The derivation of friction factor relation based on Fanno line flow and the Mach number definition is the purpose of this section. Based on this relationship, friction factors can be calculated from the flat plate test data. The required derivation is taken from John(1984) and follows.

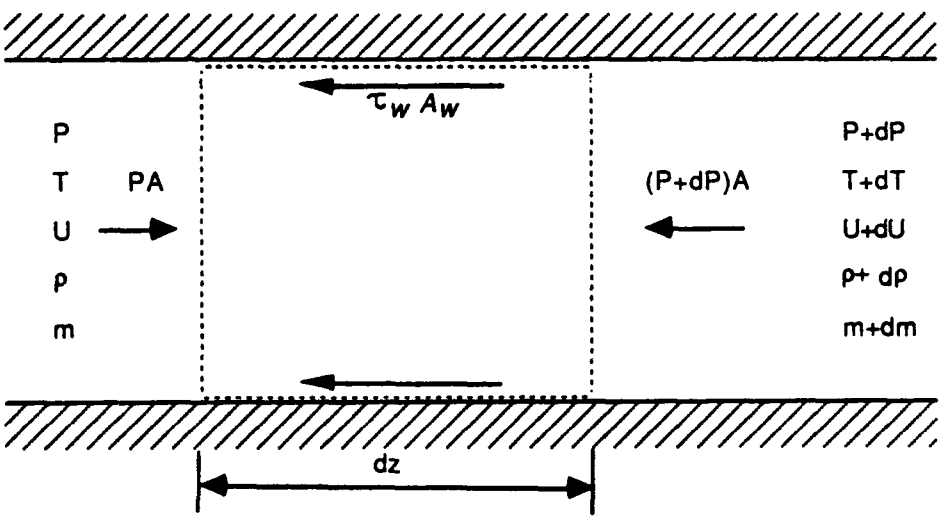

Figure 6. Control volume for analysis of adiabatic, constant area flow.

The test apparatus described in chapter II has been used to obtain pressure gradient and leakage data for smooth and honeycomb test specimens of table 1. As shown in figure 3, the flat plate tester makes a closed thin rectangular duct channel for air flow. The width to clearance ratio, W/H, is big enough to assume one dimensional flow. Air can be assumed a perfect gas, and flow is also assumed to be steady state and adiabatic. One dimensional, steady, adiabatic flow of a perfect gas with constant specific heats through a constant area duct with no external work

is called Fanno line flow. The friction factor model to be developed for the flat plate tester is based on the Fanno line flow and the Mach number definition.

Figure 6 shows the control volume taken in the closed thin retangular duct channel. The momentum equation for a control volume of length dz is

$$-AdP - \tau_w A_w = \rho AU\,du, \tag{2}$$

where A is the cross-sectional area of the duct, τ_w is the shear stress at the duct walls, and A_w is the surfacearea over whic h τ_w acts. The hydraulic diameter is defined by

$$D_h = \frac{4A}{Perimeter} \tag{3}$$

For the flat plate tester

$$D_h = \frac{4WH}{2(W+H)} \tag{4}$$

where W is the width of the duct, and H is the depth of the duct. As H is very small compared to W, D_h of the flat plate tester is 2H.

Substituting the hydraulic diameter into equation (2) yields

$$-AdP - \tau_w(dz)\frac{4A}{D_h} = \rho AU\,du \tag{5}$$

For adiabatic flow of a perfect gas, the relationship between stagnation temperature T_t and local temperature T is expressed by

$$T_t = T(1 + \frac{\gamma - 1}{2} M_a{}^2) \tag{6}$$

where M_a is the Mach number and γ is the ratio of specific heats for air. The Mach number is defined by

$$M_a = \frac{U}{\sqrt{\gamma RT}} \tag{7}$$

where R is a gas constant for air. Using equations (6) and (7), the perfect gas law and the conservation of mass, one can derive the equation for Mach number.

$$M_a = \left(\frac{-1 + \sqrt{1 + 2(\gamma - 1)(\frac{\dot{m}}{PA})^2(\frac{RT_t}{\gamma g_c})}}{(\gamma - 1)} \right)^{\frac{1}{2}} \tag{8}$$

where $\dot{m}$ is a mass flowrate through the seal and g_c is the acceleration of gravity. The relationship between friction factor f and τ_w is expressed in equation (9)

$$f = \frac{\tau_w}{0.5\rho U^2} \tag{9}$$

Using equations (5) and (9), the perfect gas law, the definition of Mach number, and the conservation of mass requirement, the friction factor, f, for the flat plate tester is :

$$f = \frac{D_h}{2} \frac{1}{M_a} \left(\frac{1 - {M_a}^2}{(1 + \frac{\gamma-1}{2}{M_a}^2)\gamma {M_a}^2} \right) \frac{dM_a}{dz} \tag{10}$$

Since all of the variables in the equation (8) are either known or measured, the Mach numbers along the axial location can be found. The Mach number gradient, dM_a/dz, can be evaluated by using a numerical method from calculated Mach numbers. Using equation (10), the friction factor also can be evaluated from the Mach number and the Mach number gradient. The evaluation of the Mach number and the friction factor will be discussed in detail in chapter V.

CHAPTER V

DATA REDUCTION AND RESULTS

Tests are carried out with smooth and honeycomb test specimens as listed in table 1 of chapter III. To determine the friction factor, the stagnation temperature, T_t, the flow rate, and pressures at 12 points along the 7.6cm length seal are measured.

Figure 7 illustrates the typical plot of the pressure distribution versus an axial length for five different Reynolds numbers. The Mach number data are evaluated using equation (8) at 6.1mm intervals along the specimen (i.e., at pressure tap locations), and figure 8 shows the Mach number distribution. As shown in figure 7 and figure 8, pressure is linearly reduced, and results in low and linearly increasing Mach numbers through the test specimen for Reynolds number 13,000, 36,000, 59,000 and 82,000. For Reynolds number 105,000, however, a big pressure drop occurs resulting in an abrupt Mach number increase to near 1.0 at the exit of the test section. This means the flow is choked.

As shown in equation (10), the friction factor is a function of Mach number and Mach number gradient along the axial location. Many possible numerical methods can be applied to evaluate the Mach number gradient, dM_a/dz. Figure 9 illustrates the comparison of quadratic and cubic least squares curve fits and a local slope method for Mach number. A quadratic least squares curve fit results in some negative friction factors in the choked case, and a cubic least squares curve fit also results in a big friction factor change through the test specimen for the choked case.

Therefore, a least-squares cubic curve fit is used for unchoked cases, and a local slope method, which directly takes the slope from the experimental data, is used

for the choked case.

The comparison of the friction factor, evaluated by different curve fitting methods and the local slope method, is presented in figure 10. In unchoked flow condition (i.e., for Reynolds numbers 13,000, 36,000, 59,000 and 82,000), there is not much differance in the friction factor for different curve fit methods, but a big difference results for choked flow conditions (i.e., for Reynolds number 105,000). As shown in figure 10, the method of curve fit for Mach number distribution is an important parameter in friction factor evaluation, especially in the choked case.

Equation (10) is used to evaluate the friction factor and the results illustrated in figure 11. For an unchoked flow condition, the friction factor is nearly uniform through the test specimen. For a choked flow condition, a big change of the friction factor occurs at the entrance and exit of the test section and also varies through the test specimen. Therefore, the shape of the friction factor distribution versus axial location depends strongly on the method of curve fit of Mach number distribution as mentioned above.

Friction factor results presented here are a Fanning friction factor defined in chapter IV and an averaged friction factor. To eliminate possible entrance and exit head losses, six data points in the middle of the test specimen are taken to find the averaged friction factor. As mentioned in chapter I, inlet pressure, Reynolds number, honeycomb width, honeycomb depth, and clearance may affect the friction factor. Discussion and plots illustrating the dependence of the friction factor on these parameters follows.

Effect of inlet pressure

Tests have been conducted with five inlet pressure conditions of 6.9 bar, 9.7

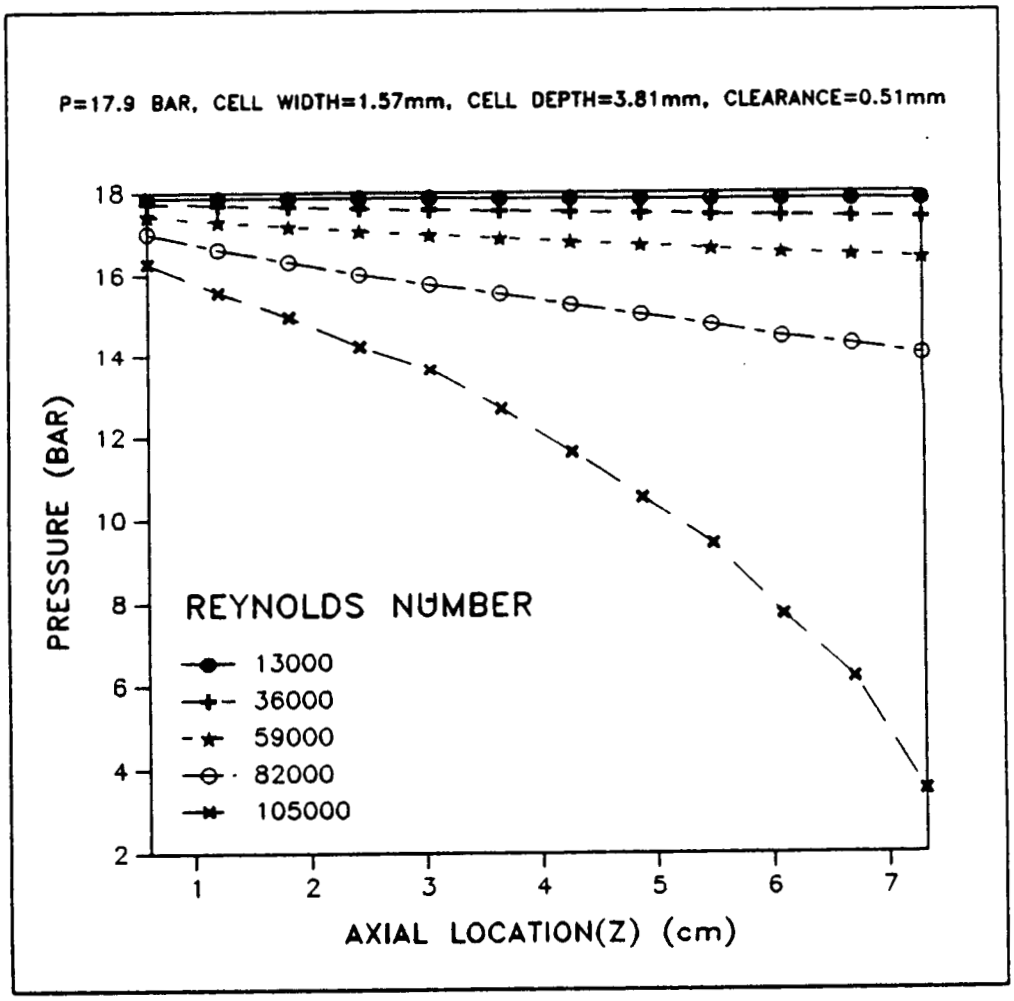

Figure 7. Pressure distribution along the axial location.

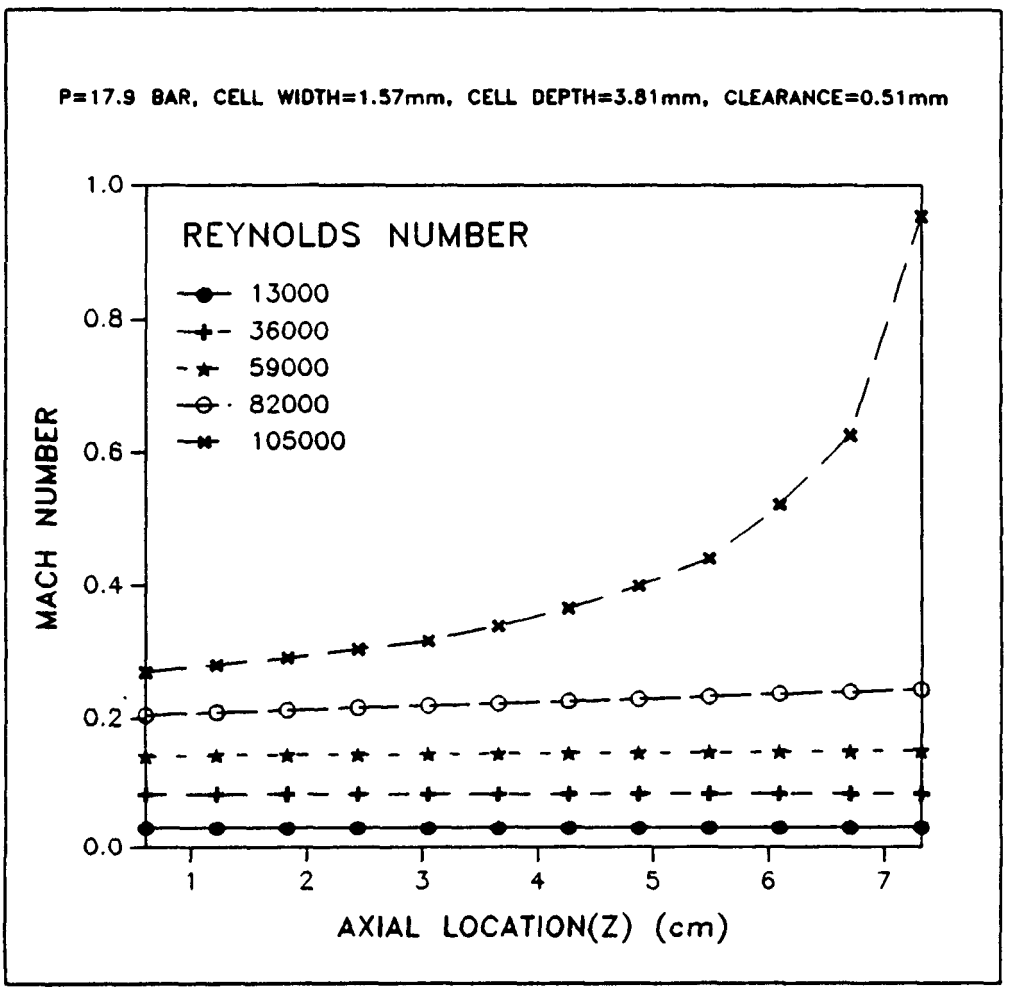

Figure 8. Mach Number distribution along the axial location.

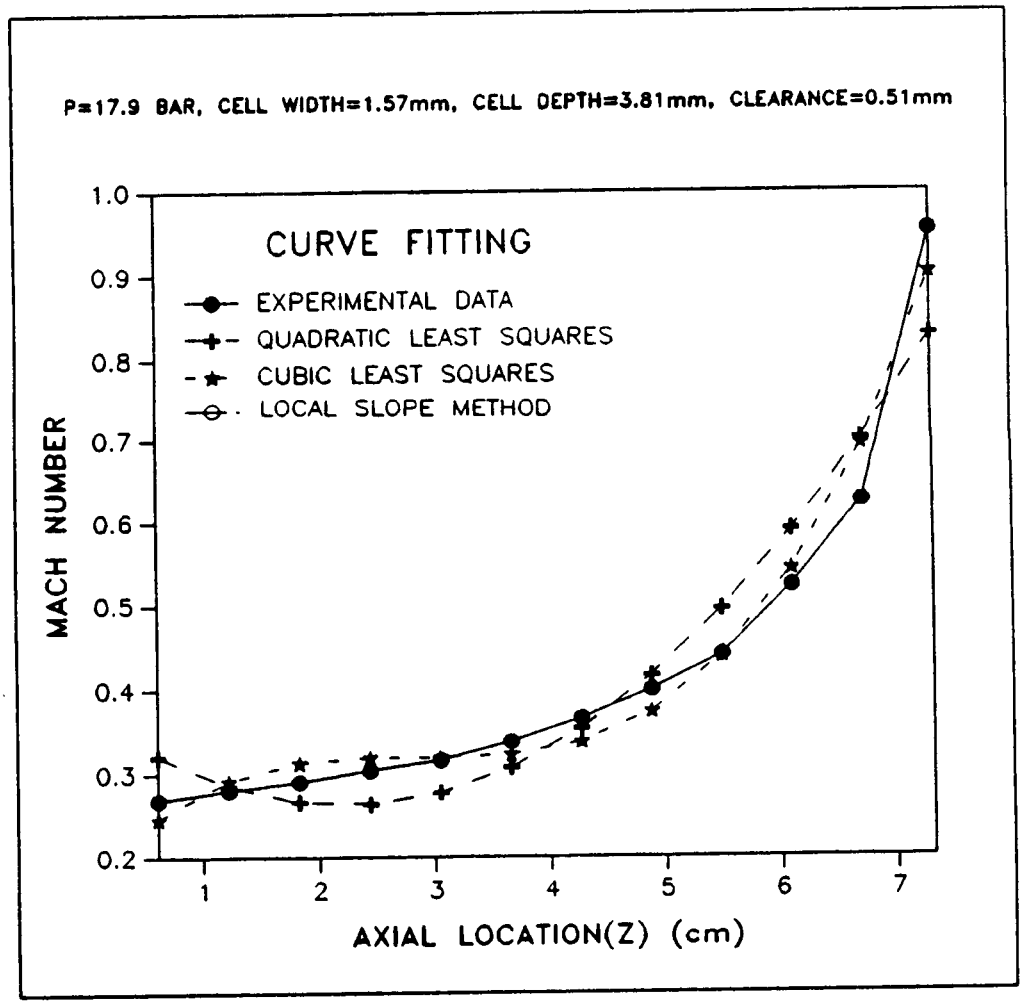

Figure 9. Comparison of Mach Number distribution with curve fitting method.

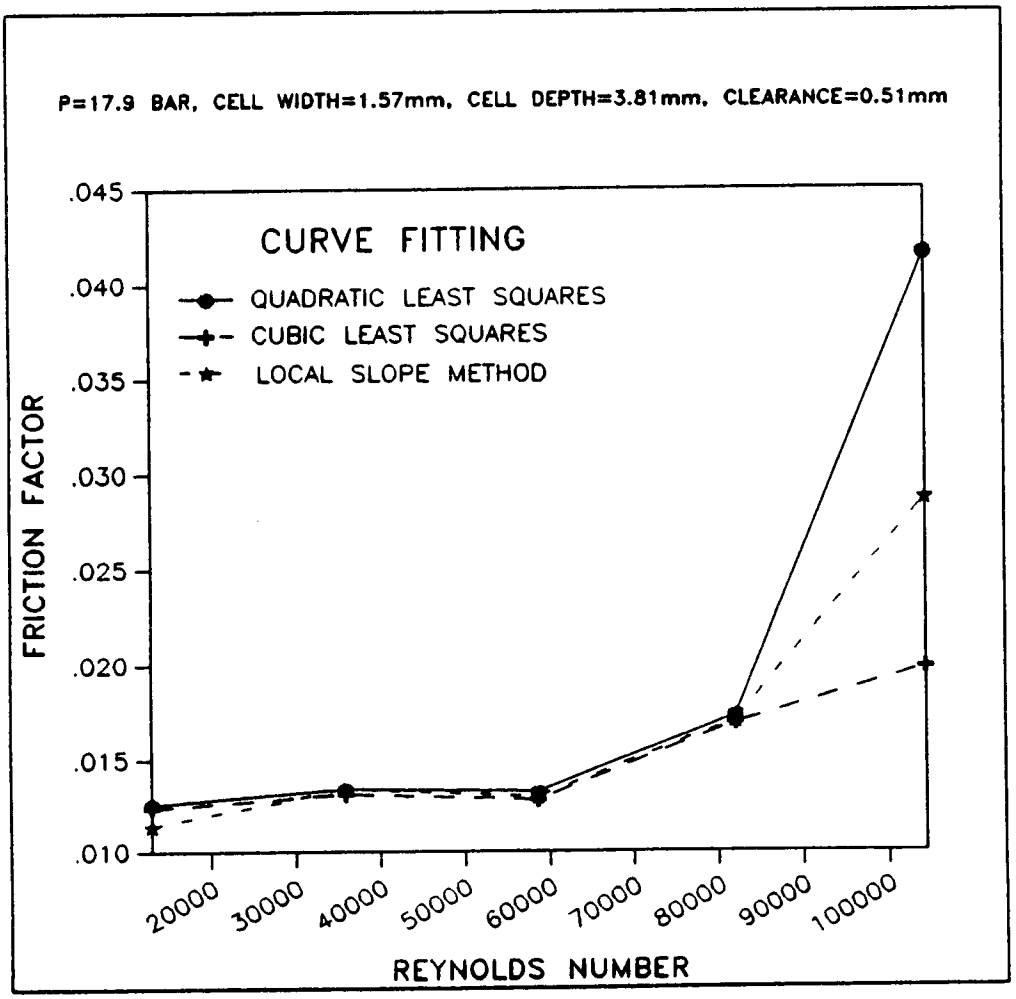

Figure 10. Comparison of friction factor with curve fitting method.

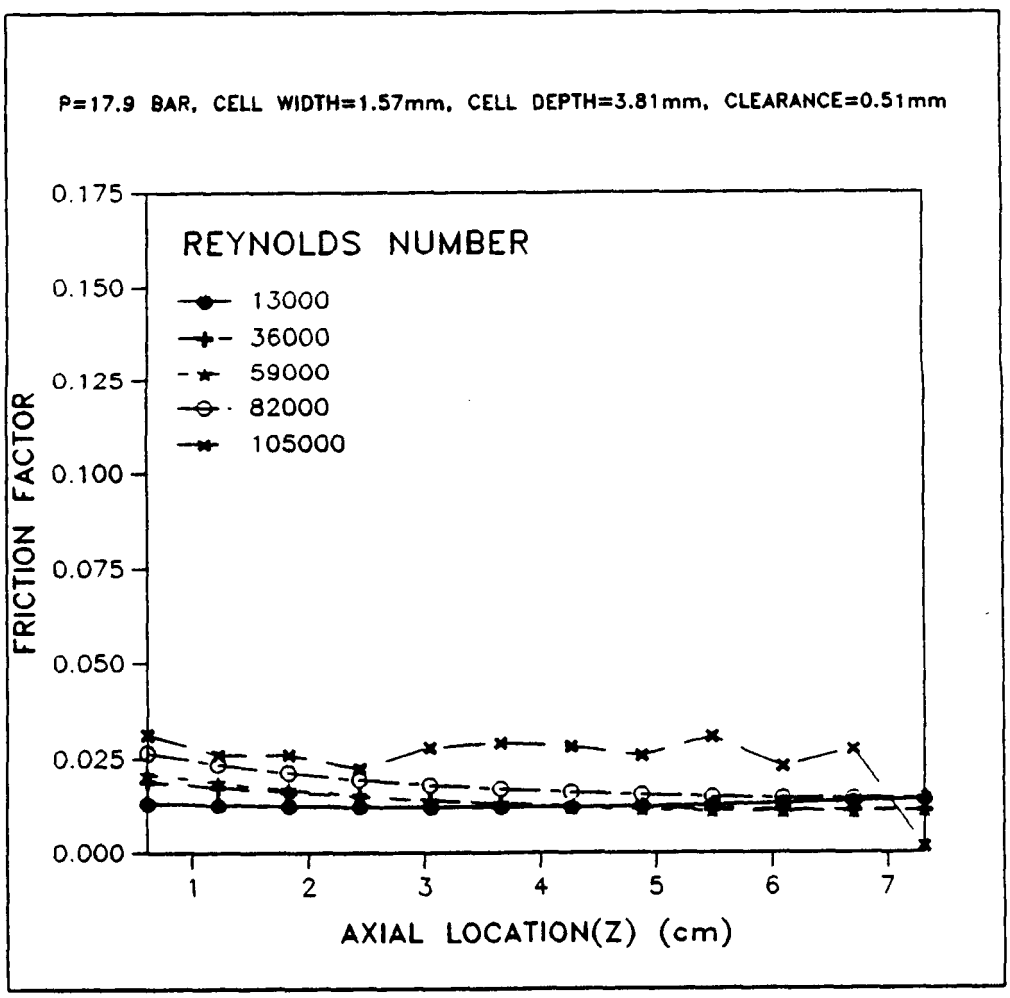

Figure 11. Friction factor distribution along the axial location.

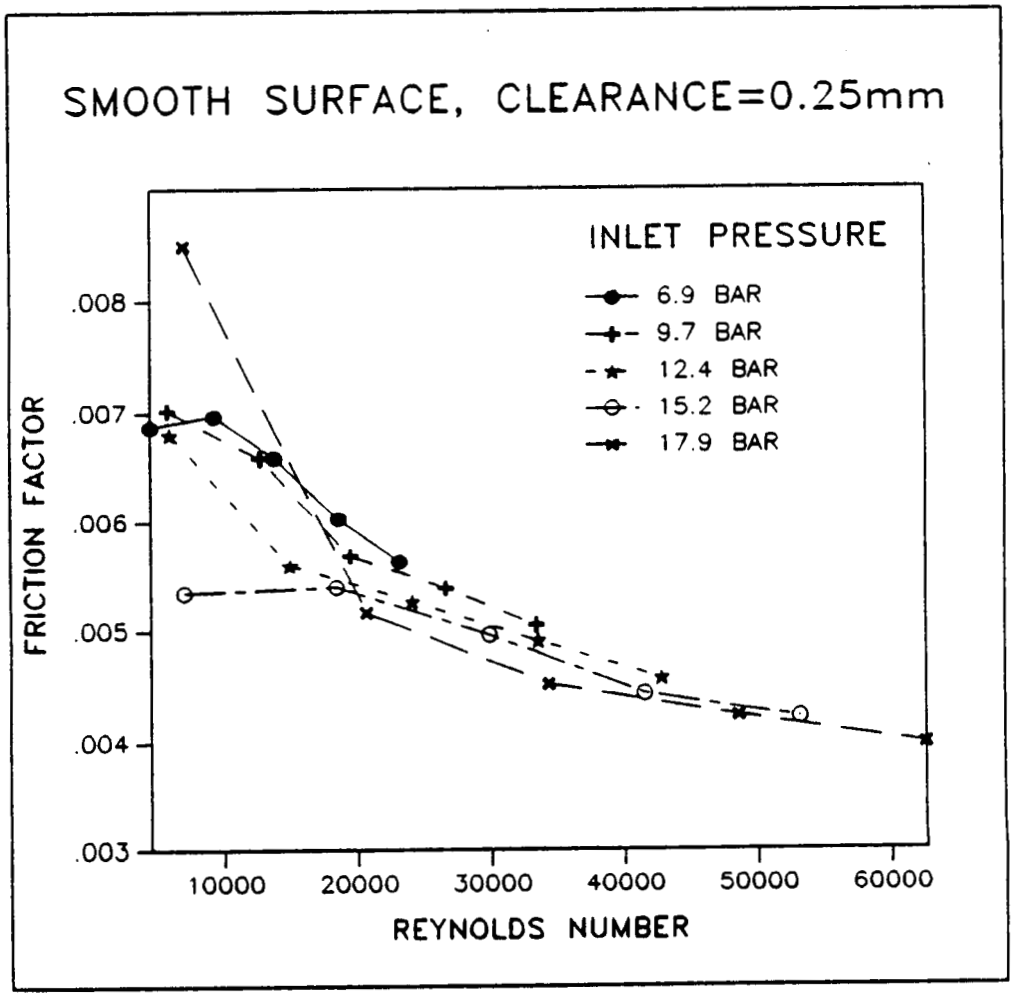

Figure 12. Effect of inlet pressure for smooth surface.

bar, 12.4 bar, 15.2 bar and 17.9 bar. For a smooth surface, figure 12 illustrates the trend that the friction factor decreases as the inlet pressure increases. For a typical honeycomb surface, the same trend holds as shown in Figure 13. For incompressible flow, the pressure gradient should affect the friction factor rather than local pressure, but in compressible flow, local pressure can affect the density of air to result in change of Mach number and Mach number gradient. As shown in equation (10), friction factor is a function of Mach number and Mach number gradient. Increasing inlet pressure results in a decrease of both Mach number and Mach number gradient. However, the decrement of the Mach number gradient is much larger than that of the Mach number. Therefore, the friction factor is reduced as the inlet pressure increases. This can be considered one reason why inlet pressure affects the friction factor.

Effect of cell width

Three honeycomb cell widths of 1.57mm, 0.79mm and 0.51mm are evaluated for the friction factor comparison. Figure 14 illustrates the typical plot of the friction factor versus Reynolds number for three cell widths, and demonstrates that the friction factor is sensitive to changes in cell widths and is also closely related to cell depth and clearance. For 3.81mm cell depth tests, an 0.79mm cell width honeycomb surface shows the biggest friction factor, followed by 0.51mm and 1.57mm for all inlet pressures, Reynolds number ranges, and 0.25mm and 0.38mm clearance, as shown in figure 14 (more plots are demonstrated on figures 23 to 32 in appendix A). For 2.29mm cell depth tests, a different trend is illustrated, as shown in a typical plot of figure 15. The 0.79mm cell width honeycomb surface also has the highest friction factor, followed by 1.57mm and 0.51mm for all inlet pressures, clearances,

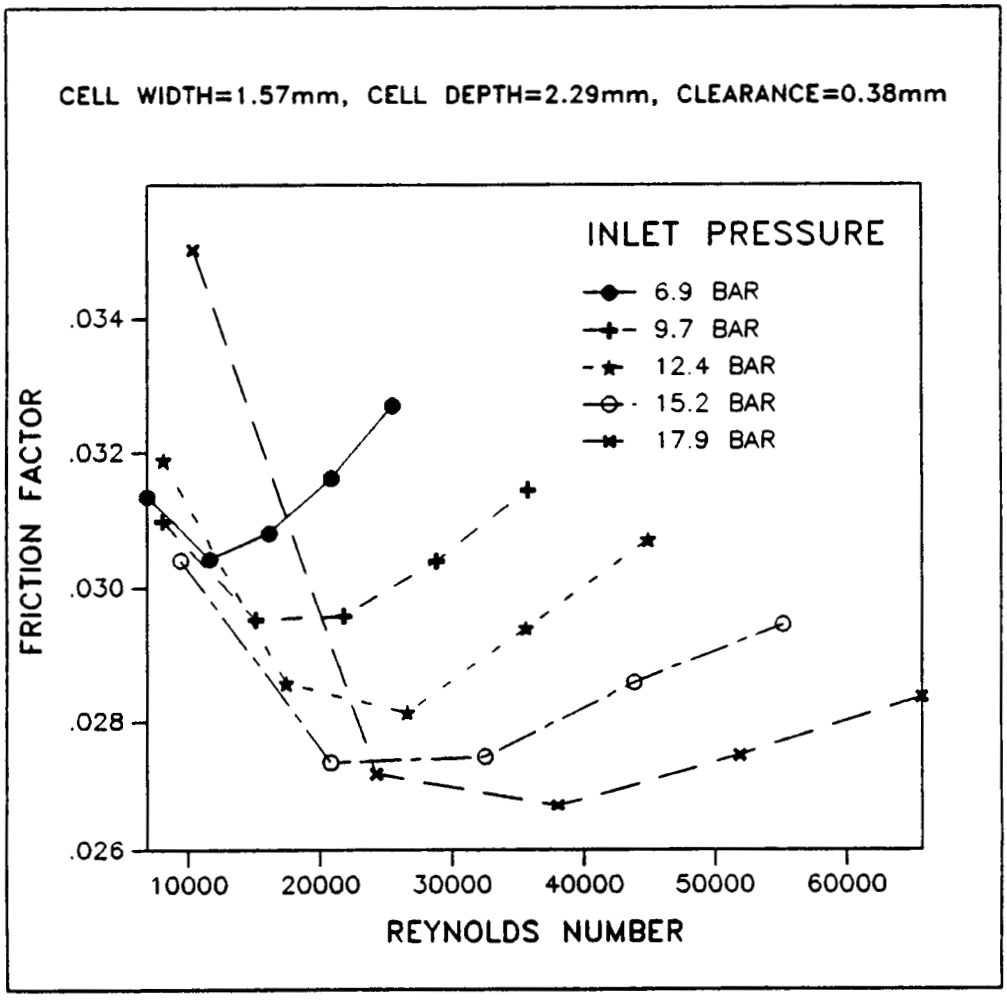

Figure 13. Effect of inlet pressure for honeycomb surface.

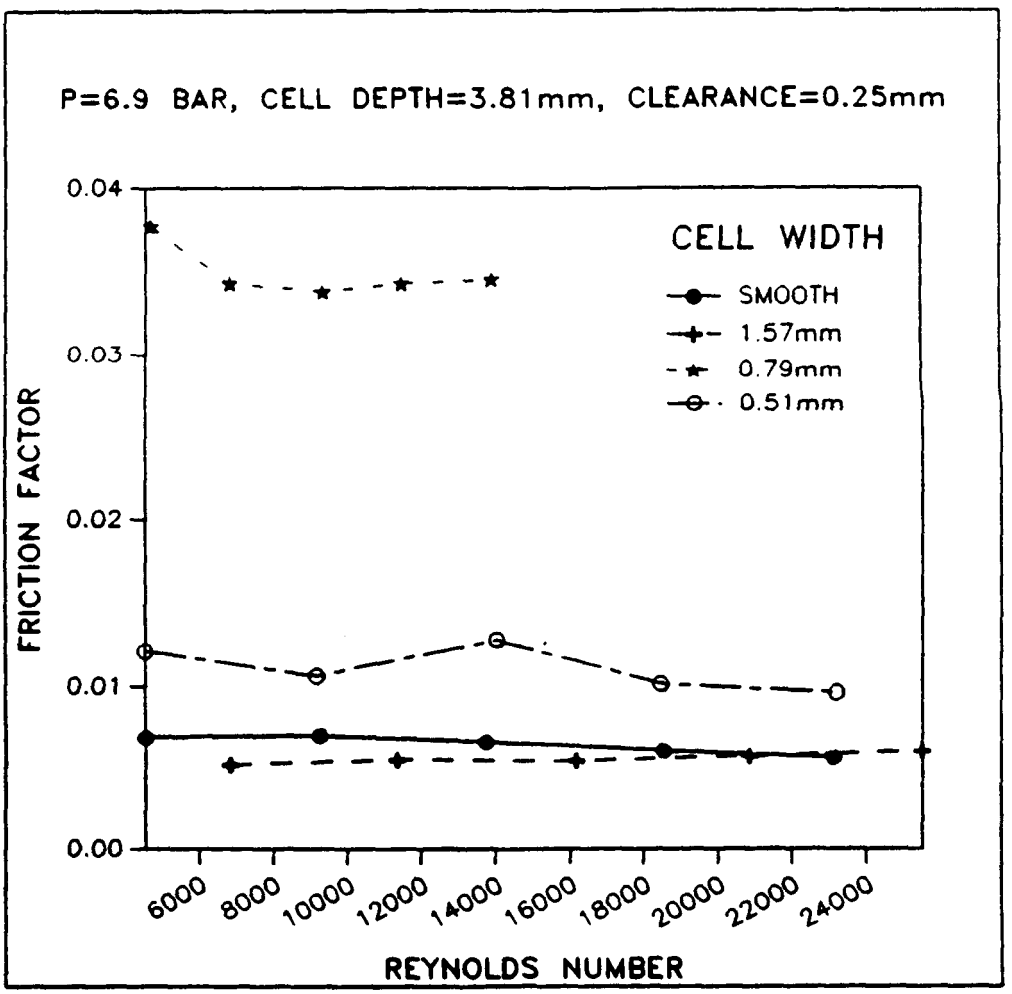

Figure 14. Comparison of friction factor with cell widths(1).

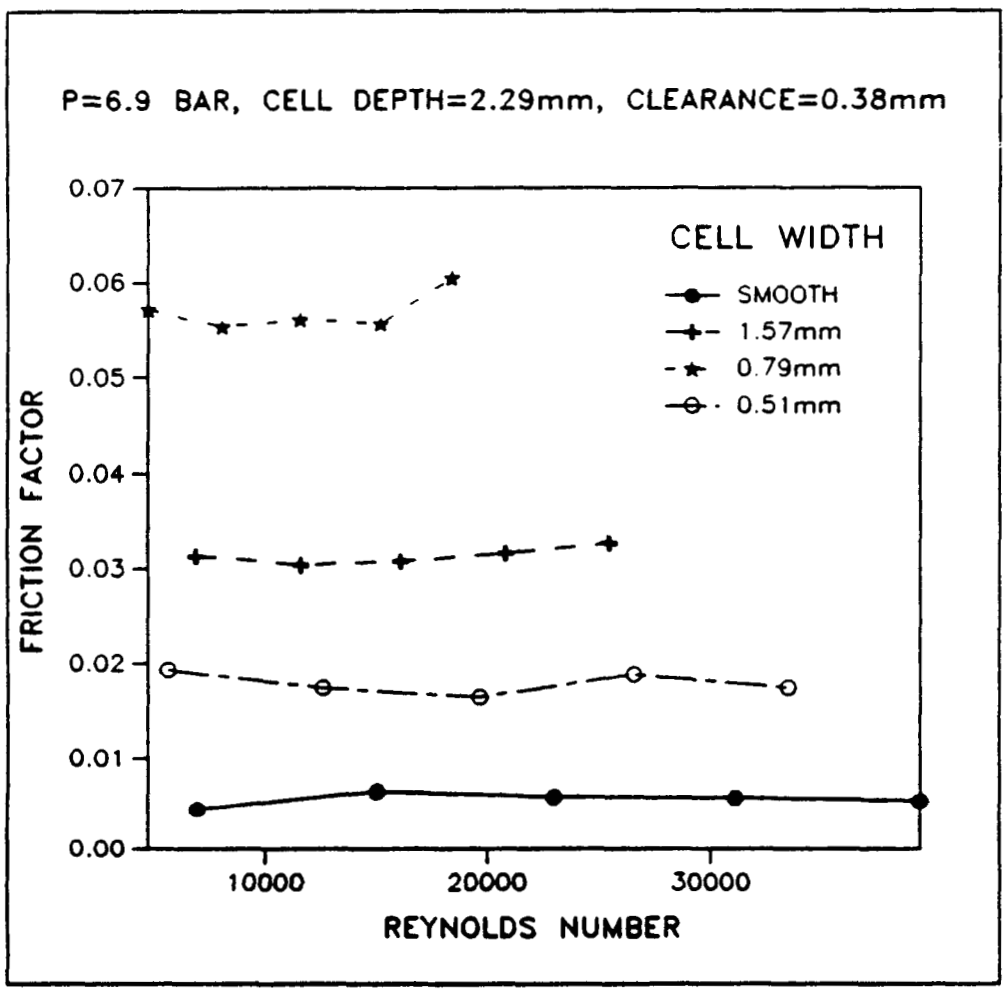

Figure 15. Comparison of friction factor with cell widths(2).

and Reynolds number ranges (more plots are demonstrated on figures 38 to 52 in appendix A). The friction factor for the honeycomb surface is much larger than that of smooth surface, as expected. However, the friction factor for 1.57mm cell width with 3.81mm cell depth and 0.25mm clearance is smaller than that of smooth surface, as shown in figure 14 (more plots are demonstrated on figures 23 to 27 in appendix A). The results of Stocker, Cox, and Holle(1977) support this result. Their results, which are taken from a four knife straight-through seal with a honeycomb land, provide that a honeycomb land can reduce leakage at 0.51 mm clearance, but at 0.31 mm clearance 1.57 mm and 3.41 mm cell width honeycomb lands leak almost twice as much as a smooth land.

Effect of Reynolds number

It is well known that friction factor is a function of two dimensionless quantities, relative roughness and Reynolds number in turbulent flow conditions. In this report, the friction factor is presented as a function of the Reynolds number which is defined based on $D = 2H$ and covers the range of 5,000 to 100,000. For a honeycomb surface, general trends show the friction factor to be nearly constant but reduced slightly as the Reynolds number increases, as shown in a typical plots of figures 14 and 15.

Effect of clearance

Clearance effects on the friction factor are investigated by varying the thickness of the spacer. Three clearances, 0.25mm, 0.38mm, and 0.51mm are evaluated for three cell widths and two cell depths. The typical plot of figure 16 illustrates that clearance is one of the important parameter of the friction factor. The trend is, however, not clear. As shown in figure 16, the friction factor increases as clearance increases for 1.57mm and 0.51mm cell width honeycomb tests with two cell depths.

For the 0.79mm cell width honeycomb test with two cell depths, the friction factor decreases as clearance increases, as shown in a typical plot of figure 17. More plots are demonstrated on figures 53 to 58 in appendix B.

Effect of cell depth

Two honeycomb depths, 2.29mm and 3.81mm, are compared for three cell widths and three clearances. Figure 18 illustrates the typical plot of the friction factor versus Reynolds number for two cell depths. In all cell widths and clearances, 2.29mm cell depth tests show bigger friction factors than 3.81mm cell depth. More plots are demonstrated on figures 59 to 67 in appendix C.

Uncertainty in Friction Factors

Generally, uncertainties in results based on measurement can be determined using the method described by Holman(1978). The uncertainty w_R in a result R which is a function of n primary measurements x_1 to x_n with uncertainties w_1 to w_n is

$$w_R = \left[\left(\frac{\partial R}{\partial x_1} w_1\right)^2 + \left(\frac{\partial R}{\partial x_2} w_2\right)^2 + \ldots + \left(\frac{\partial R}{\partial x_n} w_n\right)^2 \right]^{1/2}$$

The primary measurement in the friction factor calculations are clearance, pressure, flow rate, and stagnation temperature. The uncertainties in these measurements are about 13 μ m, 0.0096 bar, $5X10^{-5}$ m^3/min, and 0.6°K, respectively. As a result, the estimated uncertainty in Mach number and friction factor calculation are about 0.1 percent and 0.09 percent, respectively.

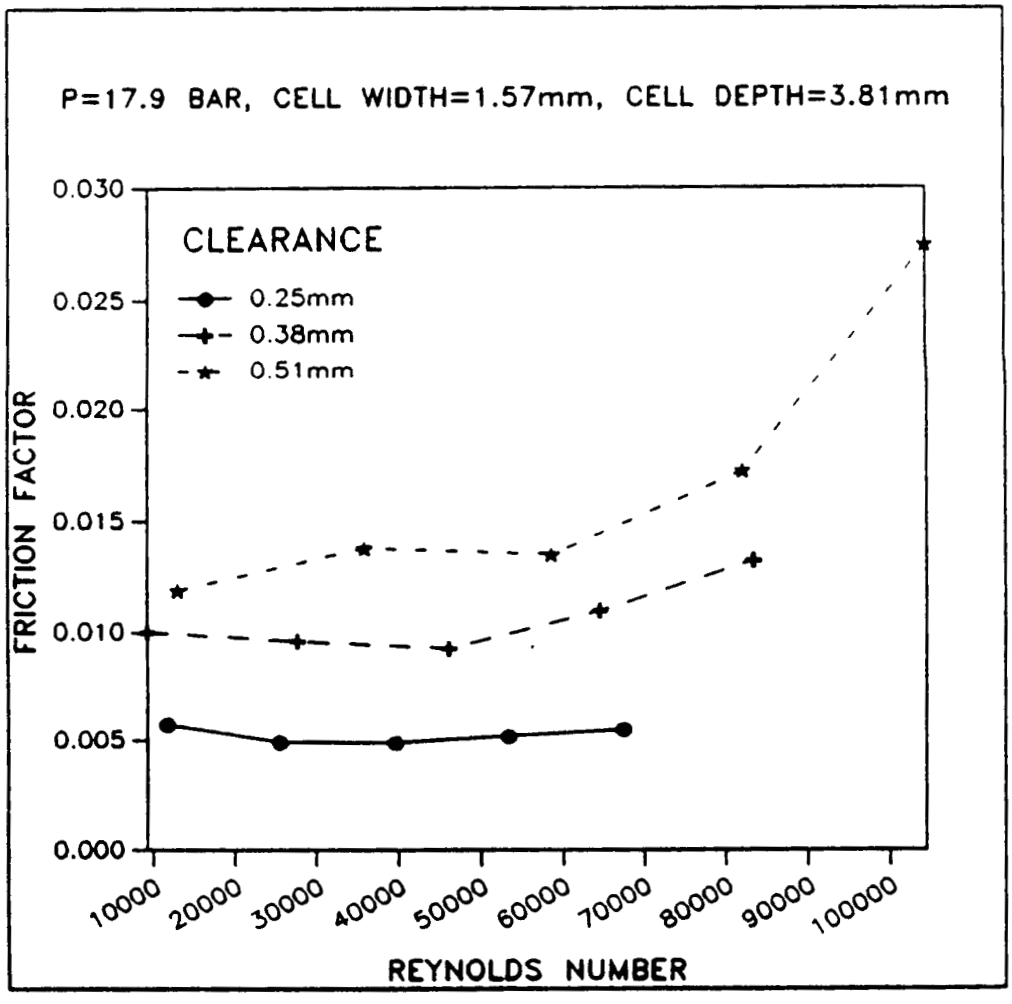

Figure 16. Comparison of friction factor with clearances(1).

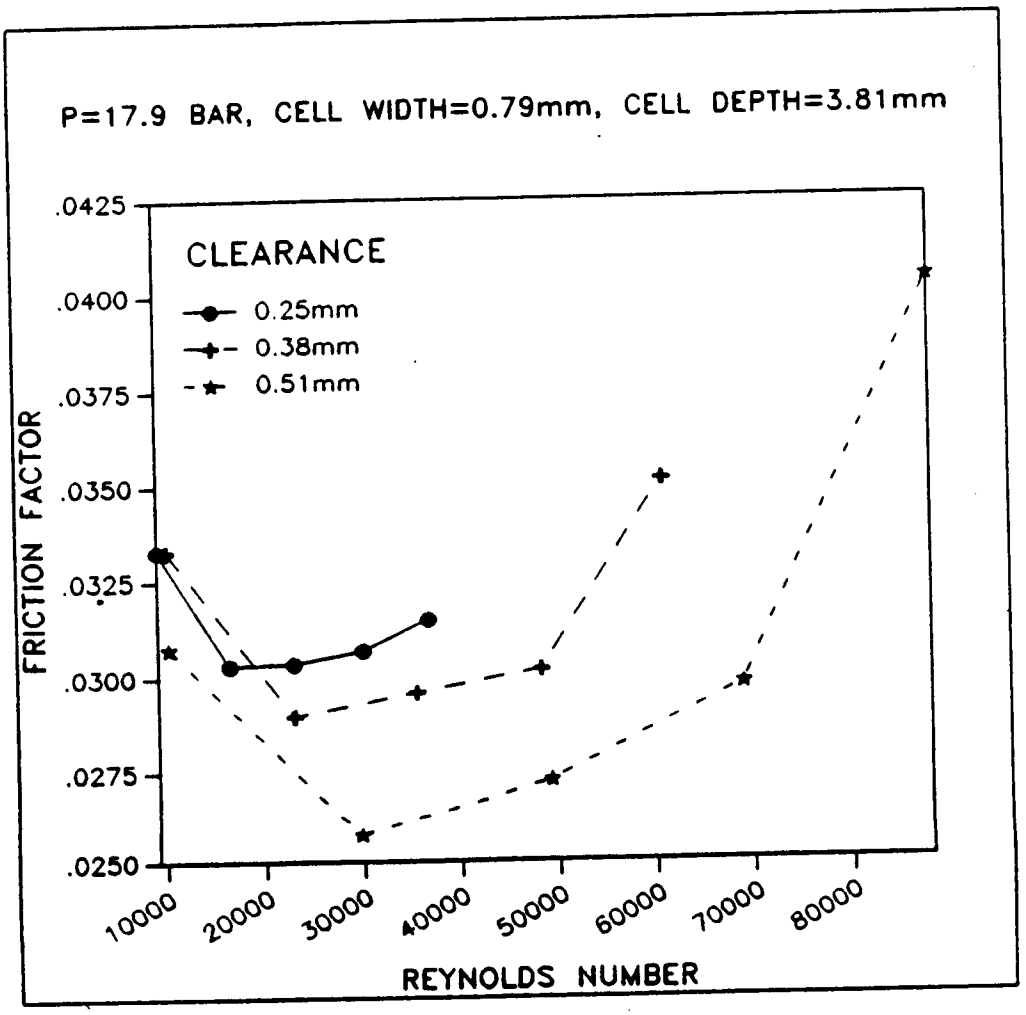

Figure 17. Comparison of friction factor with clearances(2).

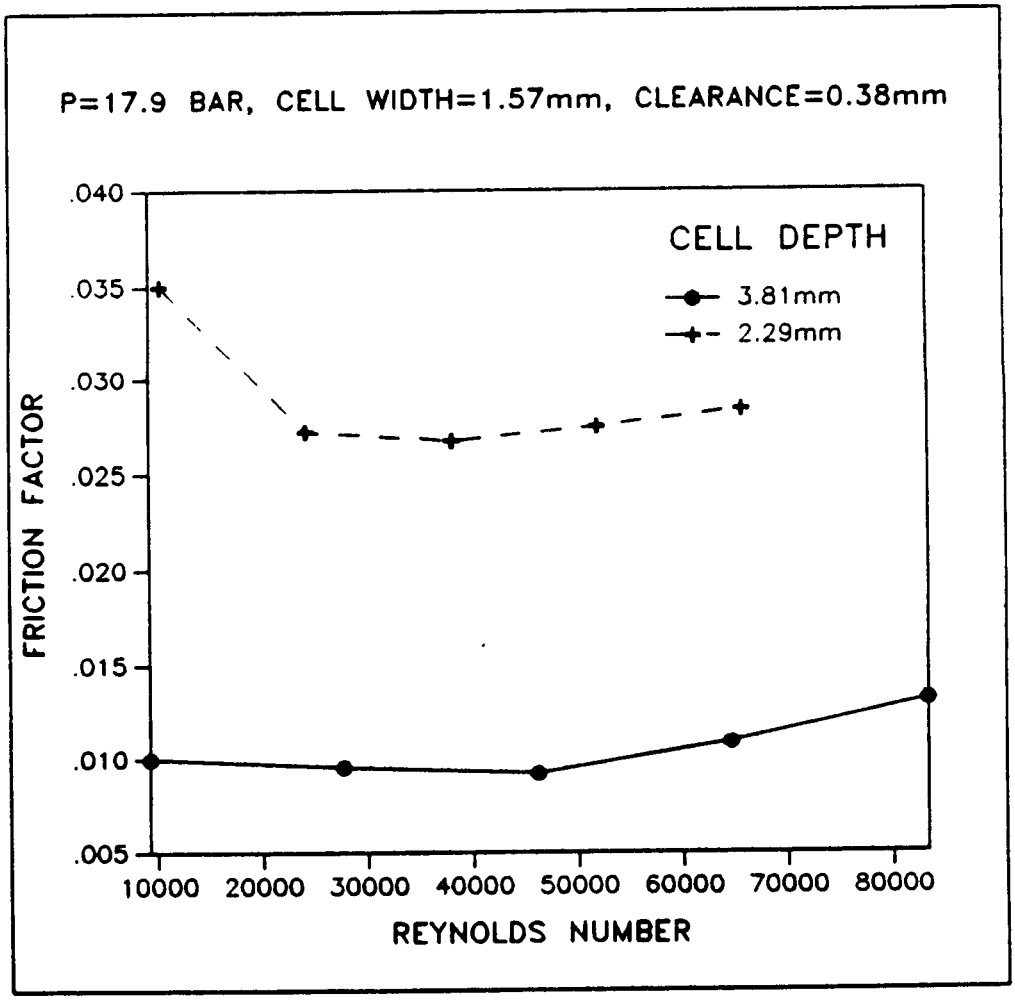

Figure 18. Comparison of friction factor with cell depths.

CHAPTER VI

CONCLUSION

The flat plate tester has been used to determine the friction factor of honeycomb surfaces. Three honeycomb cell widths, two honeycomb cell depths, and three clearances were used. Five inlet pressures and a Reynolds number range of 5,000 to 100,000 are also used for the test parameters.

Although the measurements made here are not complete enough to describe all aspects of the friction factor for honeycomb surfaces, they do bring out some of the prominent features. The comparisons in the preceding chapters support the following conclusions:

(a) Generally, honeycomb surfaces provide a much larger friction factor than a smooth surface, almost seven times.

(b) For 1.57 mm cell width with 3.81 mm cell depth and the 0.25 mm clearance, the friction factor is smaller than a smooth surface. A possible explanation is that flow may have more tendency to expand into the honeycomb cell and this action would have the effect of increasing the flow area. Therefore, while honeycomb surfaces generally reduce seal leakage, consideration must be given to the operating clearance and the honeycomb cell dimensions.

(c) The change of inlet pressure affects the Mach number and Mach number gradient to result in a change of the friction factor. Unlike an incompressible pipe flow, the friction factor for this flow condition can not defined by only two dimensionless quantities, the Reynolds number and the relative roughness.

(d) In general, the friction factor is reduced as the Reynolds number increases. Available data illustrate that the Reynolds number range covered by this report is

in the transition zone on the Moody chart.

(e) The ratio of honeycomb cell width to honeycomb cell depth(b/d) is an important parameter for the friction factor. The friction factor versus b/d, as shown in figure 19, is very similar to the results of Schlichting(1979) who presented the resistance coefficient of circular cavities of varying depth in a flat wall. Schlicting's results are illustrated in figure 20. For the available data, an optimum ratio for the friction factor is 2.9 (i.e., 0.79mm cell width and 2.29mm cell depth) in a 0.25mm clearance.

(f) The ratio of honeycomb cell width to clearance(b/H) is also an important parameter. Figure 21 shows the friction factor versus b/H for two cell depths. For the available data, an optimum value results at the ratio of 3.1 (i.e., 0.79mm cell width and 0.25mm clearance) in 2.29mm cell depth.

(g) The effect of honeycomb material in reducing seal leakage appears to be a function of the cell width, cell depth, and clearance. The data obtained from these tests indicate the maximum friction factor is about 0.073 when b/d is 2.9 and clearance is 0.25 mm.

(h)The friction factor, generally, is a function of the relative roughness of the surface and the Reynolds number. Relative roughness is defined by an absolute roughness to the diameter ratio. However, for honeycomb surfaces, the absolute roughness is an hole. Therefore, geometrical relative roughness does not have any meaning. The friction factor of honeycomb surfaces can be inserted to the Moody diagram, and an effective relative roughness can be estimated by this approach. As shown figure 22, the maximum effective relative roughness is extended to the order of about 0.4 for this tests.

(i) Further experimental investigation with various b/d and b/H ratios would

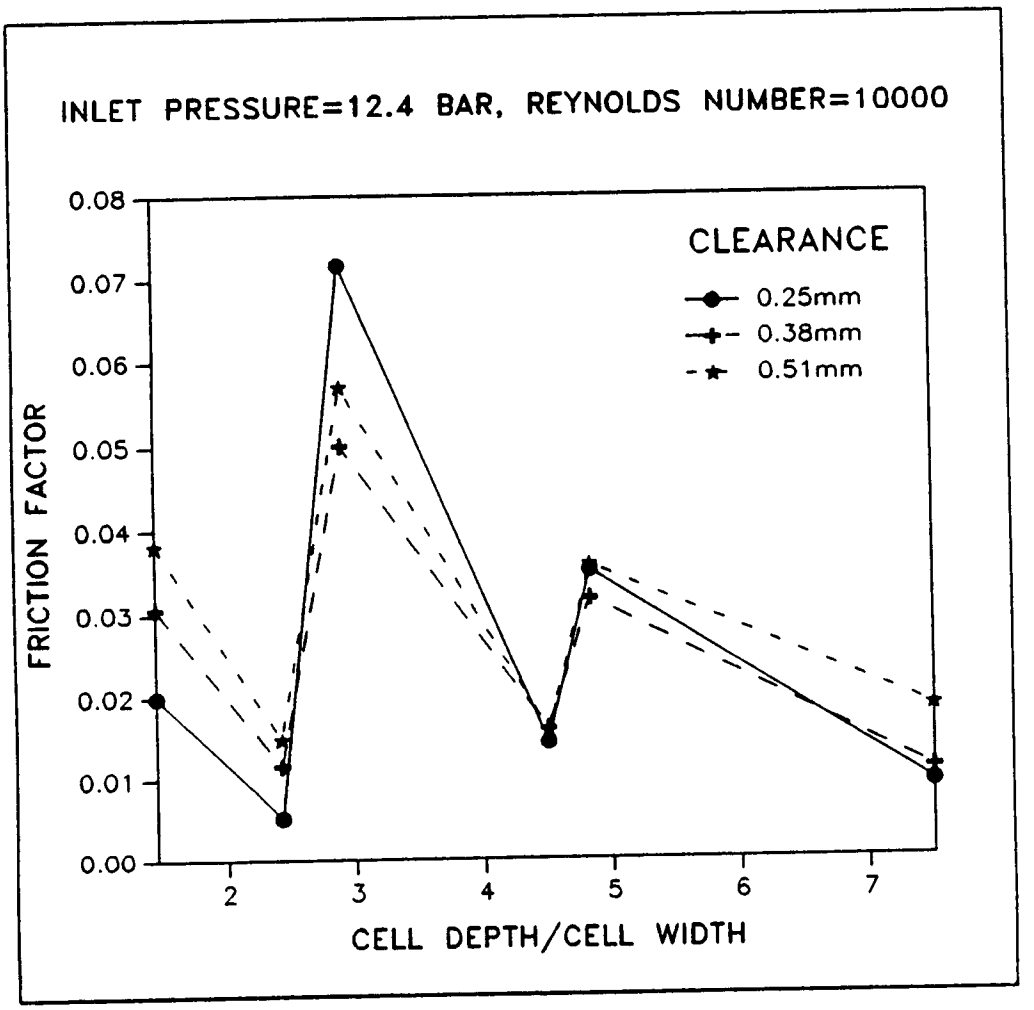

Figure 19. Friction factor versus the ratio of cell width to cell depth.

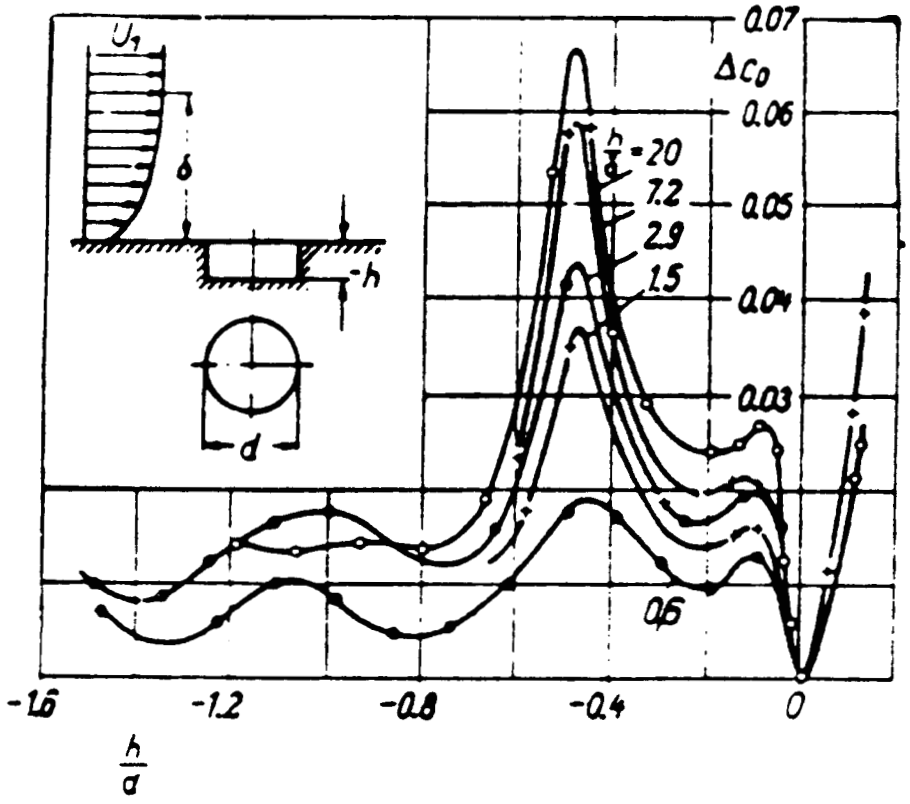

Figure 20. Resistance coefficient of circular cavities of varying depth in a flat wall.

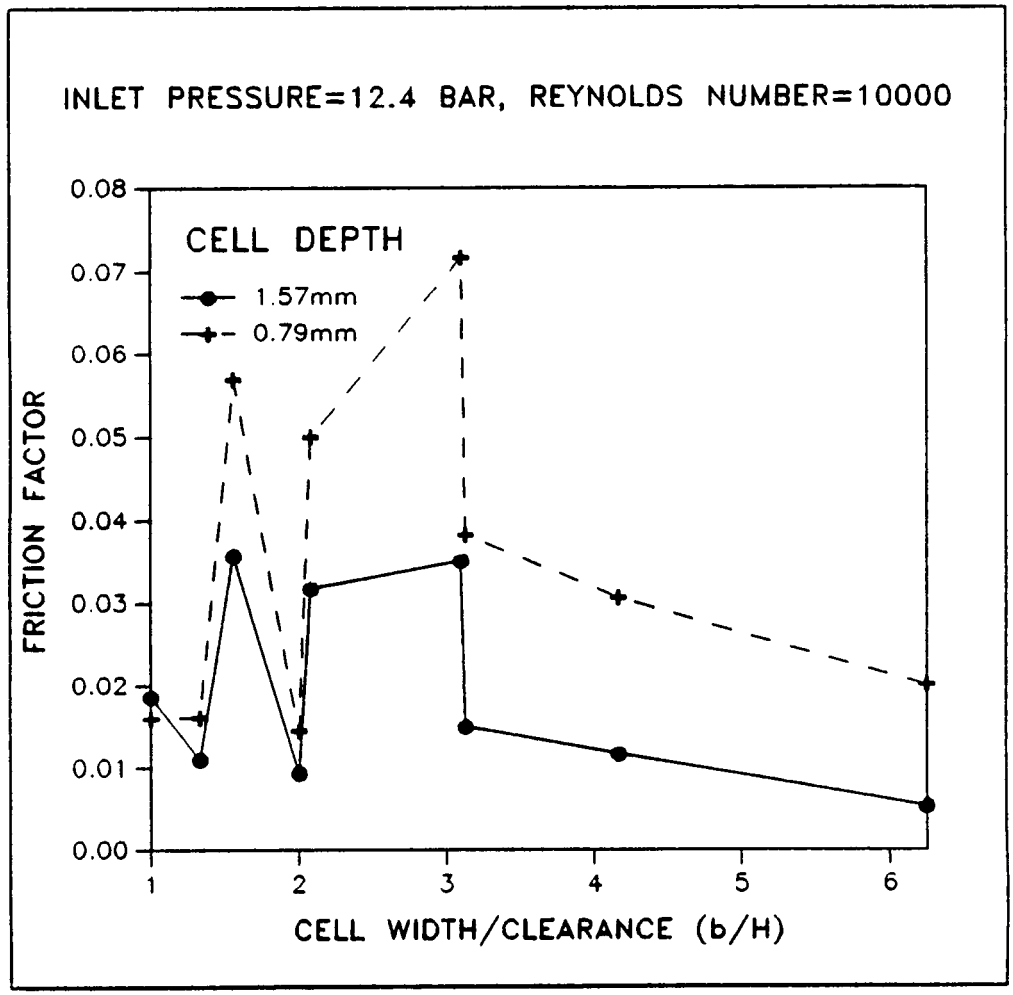

Figure 21. Friction factor versus the ratio of cell width to clearance.

ORIGINAL PAGE IS
OF POOR QUALITY

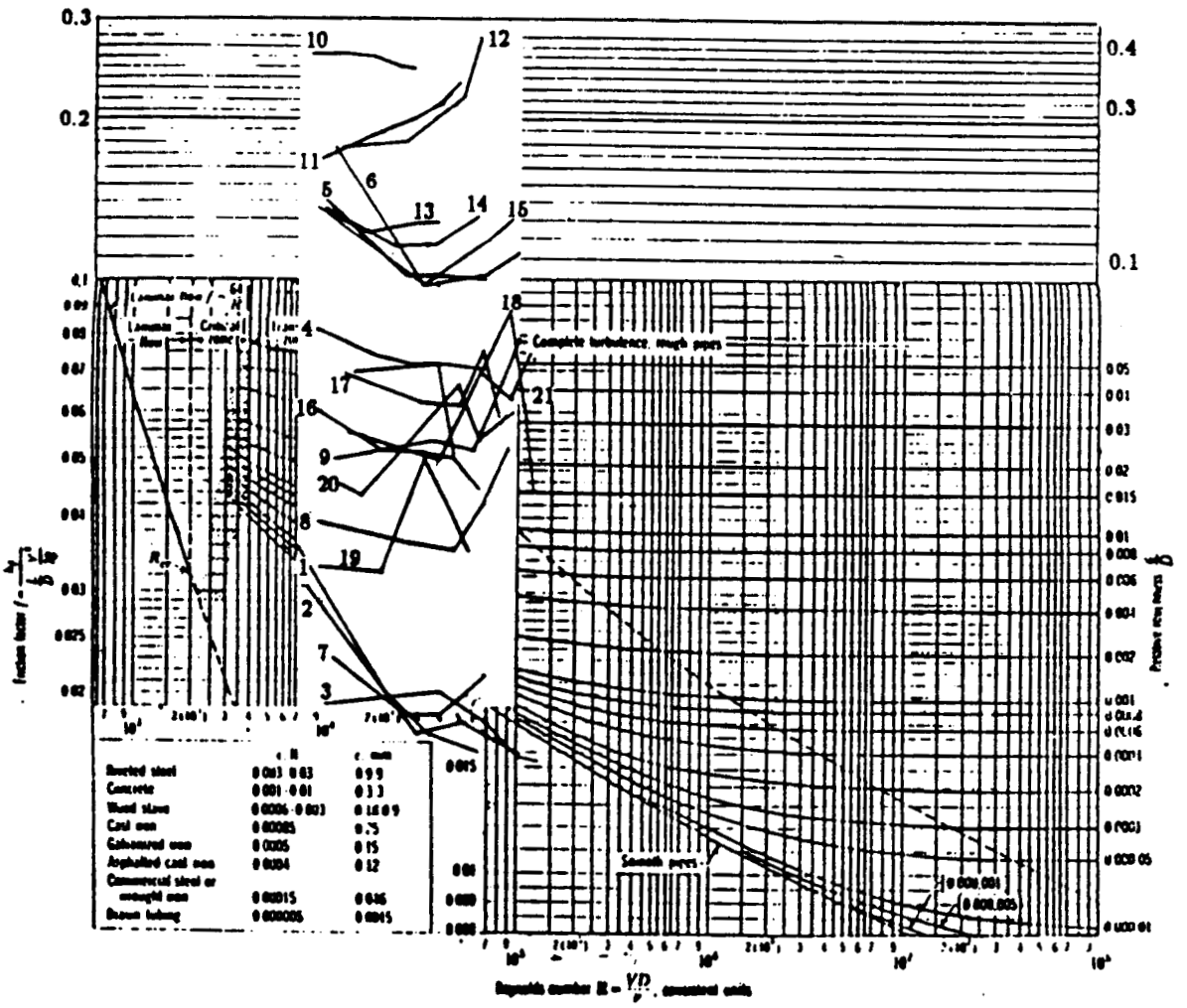

Figure 22. Relative roughness estimation from the Moody diagram.

help to find optimum ratios for the maximum surface friction factors.

REFERENCES

Childs, D. W., and Kim, C. H., 1985, "Analysis and Testing for Rotor Dynamic Coefficients of Turbulent Annular Seals with Different Directionally Homogeneous Surface Roughness Treatment for Rotor and Stator Elements," ASME Journal of Tribology Technology, vol. 107, pp. 296-306.

Childs, D. W., and Kim, C. H., 1986, "Test Results for Round-Hole Pattern Damper Seals: Optimum Configurations and Dimension for Maximum Net Damping," ASME Journal of Tribology, vol. 108, pp. 605-611.

Childs, D. W., Elrod, D., and Hale, K., 1988, "Annular Honeycomb Seals: Test Results for Leakage and Rotordynamic Coefficients; Comparisons to Labyrinth and Smooth Configurations," ASME Paper 88-Trib-35, ASME/STLE Joint Tribology Conference.

Childs, D. W., and Moyer, D., 1985, "Vibration Characteristics of The HPOTP(High Pressure Oxygen Turbopump) of The SSME(Space Shuttle Main Engine)," ASME Journal of Engineering for Gas Turbine and Power, vol. 107, no. 1, pp. 152-159.

Elrod,D., 1988, "Entrance and Exit Region Friction Factor Models for Annular Seal Analysis," Ph.D Dissertation, Texas A&M University, College Station, Texas.

Frössel, W., 1938, "Flow in Smooth Straight Pipes at Velocities Above and Below Sound Velocity," N.A.C.A. TM, no. 844.

Grashof, F., 1875, Theoretische Maschinenlehre, L. Voss, Leipzig, Germany, pp. 593-597.

Holman, J. P., 1978, Experimental Methods for Engineers, McGraw-Hill, New York, NY, p. 45.

John, J. E. A., 1984, Gas Dynamics,Allyn and Bacon, Newton, MA.

Keenan, Joseph H., 1939, "Friction Coefficients for the Compressible Flow of Steam," Journal of Applied Mechanics, Trans. A.S.M.E., vol. 61, pp. A-11.

Moody, L. F., 1944, "Friction Factors for Pipe Flow," Trans. Am. Soc. Mech. Engrs. 66, pp. 671-684.

Nelson, C. C., 1984, "Analysis for Leakage and Rotordynamic Coefficients of Surface Roughened Tapered Annular Gas Seals," ASME Journal of Engineering for Power, vol. 106, no. 4, pp. 927-934.

Schlichting, H., 1979, Boundary-Layer Theory, 7th Ed., McGraw-Hill, New York, NY, p. 656.

Stocker, H. L., Cox, D. M., and Holle, G. F., 1977, "Aerodynamic Performance of Conventional and Advanced Design Labyrinth Seals with Solid-Smooth, Abradable, and Honeycomb Lands", Detroit Diesel Allison, NASA CR-135307.

Stodola, A., 1927, Steam and Gas Turbines, New York, N. Y., McGraw-Hill Book Company, Inc., vol. 1, p. 61.

Zeuner, G., 1900, Technical Thermodynamics, Leipzig, Germany, pp. 264-273.

APPENDIX A

FRICTION FACTOR VERSUS REYNOLDS NUMBER FOR A SMOOTH SURFACE AND HONEYCOMB SURFACES WITH THREE CELL WIDTHS

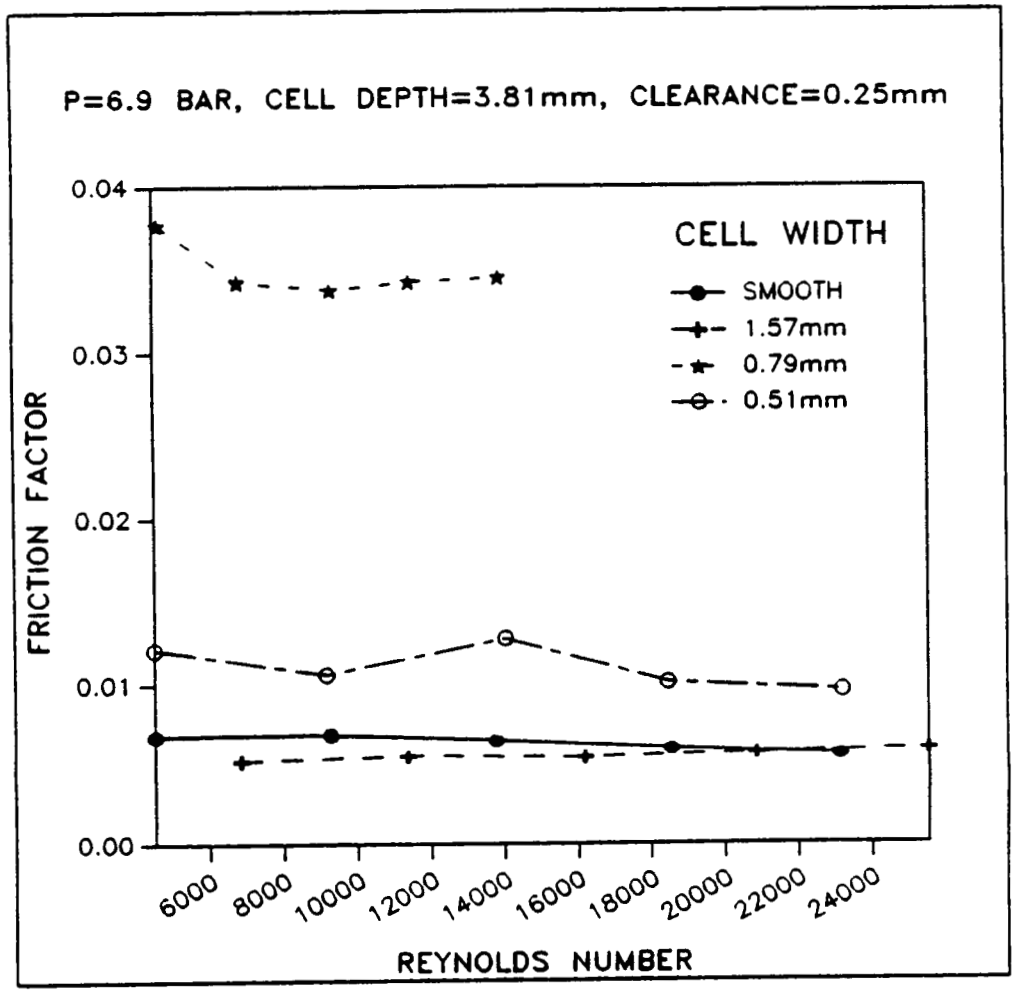

Figure 23. Friction factor versus Reynolds number for tests 1,4,10 and 16 of table 1 with inlet pressure 6.9 bar.

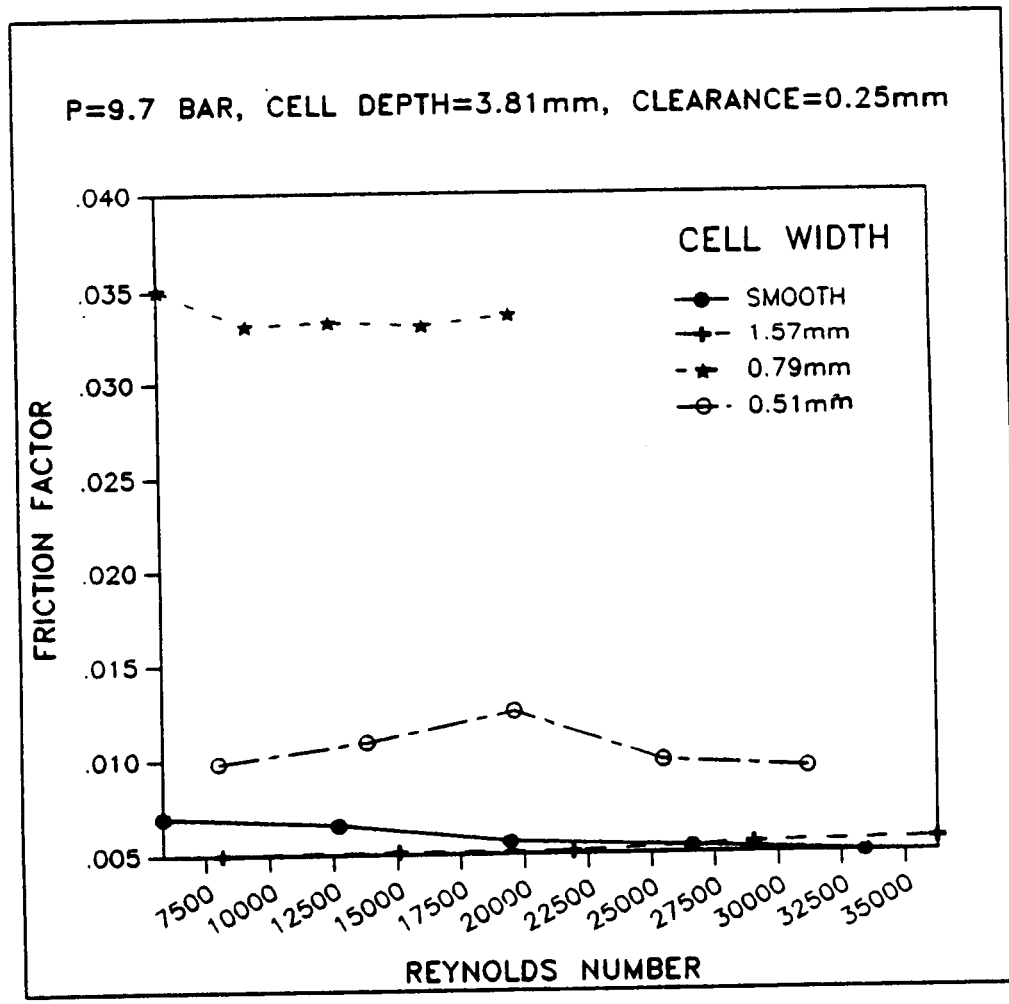

Figure 24. Friction factor versus Reynolds number for tests 1,4,10 and 16 of table 1 with inlet pressure 9.7 bar.

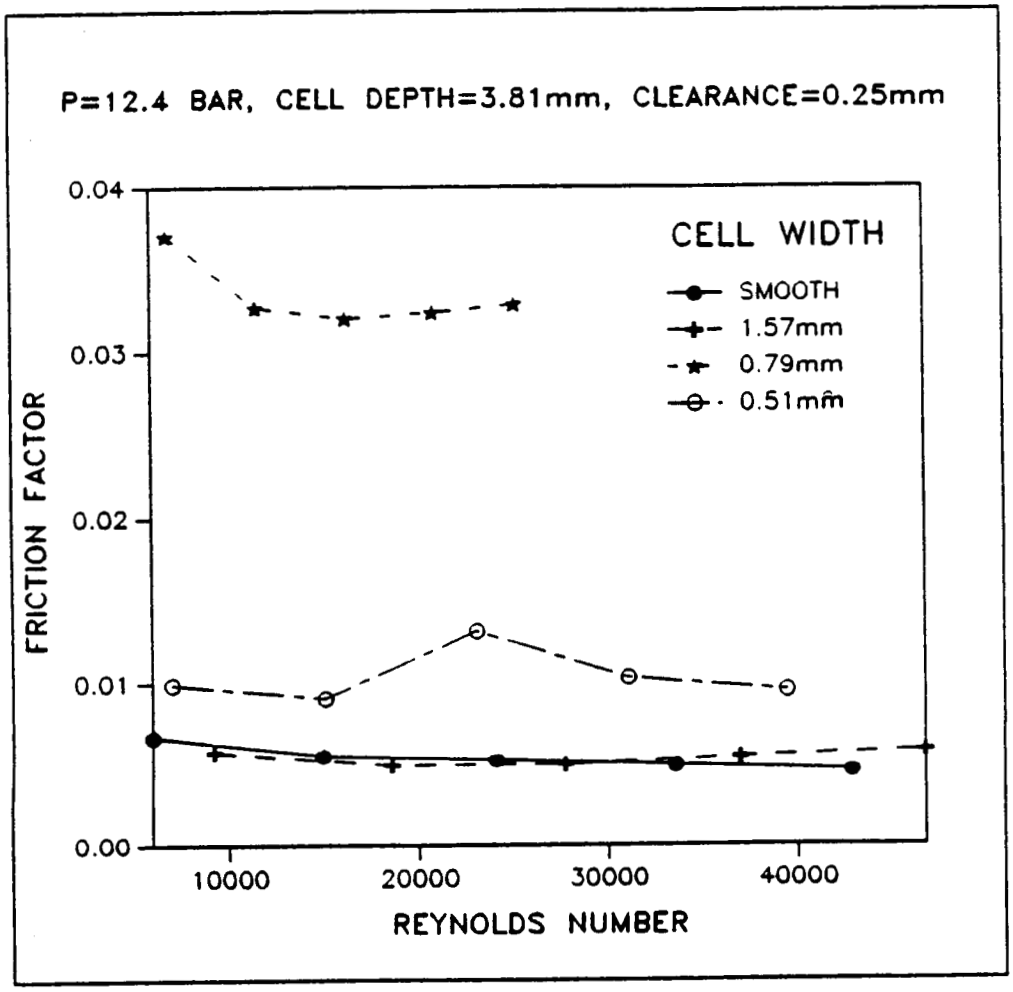

Figure 25. Friction factor versus Reynolds number for tests 1,4,10 and 16 of table 1 with inlet pressure 12.4 bar.

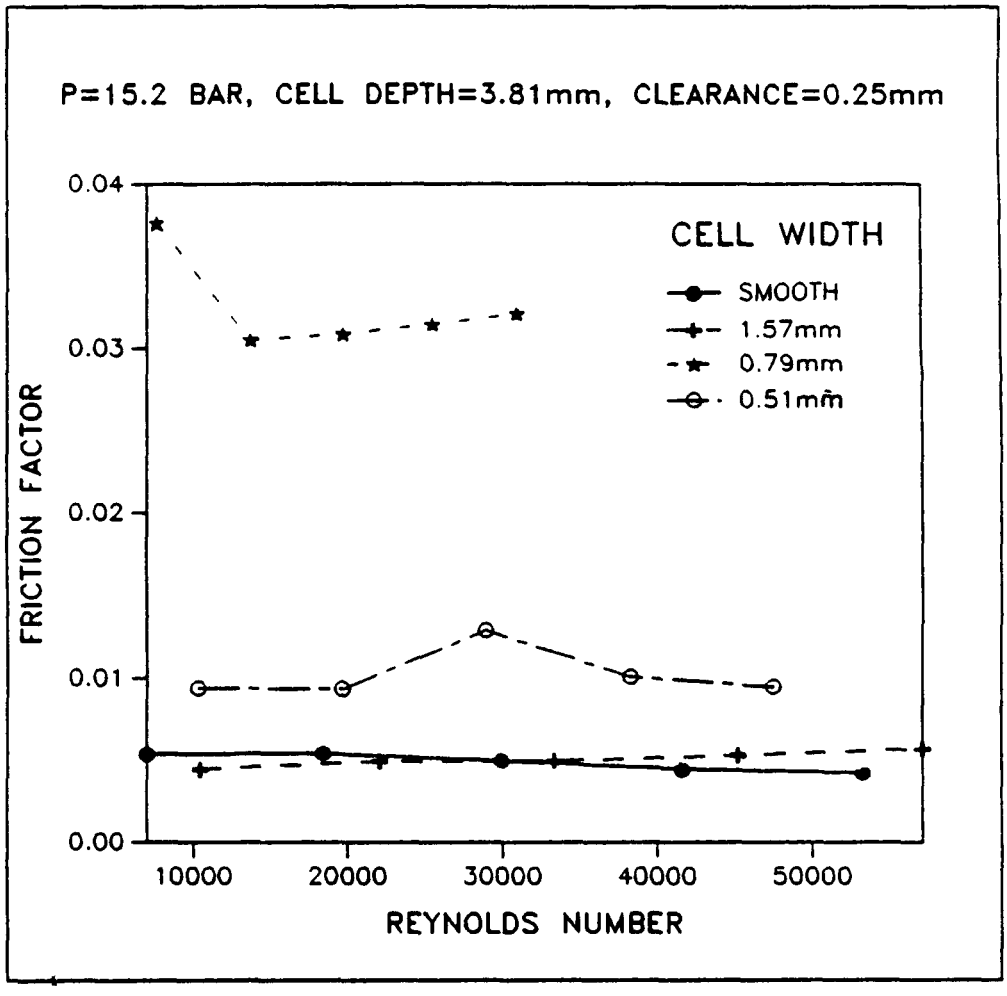

Figure 26. Friction factor versus Reynolds number for tests 1,4,10 and 16 of table 1 with inlet pressure 15.2 bar.

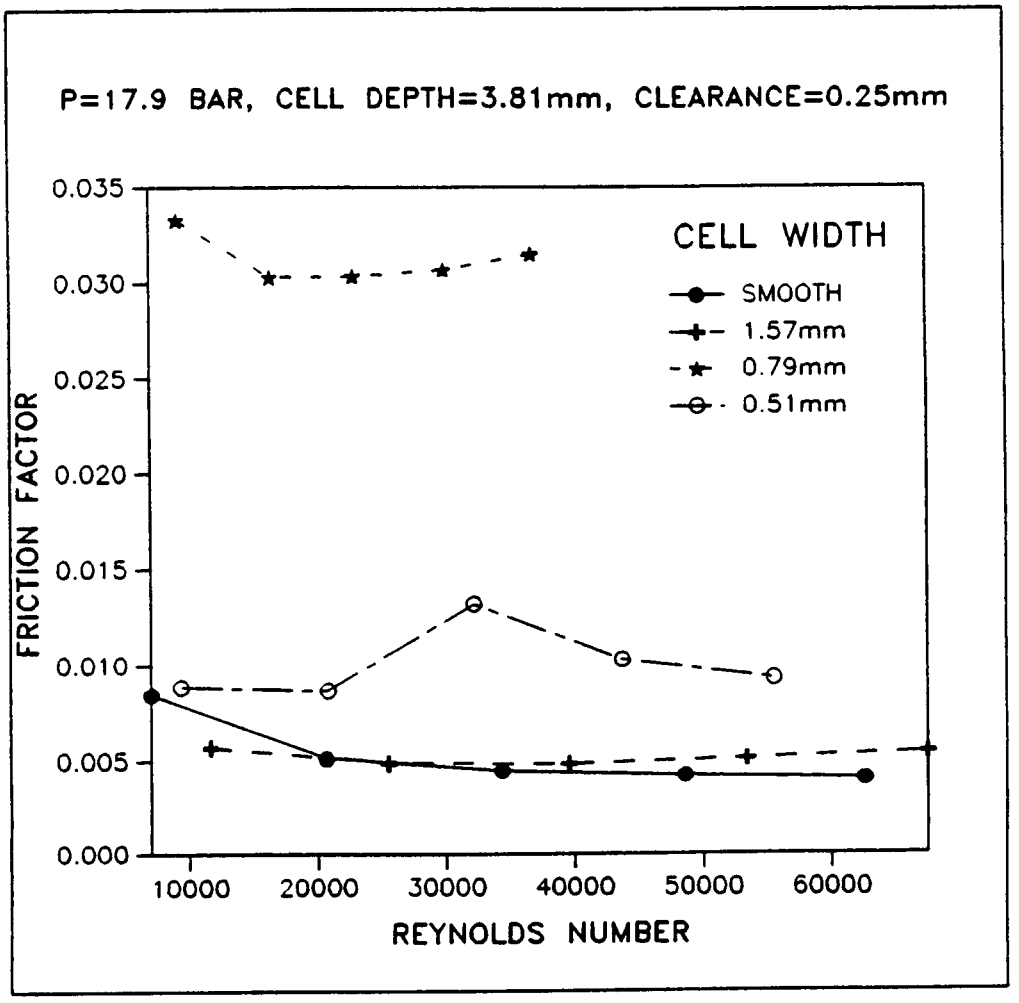

Figure 27. Friction factor versus Reynolds number for tests 1,4,10 and 16 of table 1 with inlet pressure 17.9 bar.

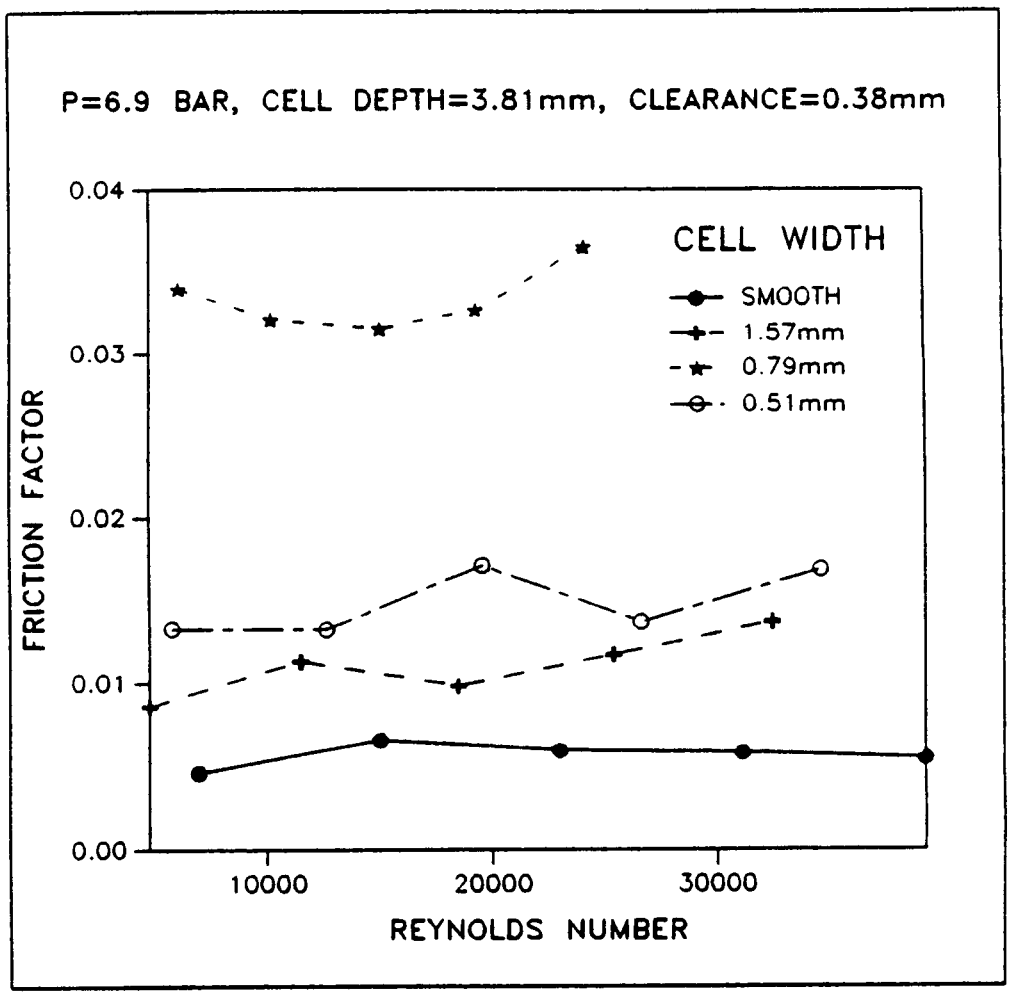

Figure 28. Friction factor versus Reynolds number for tests 2,5,11 and 17 of table 1 with inlet pressure 6.9 bar.

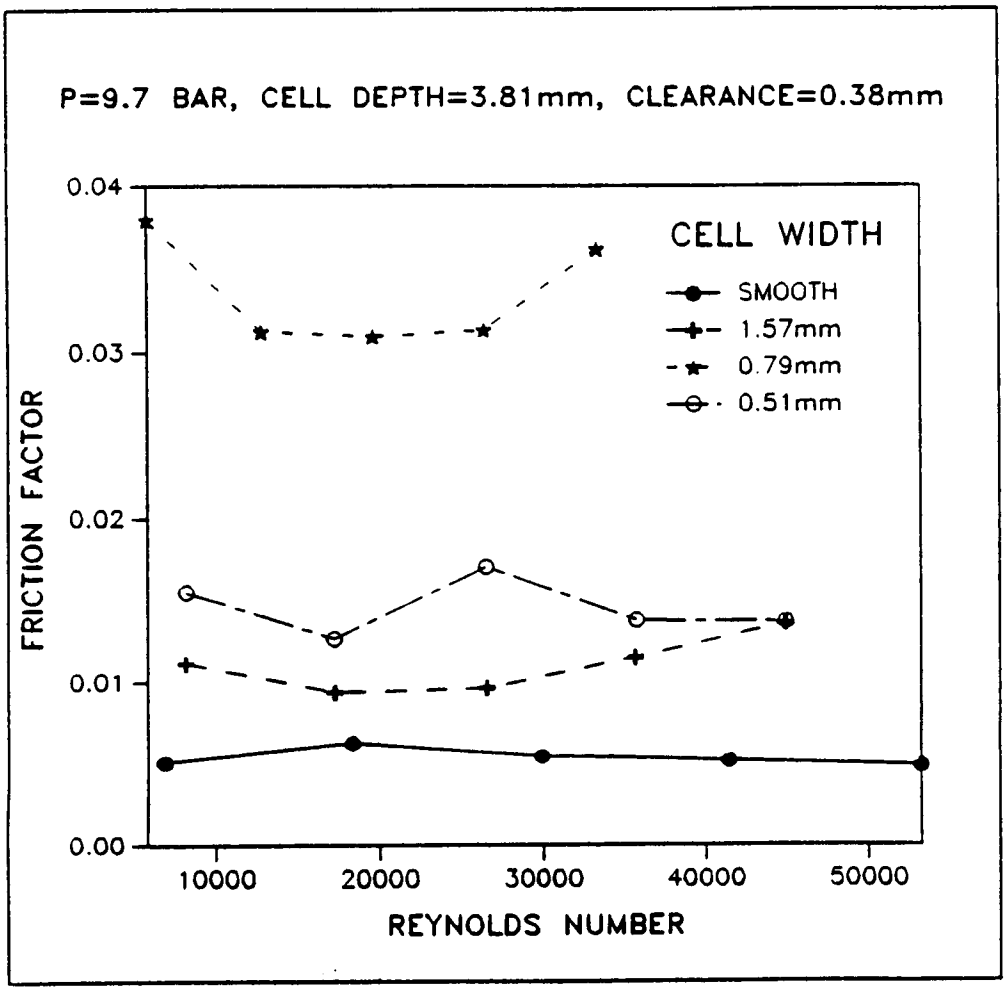

Figure 29. Friction factor versus Reynolds number for tests 2,5,11 and 17 of table 1 with inlet pressure 9.7 bar.

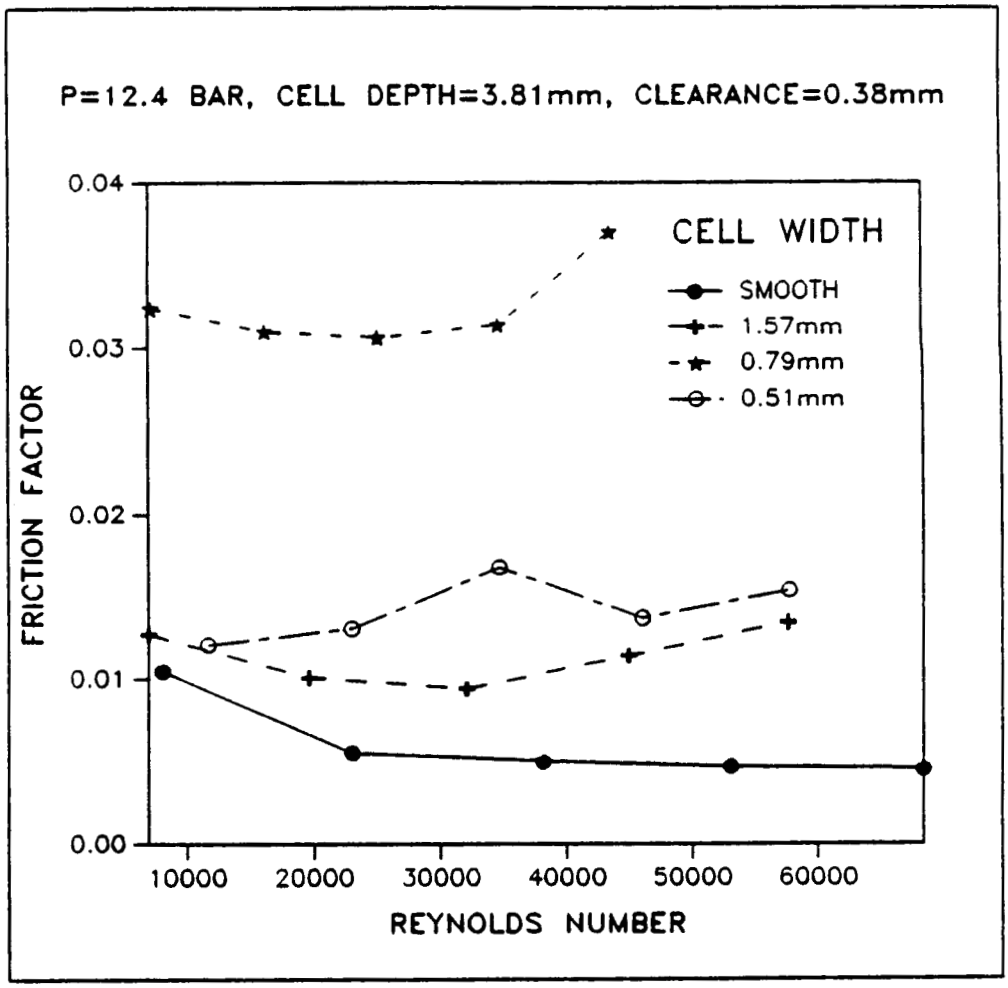

Figure 30. Friction factor versus Reynolds number for tests 2,5,11 and 17 of table 1 with inlet pressure 12.4 bar.

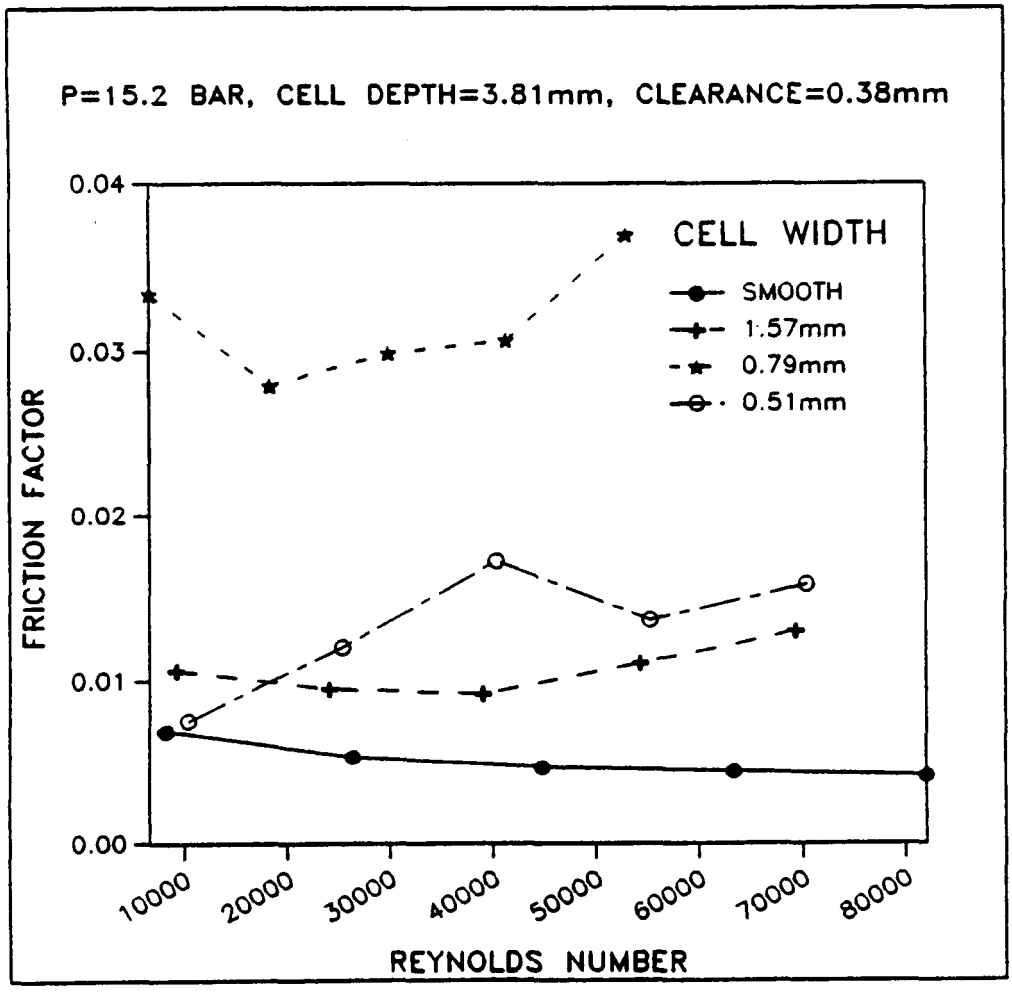

Figure 31. Friction factor versus Reynolds number for tests 2,5,11 and 17 of table 1 with inlet pressure 15.2 bar.

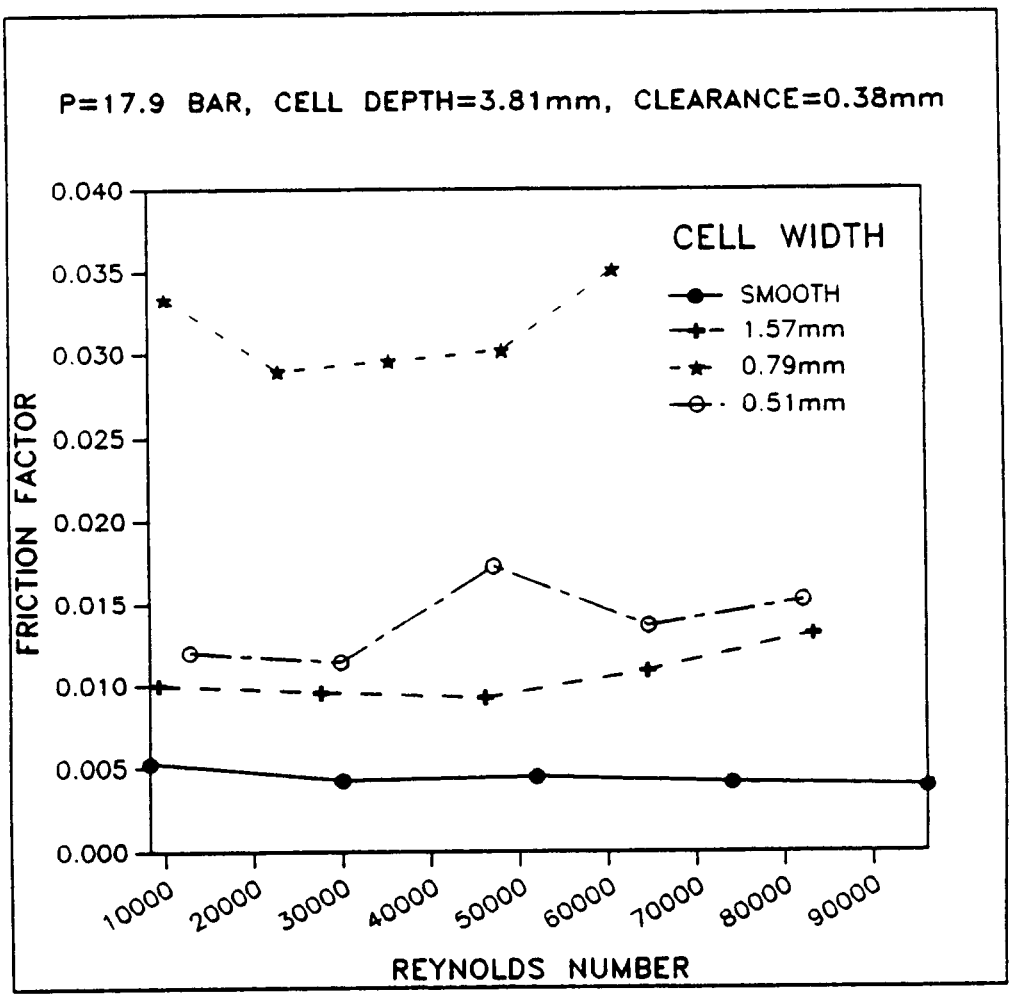

Figure 32. Friction factor versus Reynolds number for tests 2,5,11 and 17 of table 1 with inlet pressure 17.9 bar.

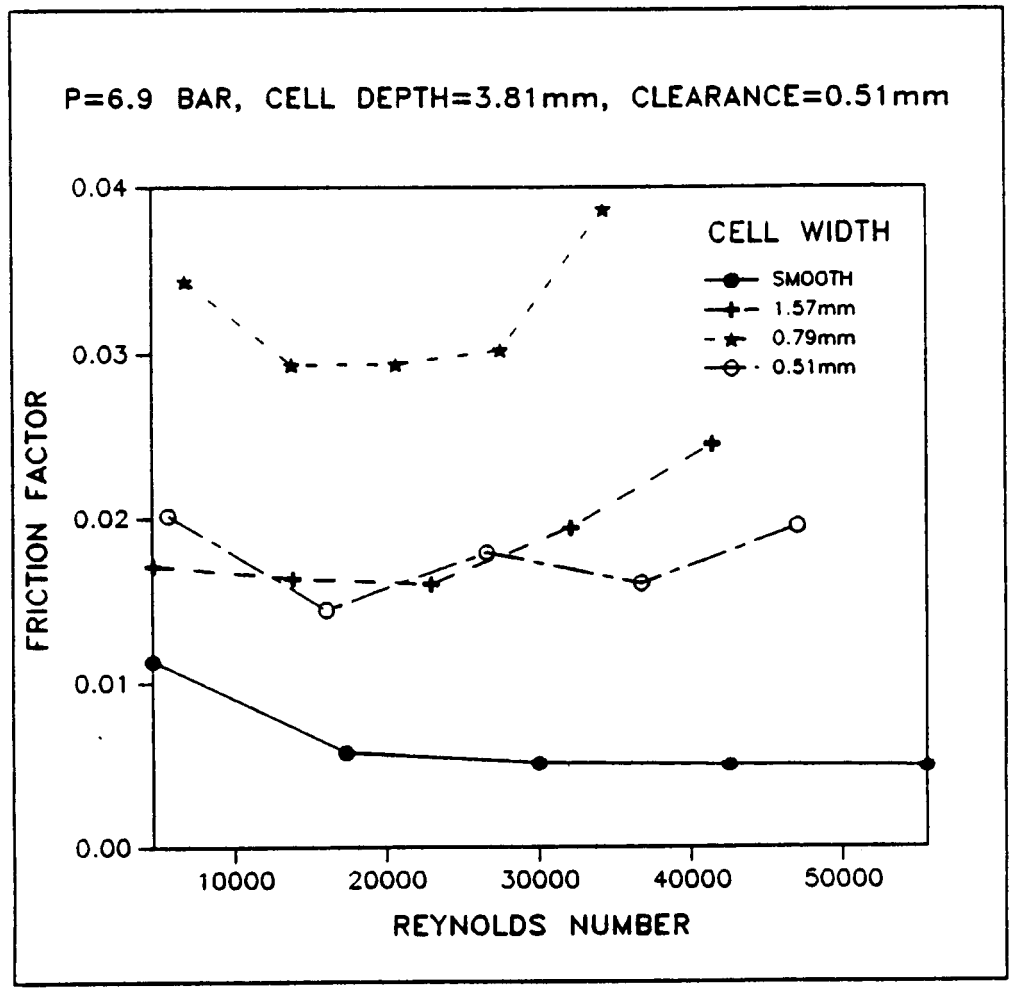

Figure 33. Friction factor versus Reynolds number for tests 3,6,12 and 18 of table 1 with inlet pressure 6.9 bar.

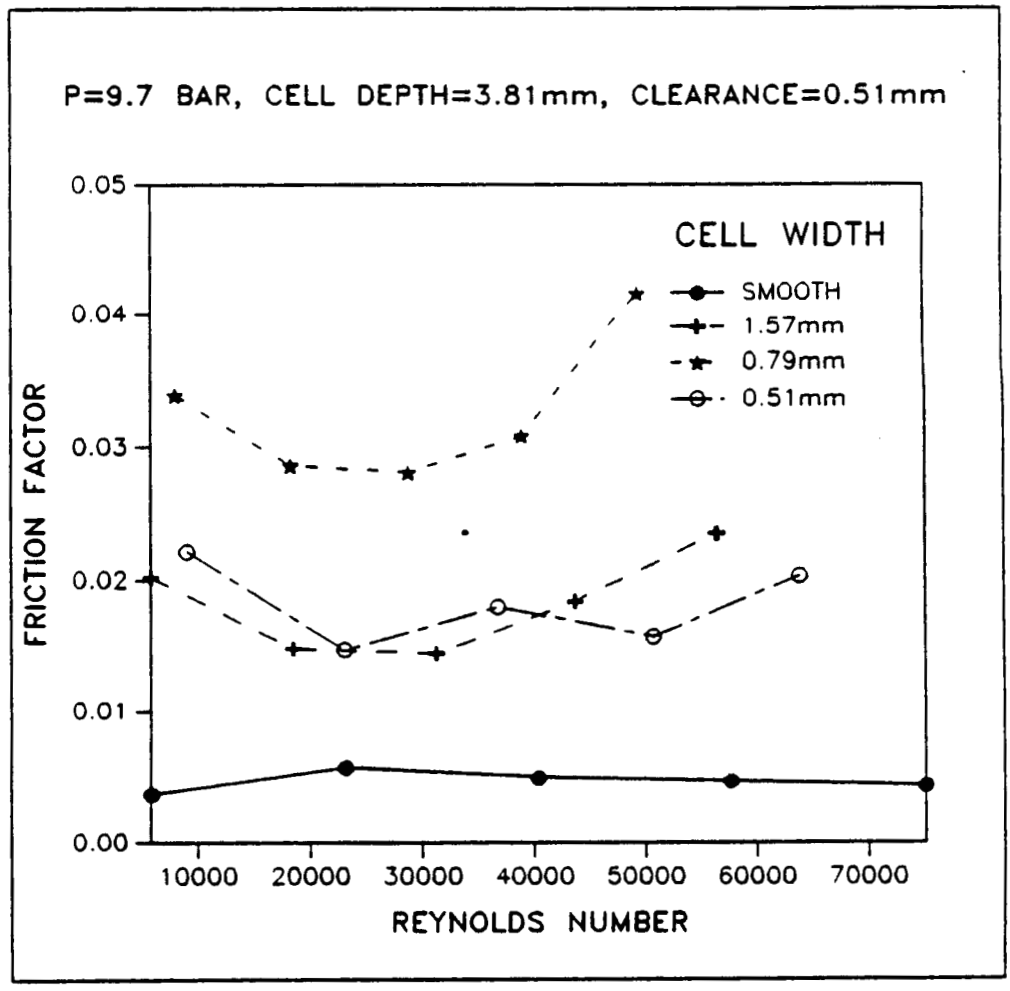

Figure 34. Friction factor versus Reynolds number for tests 3,6,12 and 18 of table 1 with inlet pressure 9.7 bar.

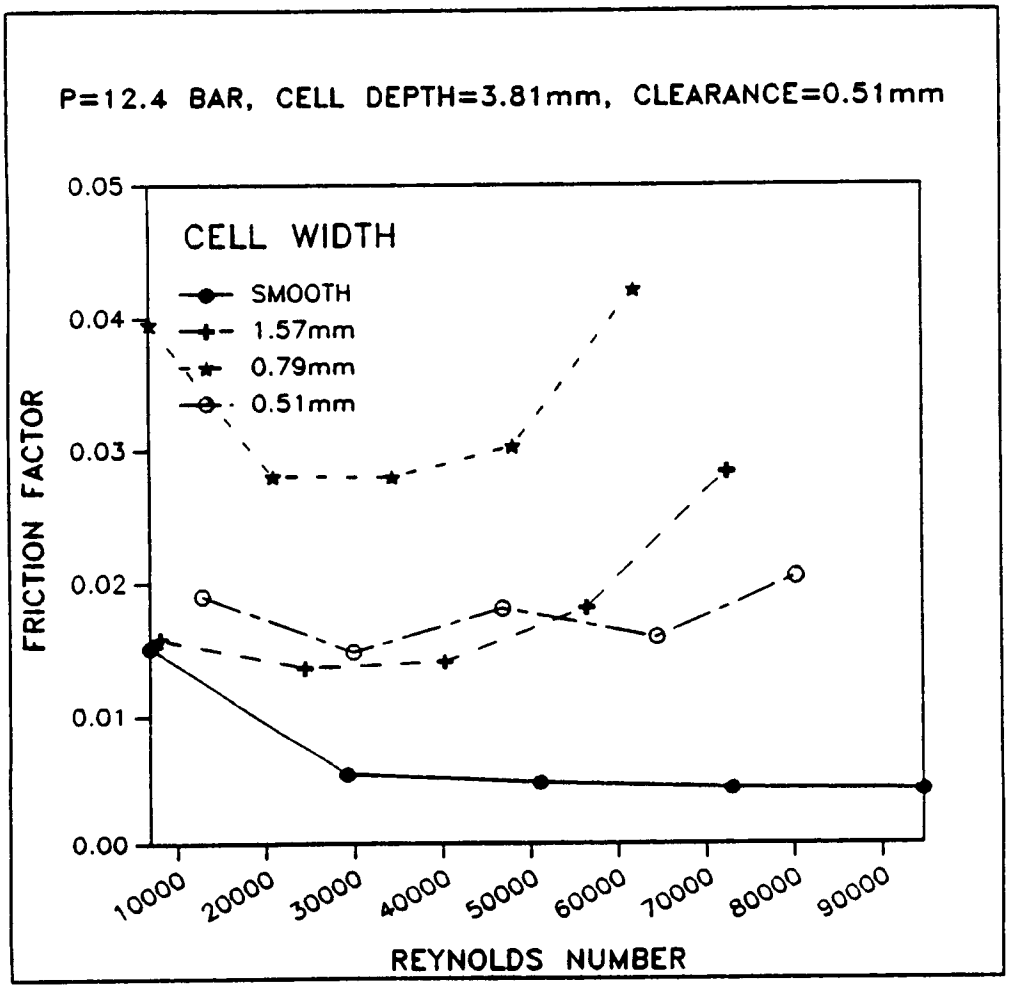

Figure 35. Friction factor versus Reynolds number for tests 3,6,12 and 18 of table 1 with inlet pressure 12.4 bar.

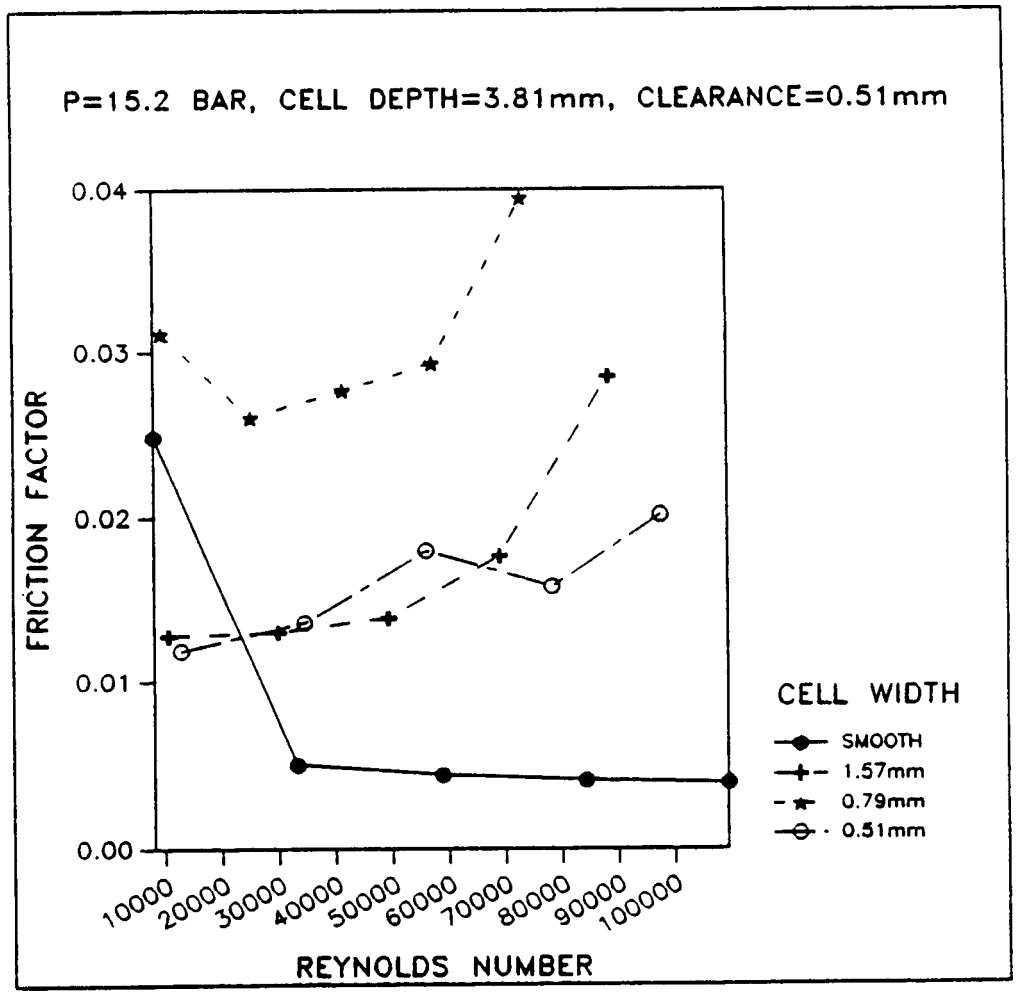

Figure 36. Friction factor versus Reynolds number for tests 3,6,12 and 18 of table 1 with inlet pressure 15.2 bar.

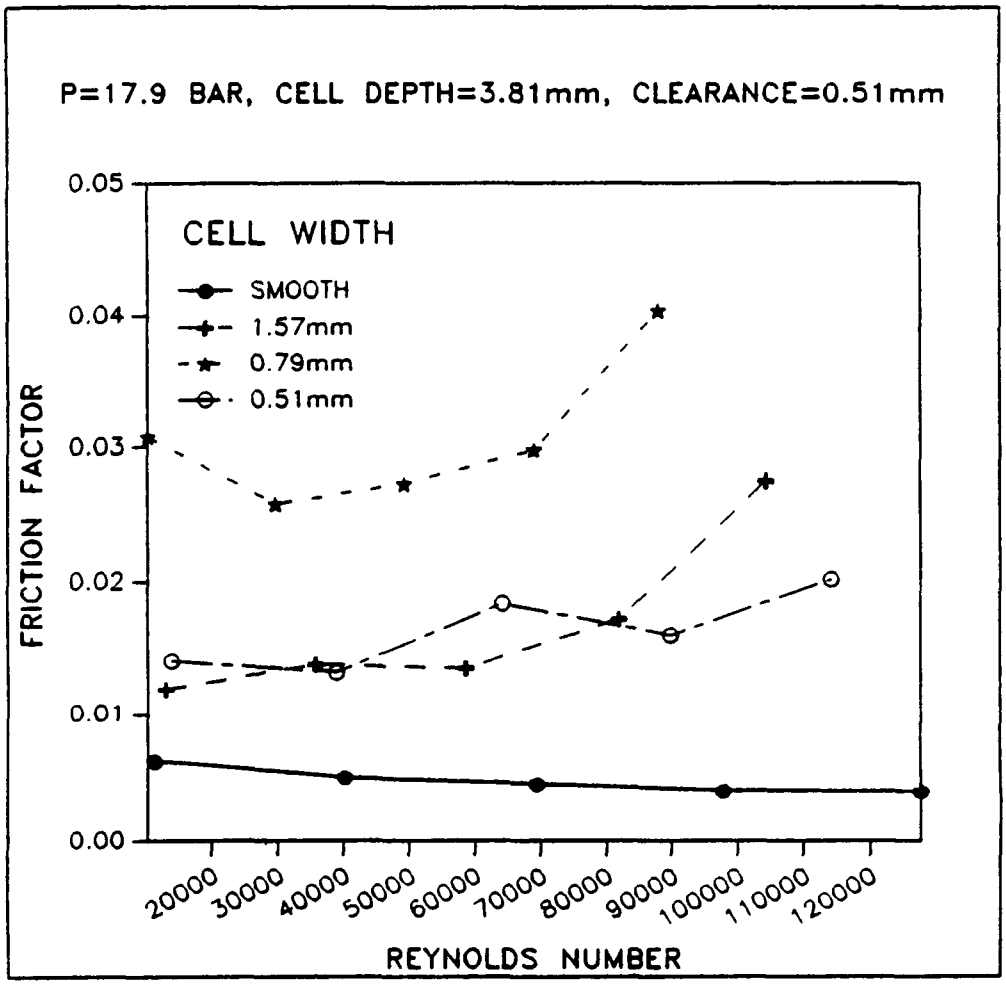

Figure 37. Friction factor versus Reynolds number for tests 3,6,12 and 18 of table 1 with inlet pressure 17.9 bar.

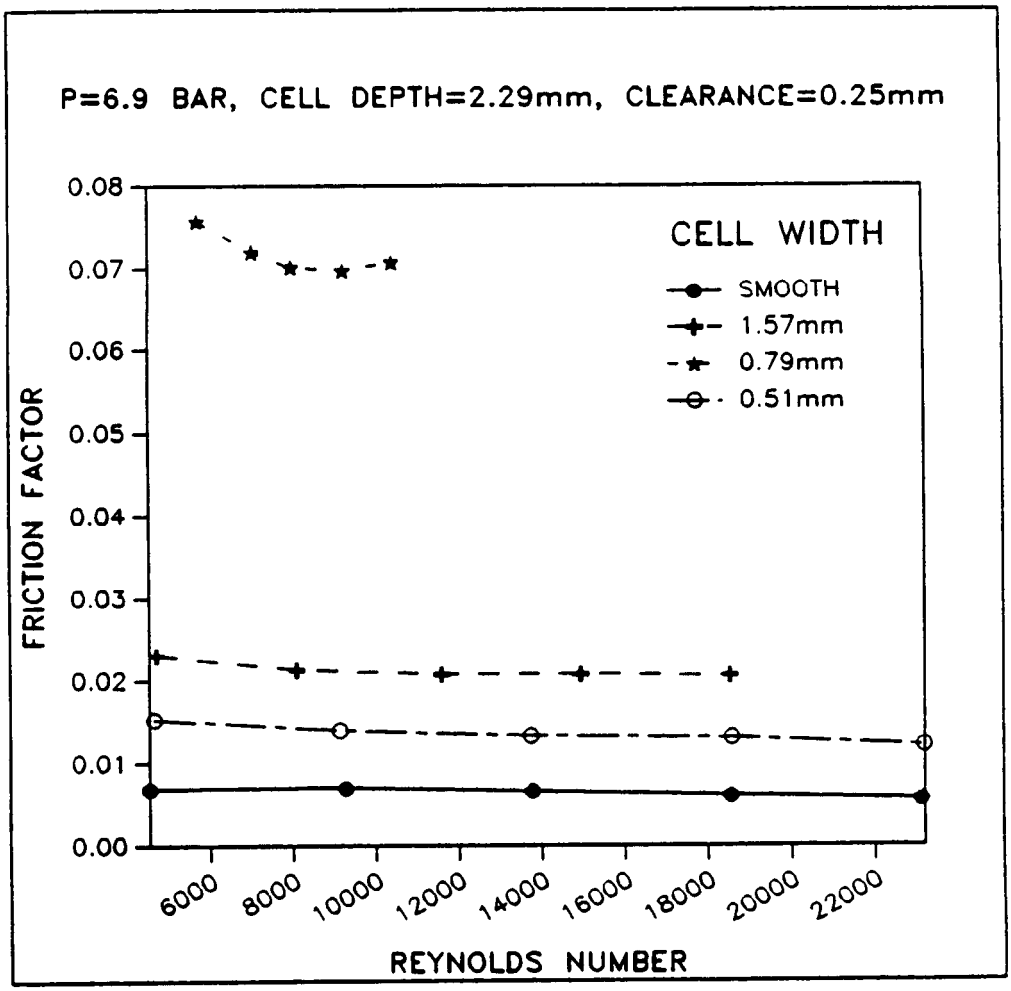

Figure 38. Friction factor versus Reynolds number for tests 1,7,13 and 19 of table 1 with inlet pressure 6.9 bar.

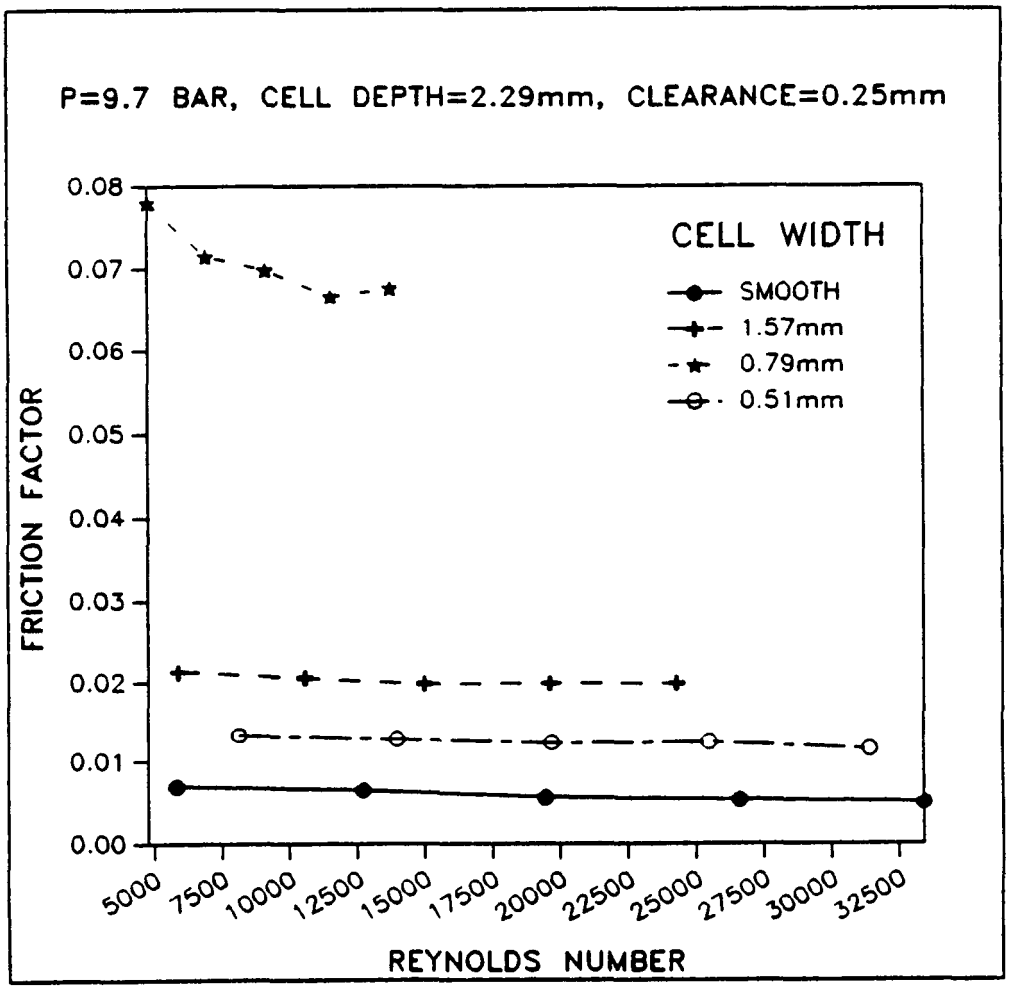

Figure 39. Friction factor versus Reynolds number for tests 1,7,13 and 19 of table 1 with inlet pressure 9.7 bar.

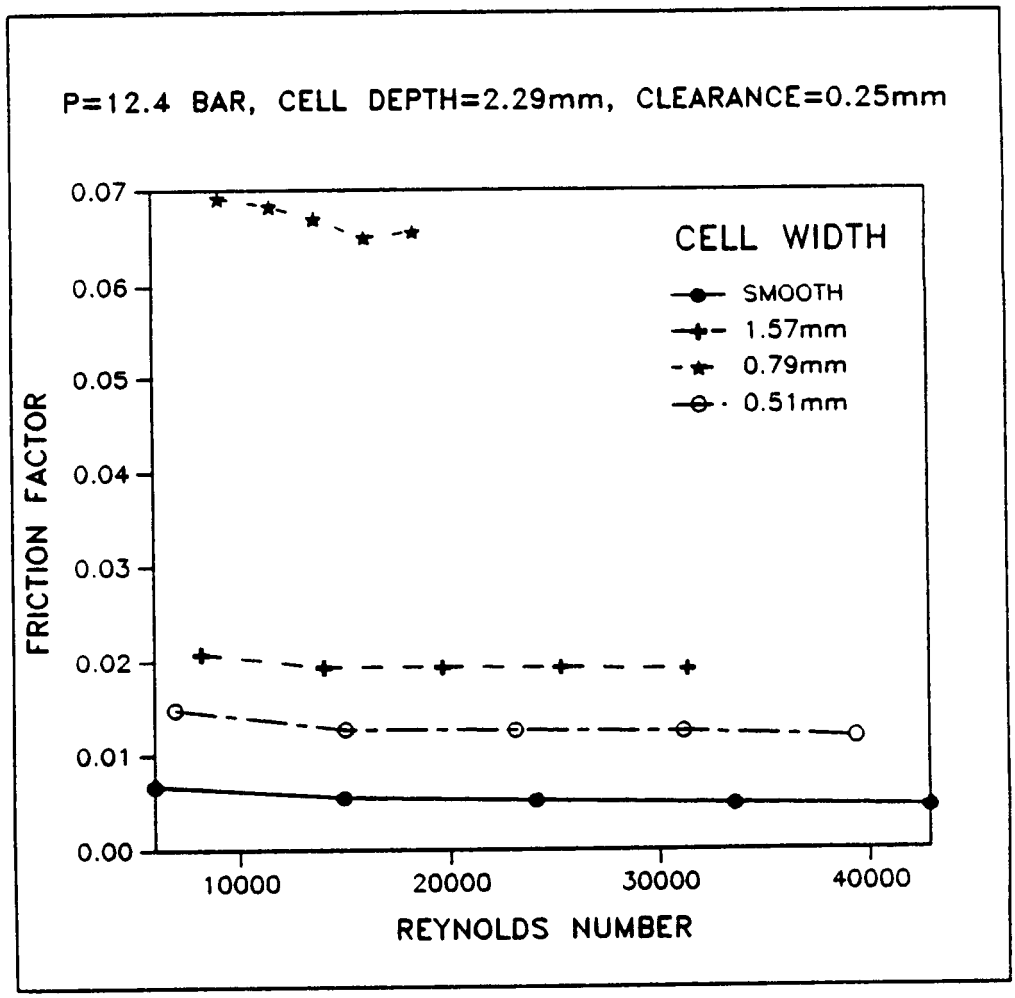

Figure 40. Friction factor versus Reynolds number for tests 1,7,13 and 19 of table 1 with inlet pressure 12.4 bar.

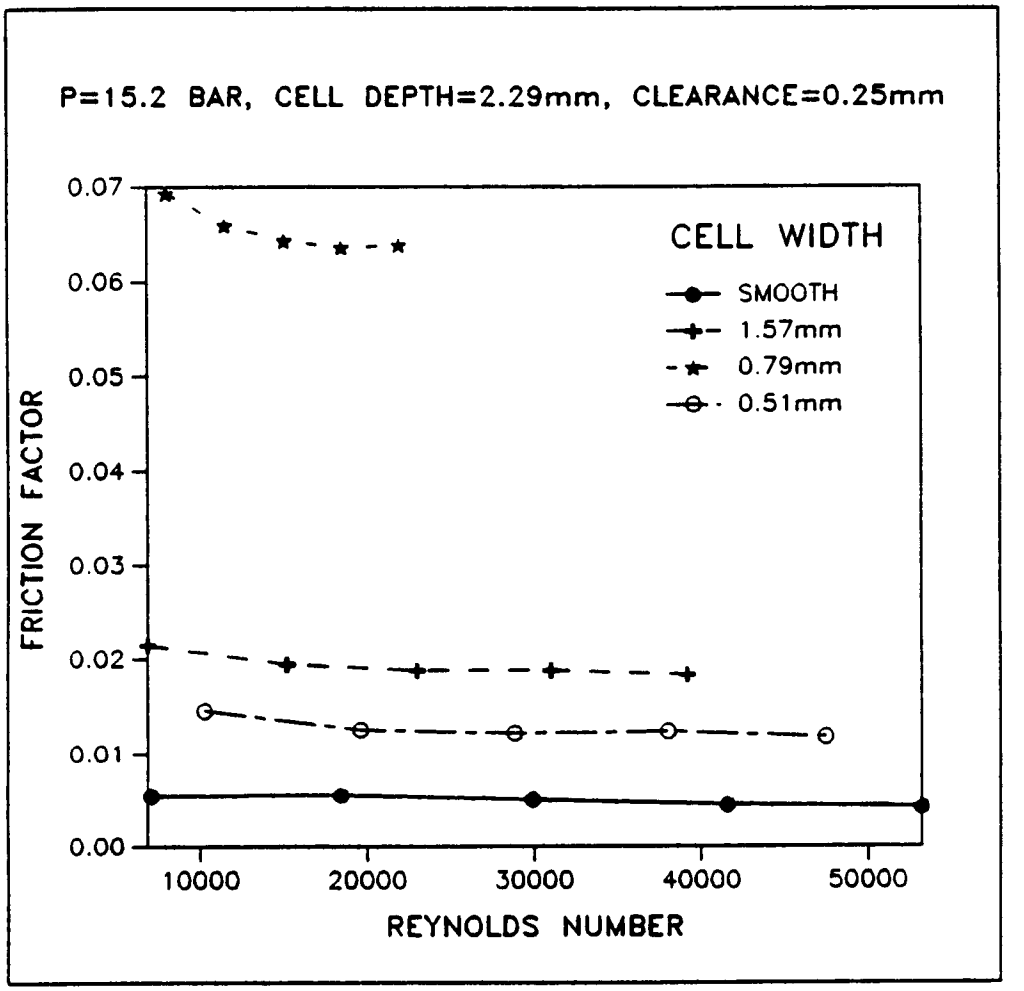

Figure 41. Friction factor versus Reynolds number for tests 1,7,13 and 19 of table 1 with inlet pressure 15.2 bar.

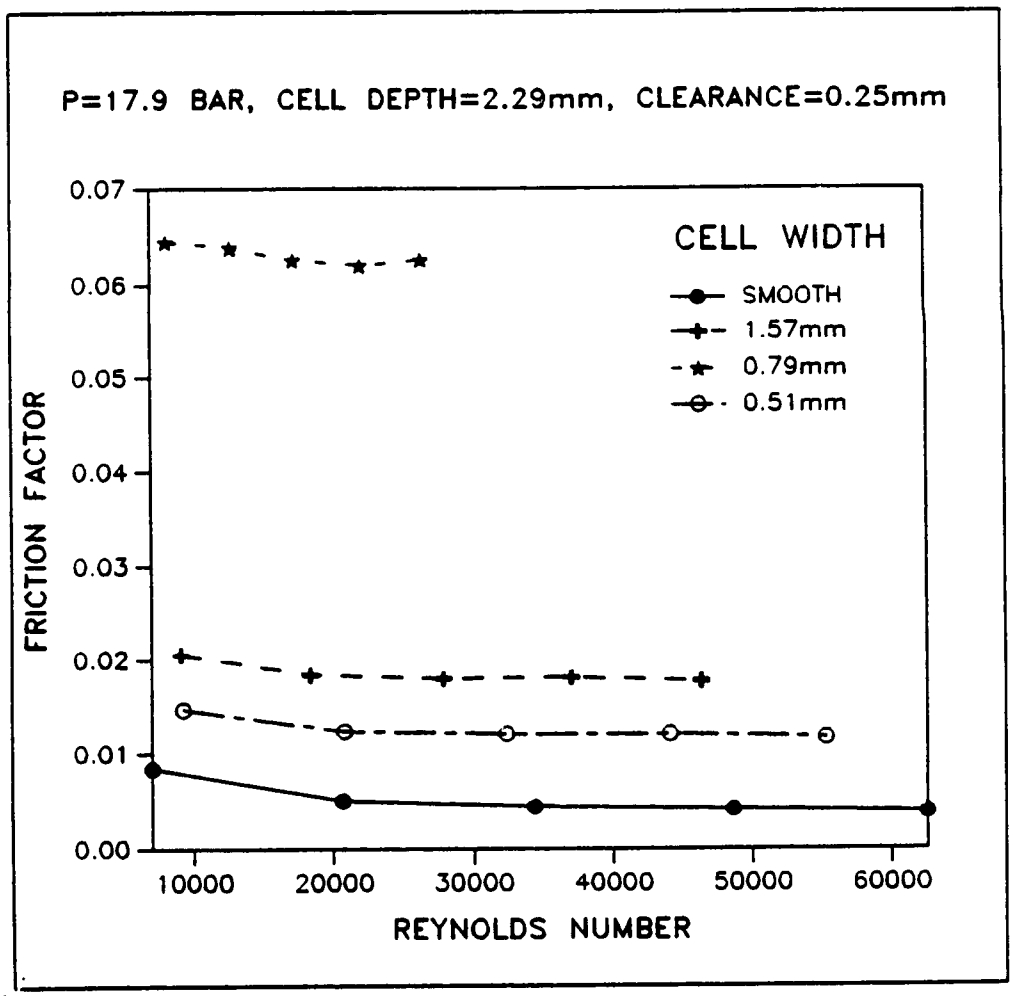

Figure 42. Friction factor versus Reynolds number for tests 1,7,13 and 19 of table 1 with inlet pressure 17.9 bar.

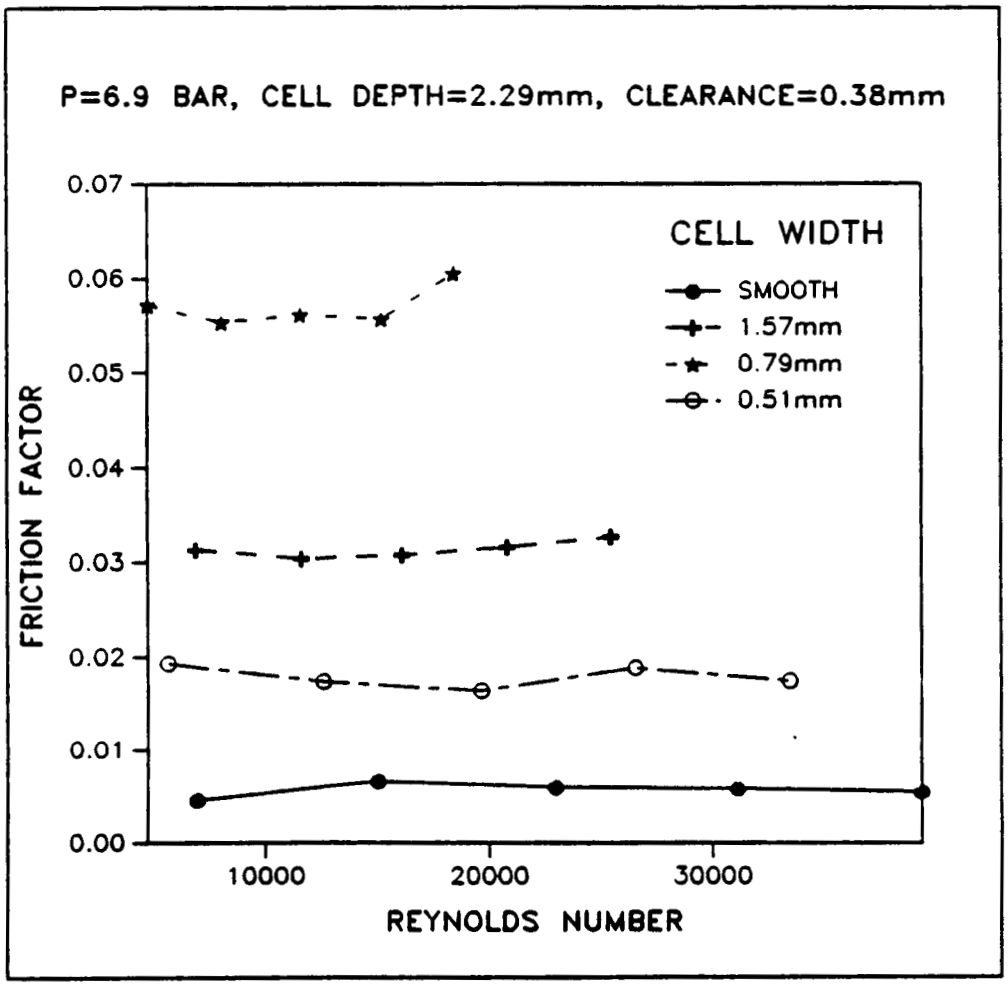

Figure 43. Friction factor versus Reynolds number for tests 2,8,14 and 20 of table 1 with inlet pressure 6.9 bar.

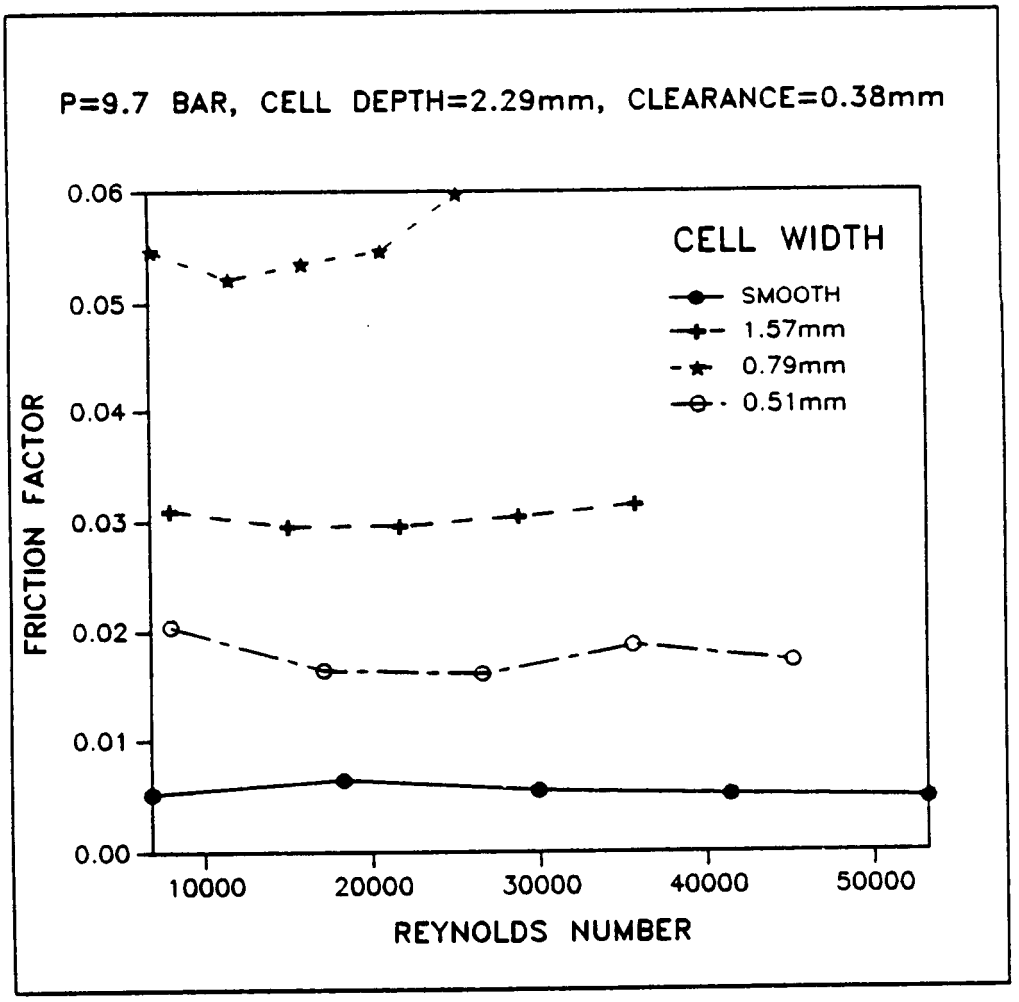

Figure 44. Friction factor versus Reynolds number for tests 2,8,14 and 20 of table 1 with inlet pressure 9.7 bar.

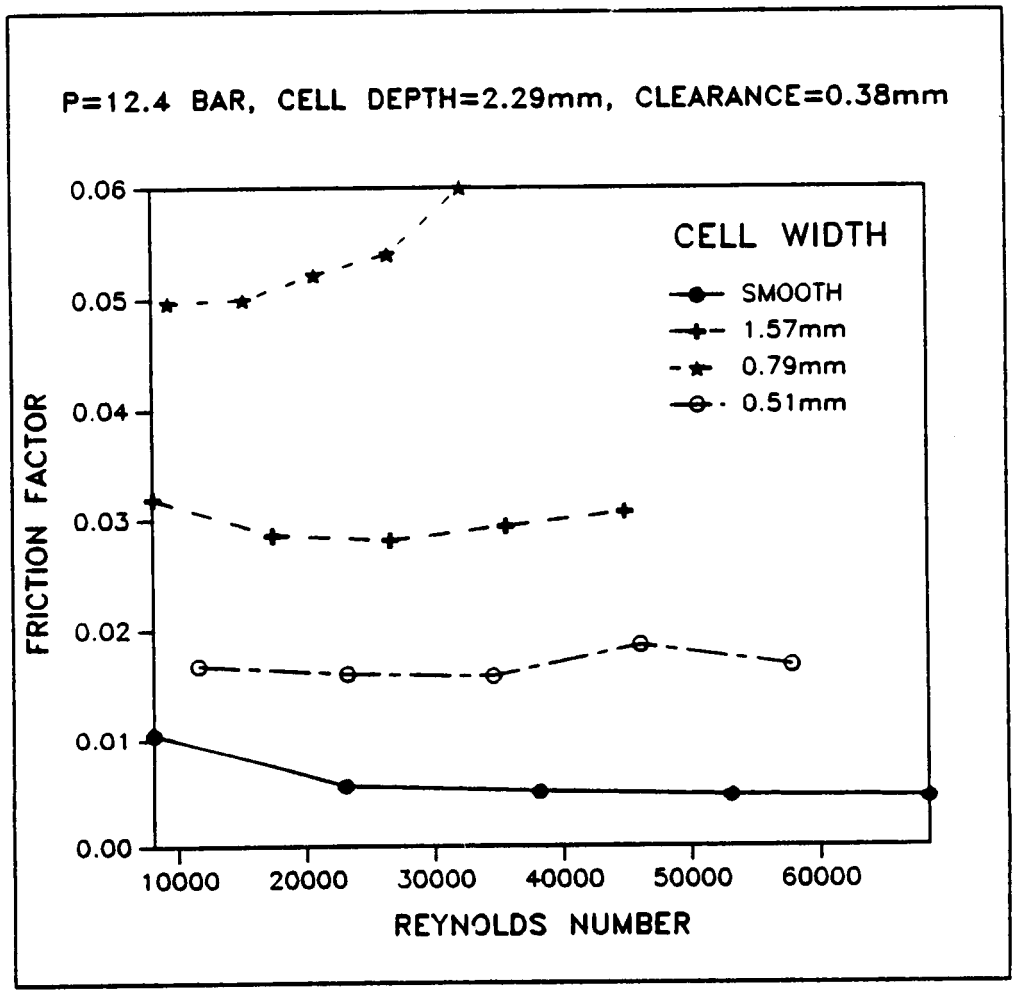

Figure 45. Friction factor versus Reynolds number for tests 2,8,14 and 20 of table 1 with inlet pressure 12.4 bar.

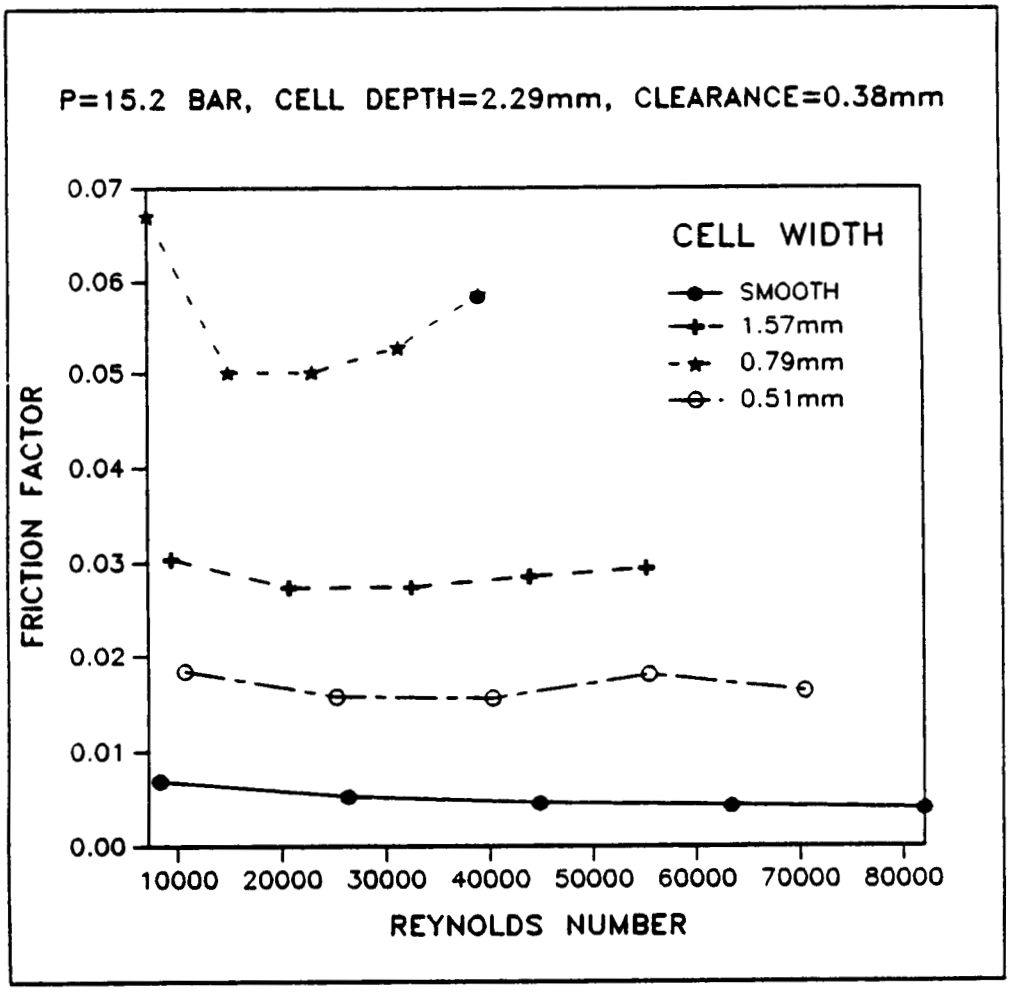

Figure 46. Friction factor versus Reynolds number for tests 2,8,14 and 20 of table 1 with inlet pressure 15.2 bar.

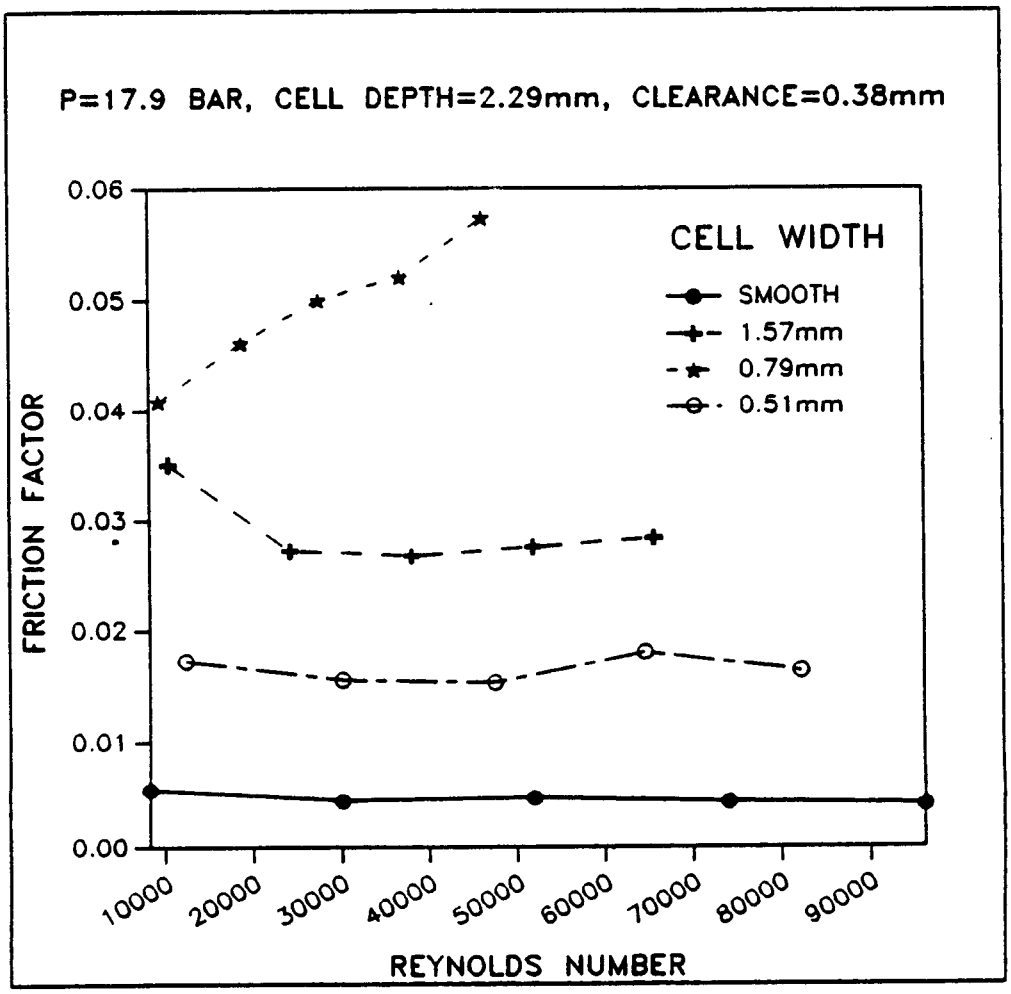

Figure 47. Friction factor versus Reynolds number for tests 2,8,14 and 20 of table 1 with inlet pressure 17.9 bar.

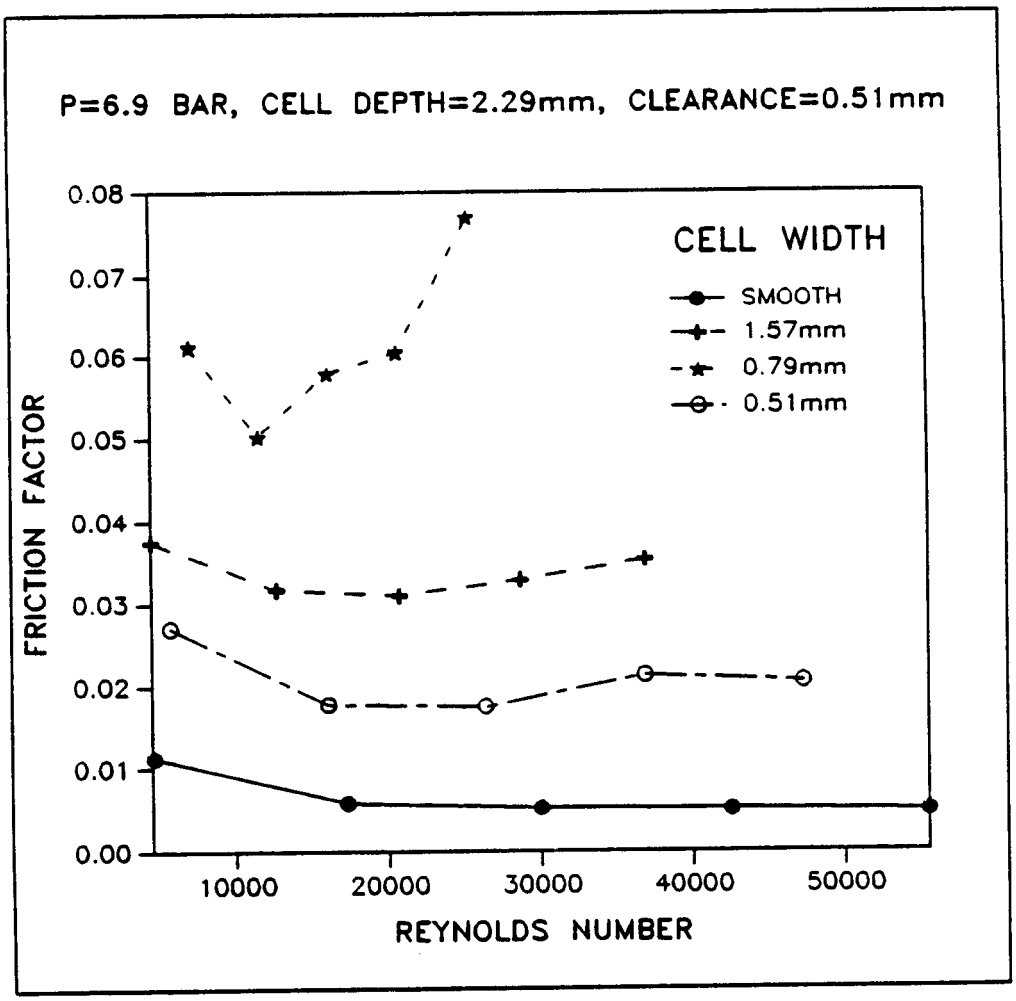

Figure 48. Friction factor versus Reynolds number for tests 3,9,15 and 21 of table 1 with inlet pressure 6.9 bar.

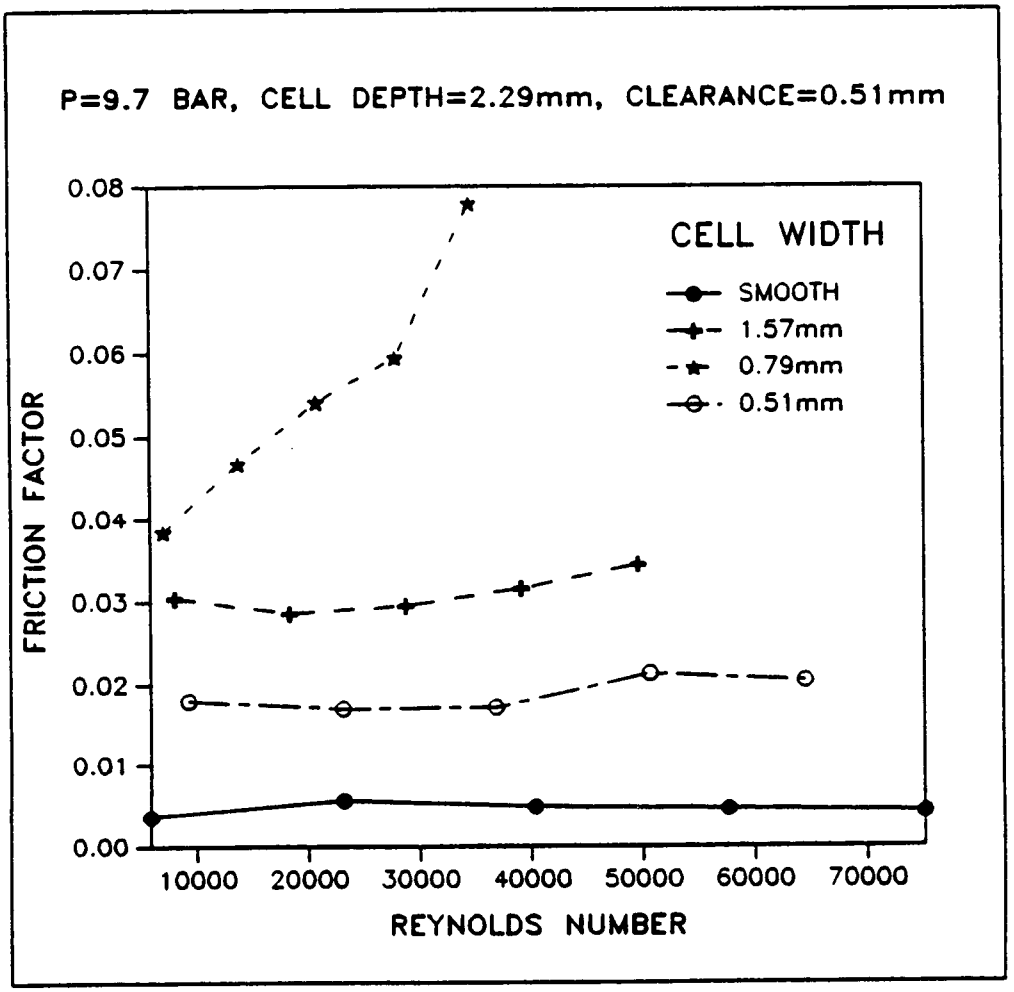

Figure 49. Friction factor versus Reynolds number for tests 3,9,15 and 21 of table 1 with inlet pressure 9.7 bar.

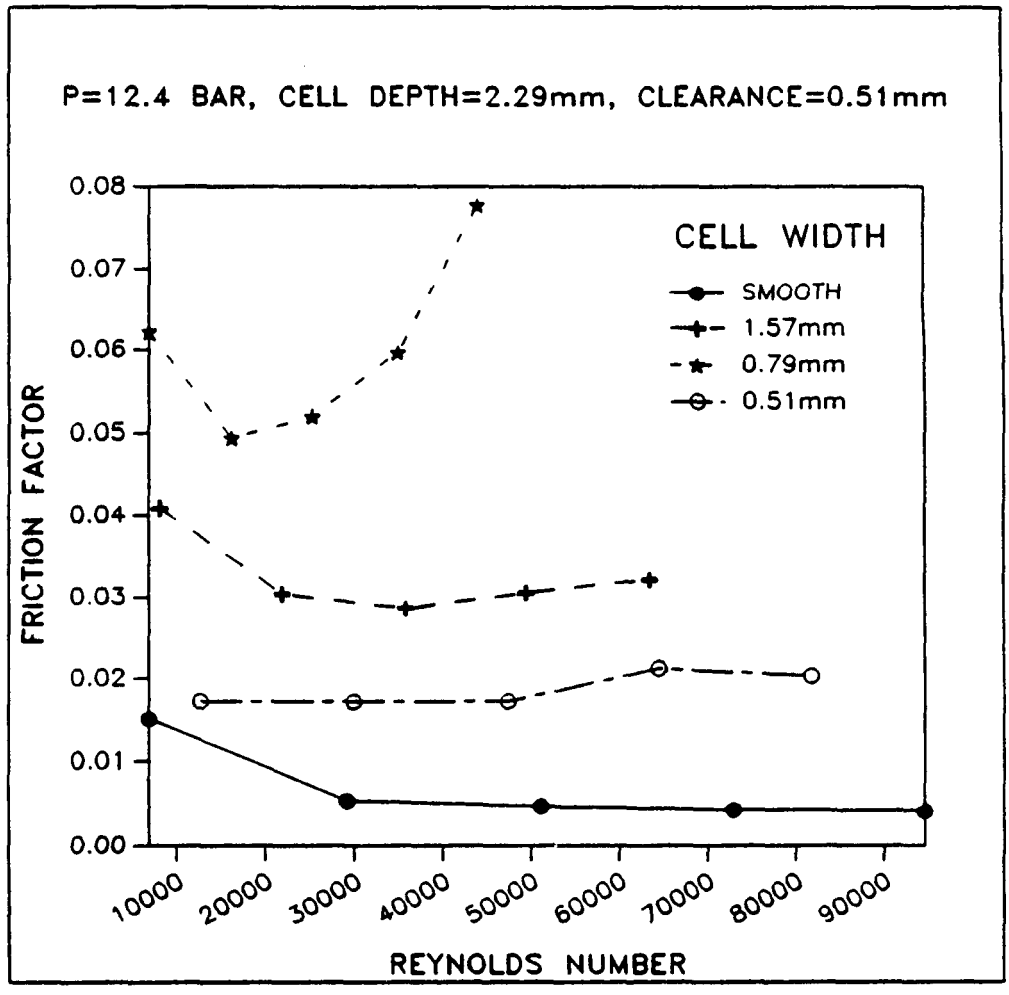

Figure 50. Friction factor versus Reynolds number for tests 3,9,15 and 21 of table 1 with inlet pressure 12.4 bar.

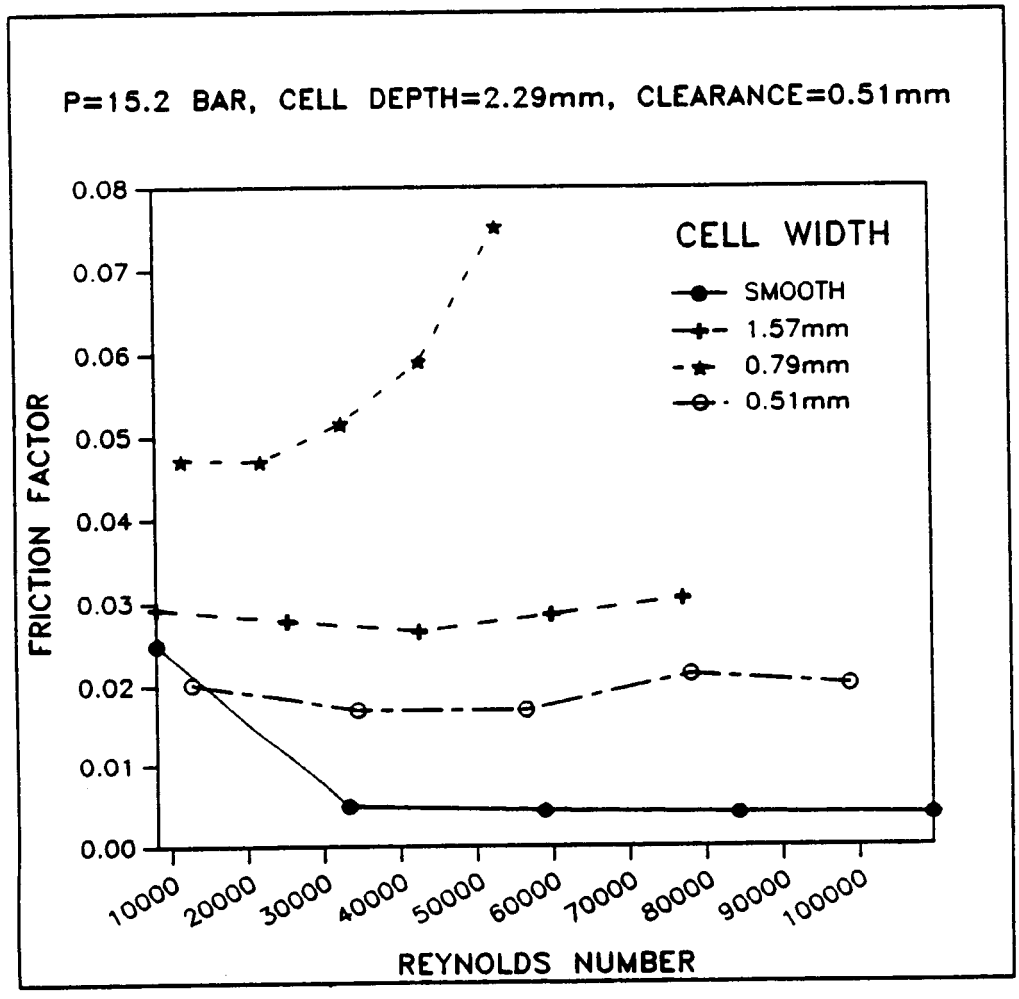

Figure 51. Friction factor versus Reynolds number for tests 3,9,15 and 21 of table 1 with inlet pressure 15.2 bar.

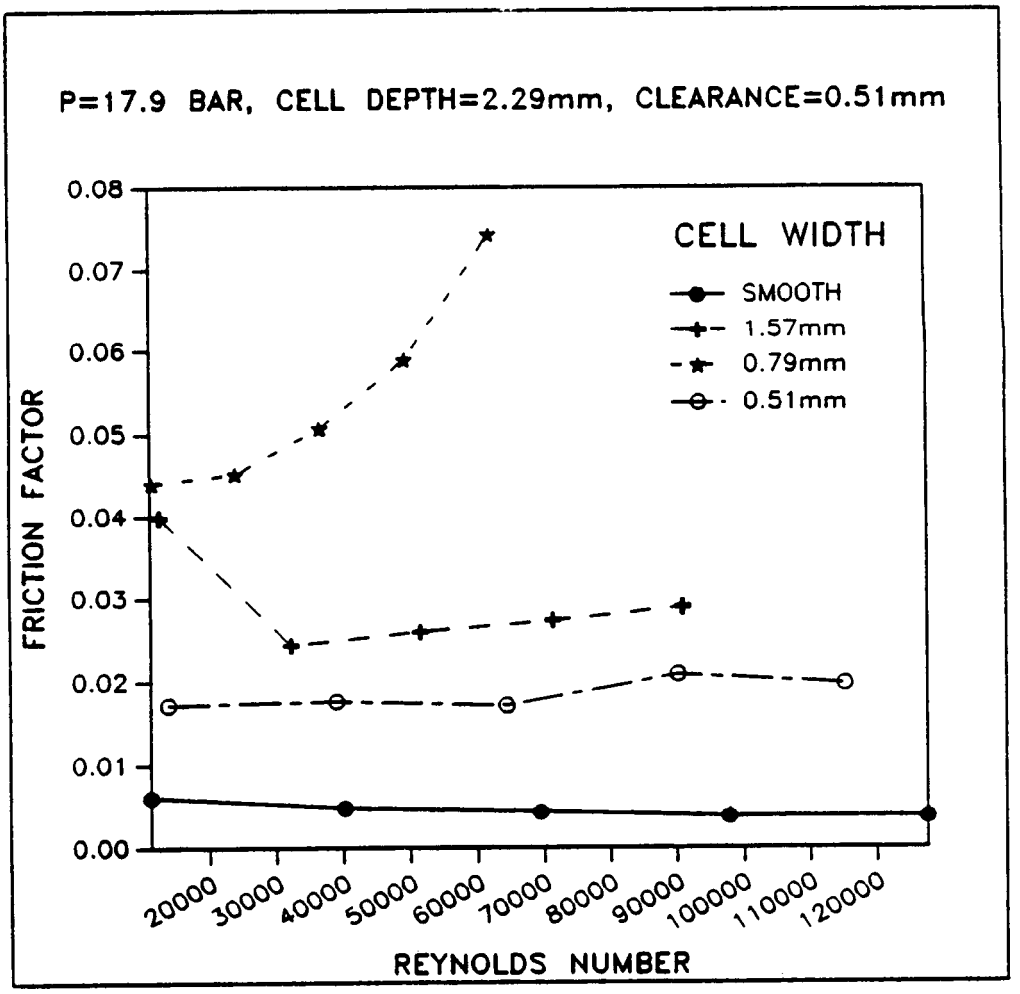

Figure 52. Friction factor versus Reynolds number for tests 3,9,15 and 21 of table 1 with inlet pressure 17.9 bar.

APPENDIX B

FRICTION FACTOR VERSUS REYNOLDS NUMBER FOR HONEYCOMB SURFACES WITH THREE CLEARANCES

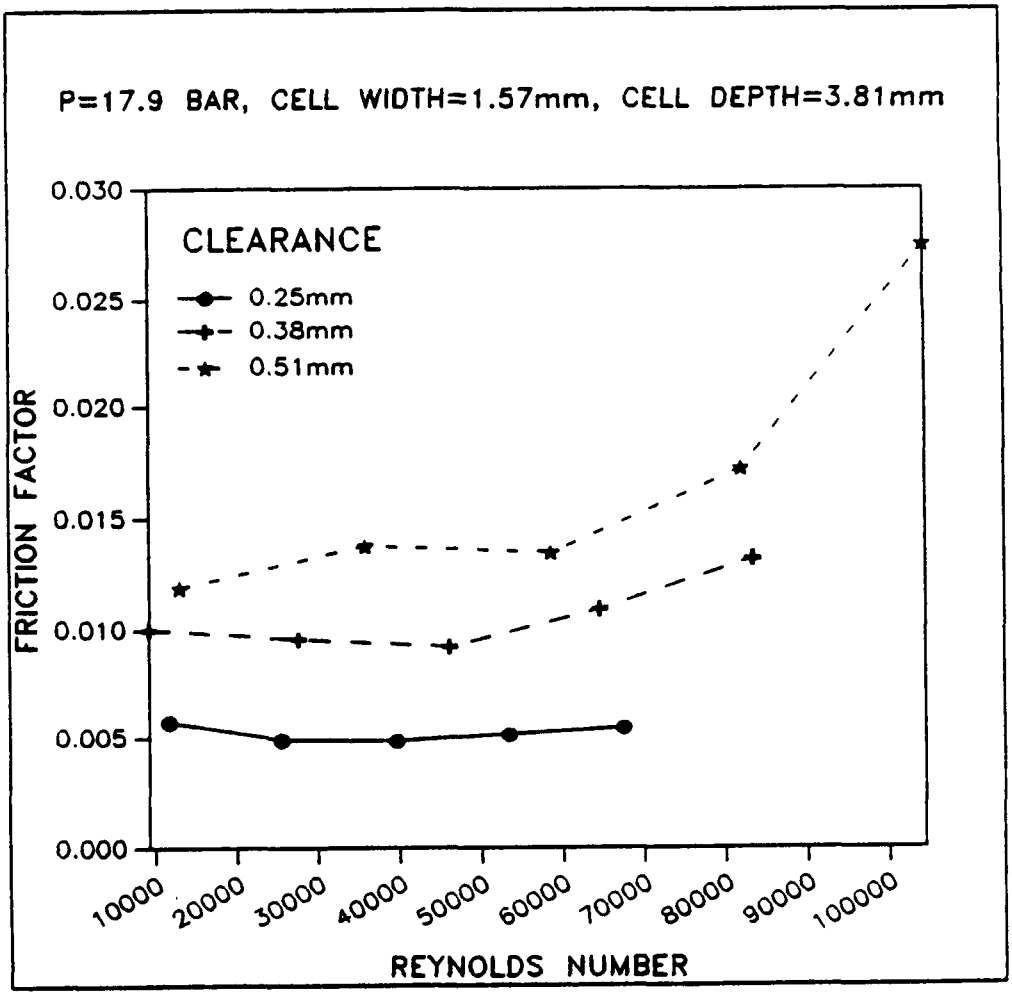

Figure 53. Friction factor versus Reynolds number for tests 4,5 and 6 of table 1 with inlet pressure 17.9 bar.

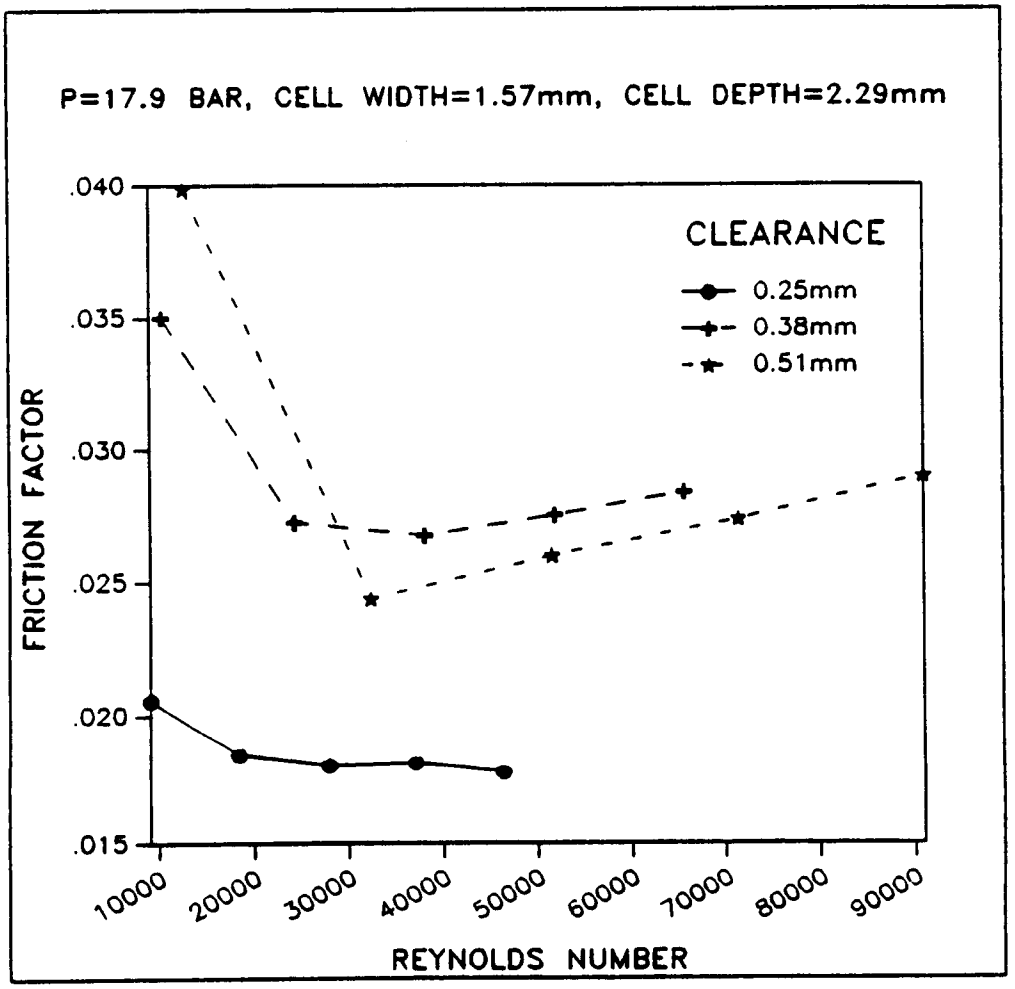

Figure 54. Friction factor versus Reynolds number for tests 7,8 and 9 of table 1 with inlet pressure 17.9 bar.

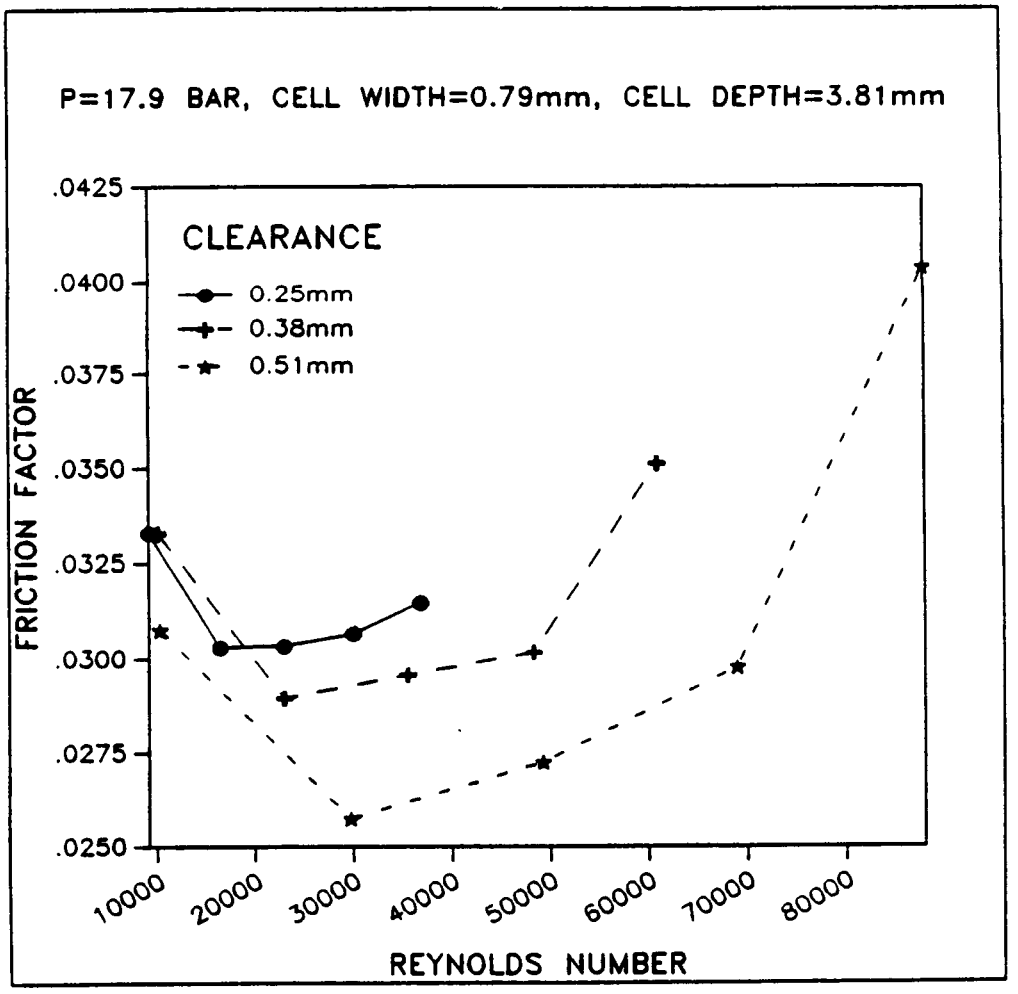

Figure 55. Friction factor versus Reynolds number for tests 10,11 and 12 of table 1 with inlet pressure 17.9 bar.

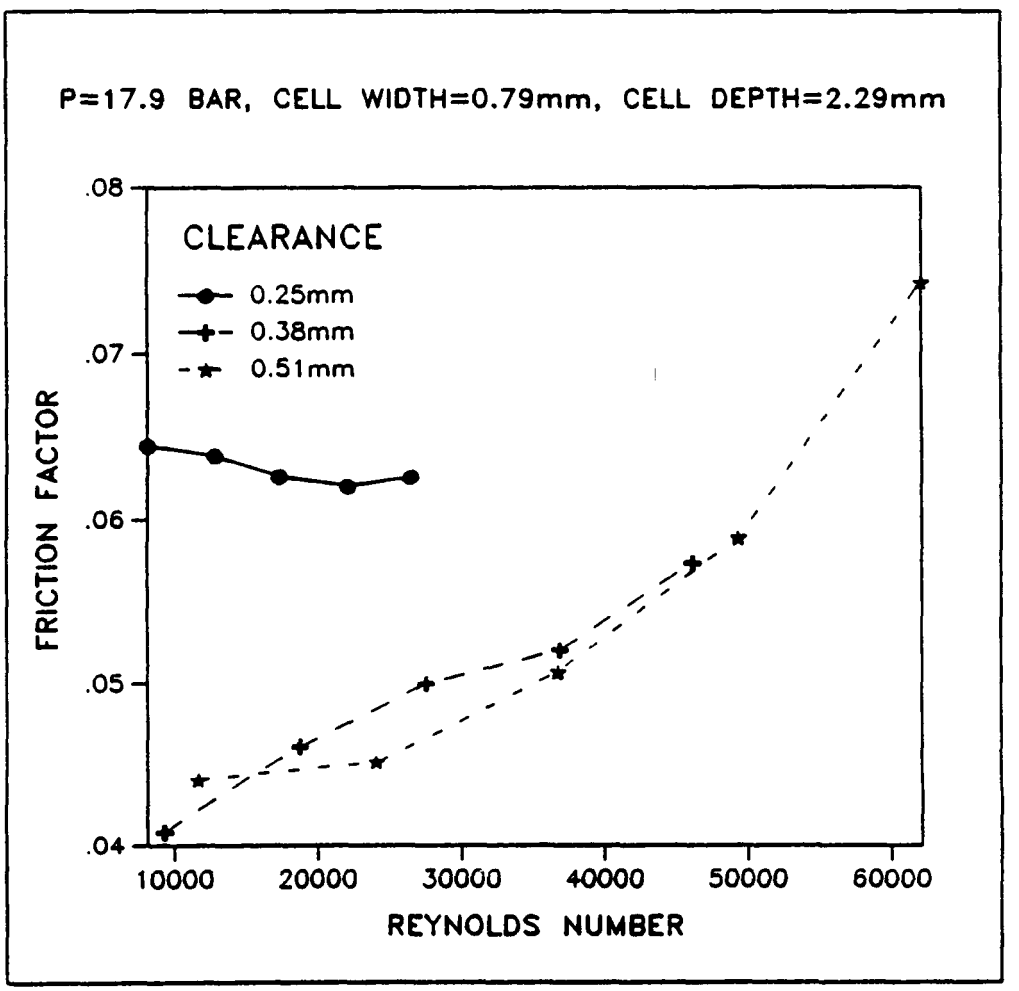

Figure 56. Friction factor versus Reynolds number for tests 13,14 and 15 of table 1 with inlet pressure 17.9 bar.

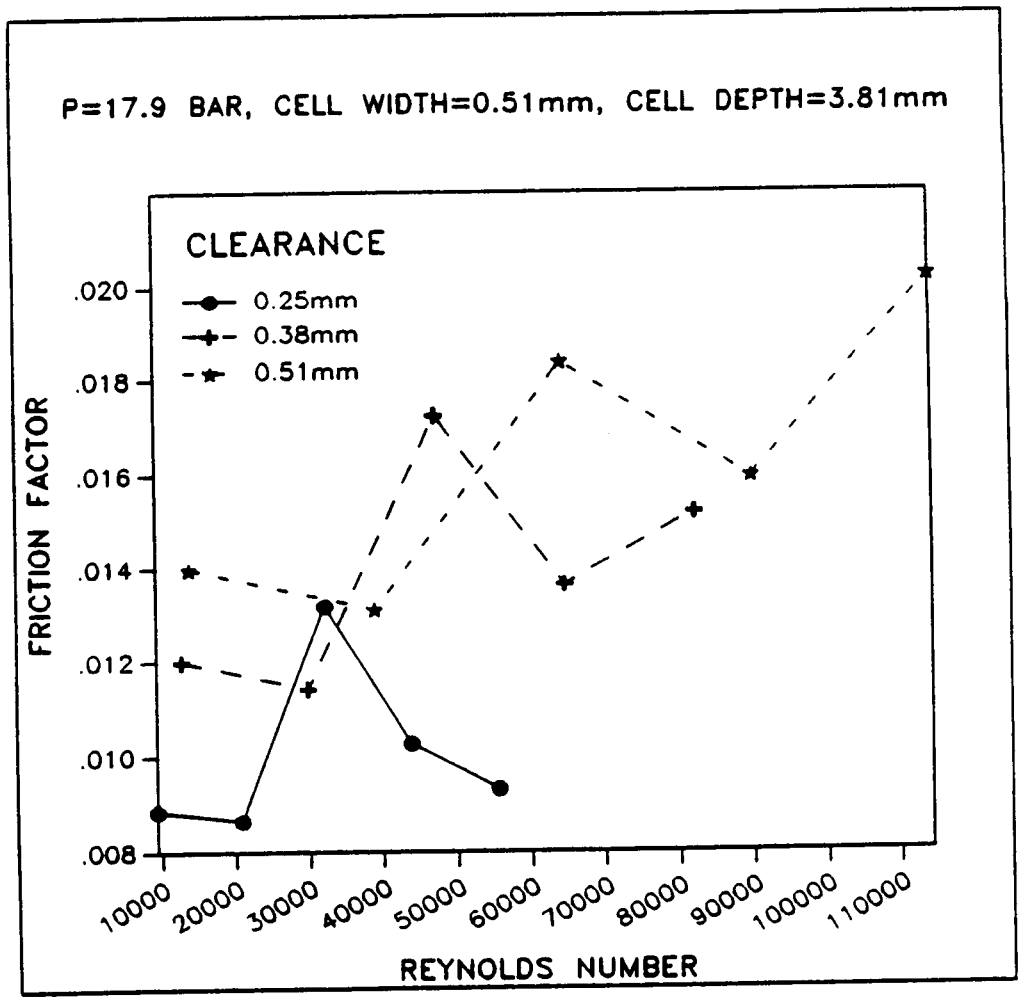

Figure 57. Friction factor versus Reynolds number for tests 16,17 and 18 of table 1 with inlet pressure 17.9 bar.

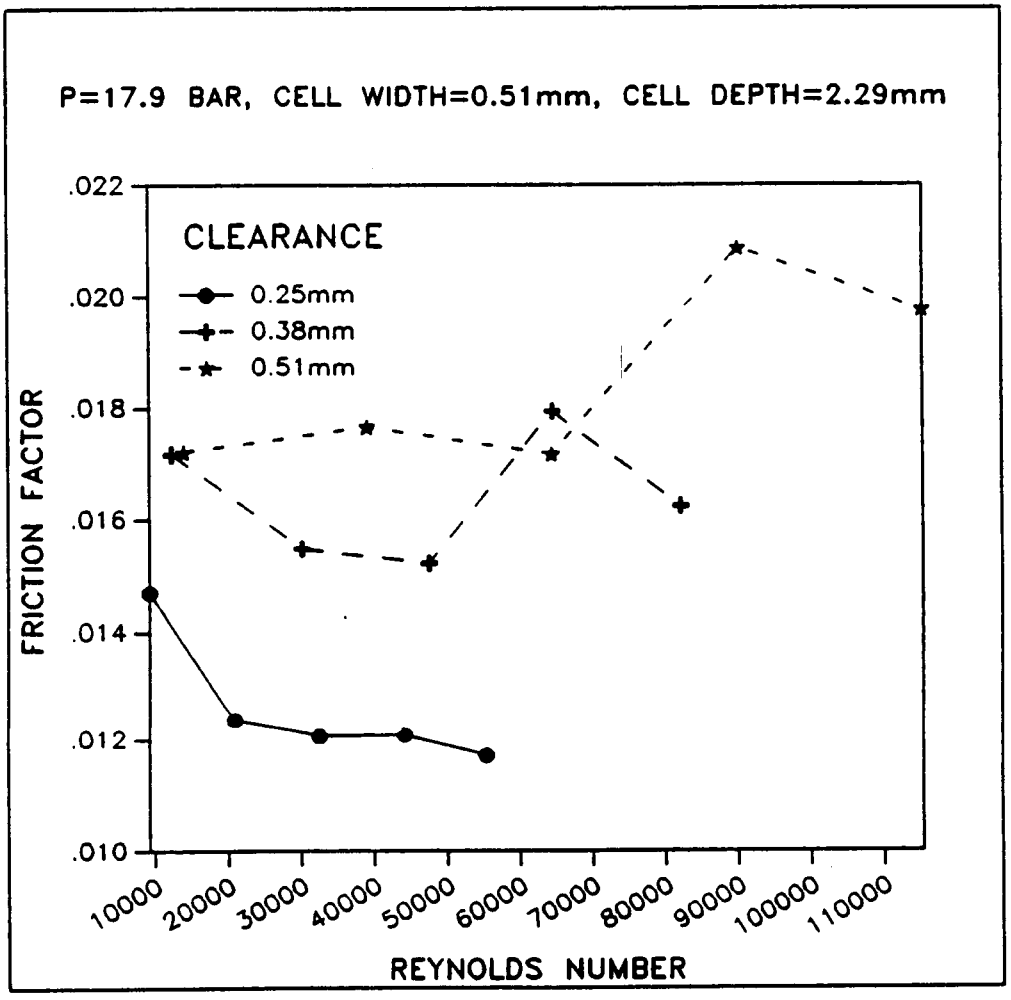

Figure 58. Friction factor versus Reynolds number for tests 19,20 and 21 of table 1 with inlet pressure 17.9 bar.

APPENDIX C

FRICTION FACTOR VERSUS REYNOLDS NUMBER FOR HONEYCOMB SURFACES WITH TWO CELL DEPTHS

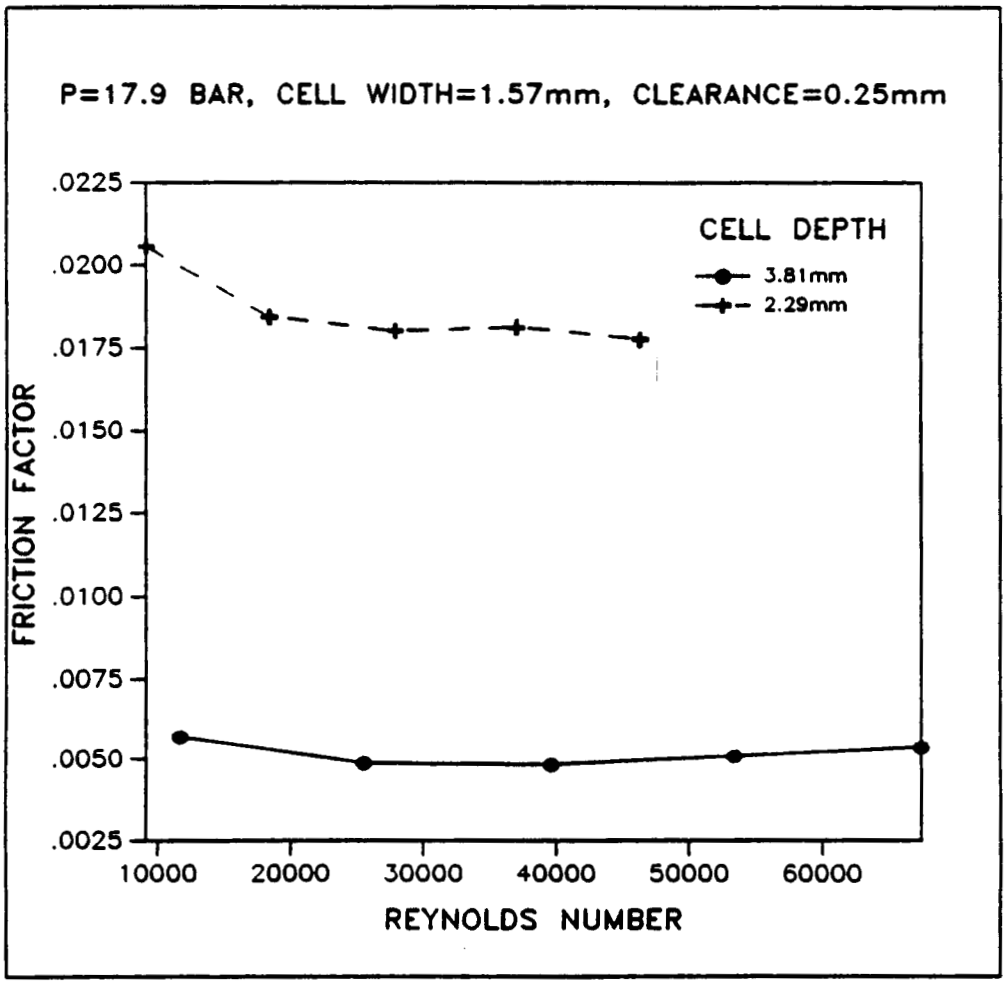

Figure 59. Friction factor versus Reynolds number for tests 4 and 7 of table 1 with inlet pressure 17.9 bar.

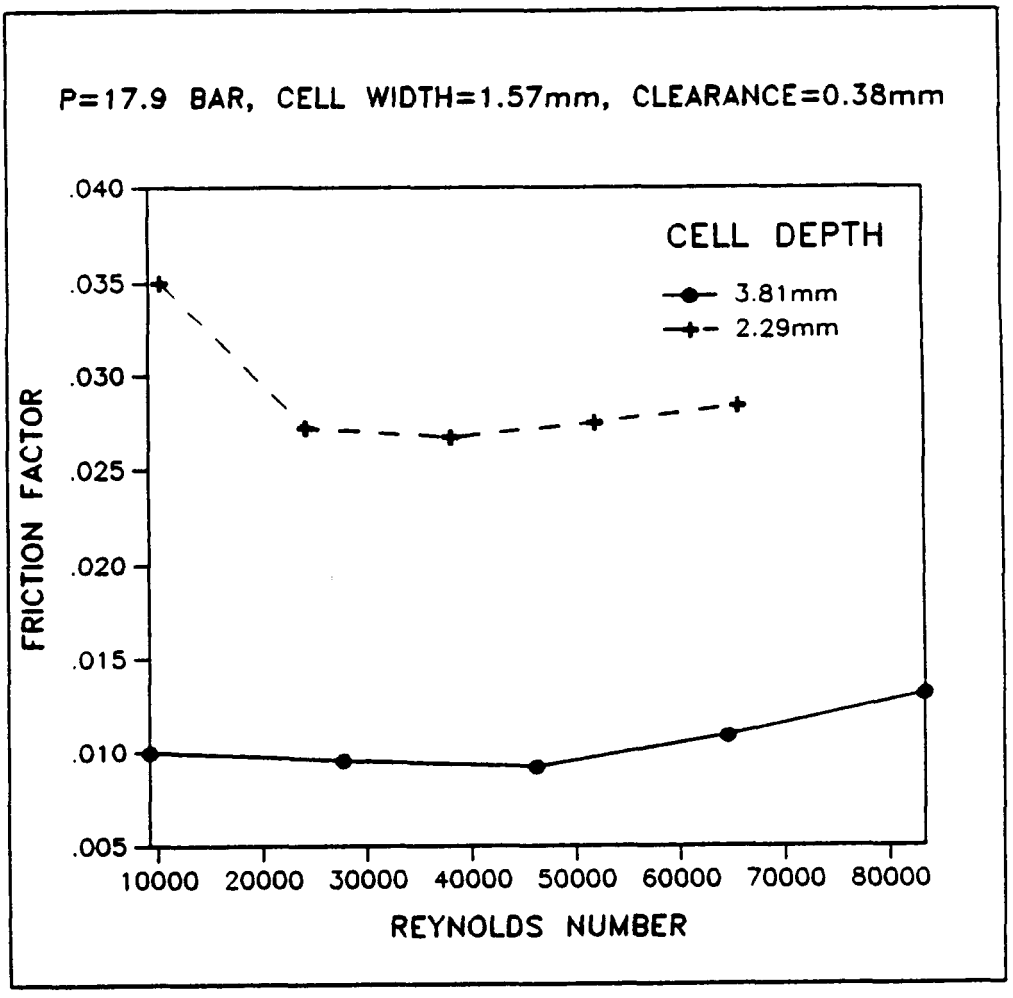

Figure 60. Friction factor versus Reynolds number for tests 5 and 8 of table 1 with inlet pressure 17.9 bar.

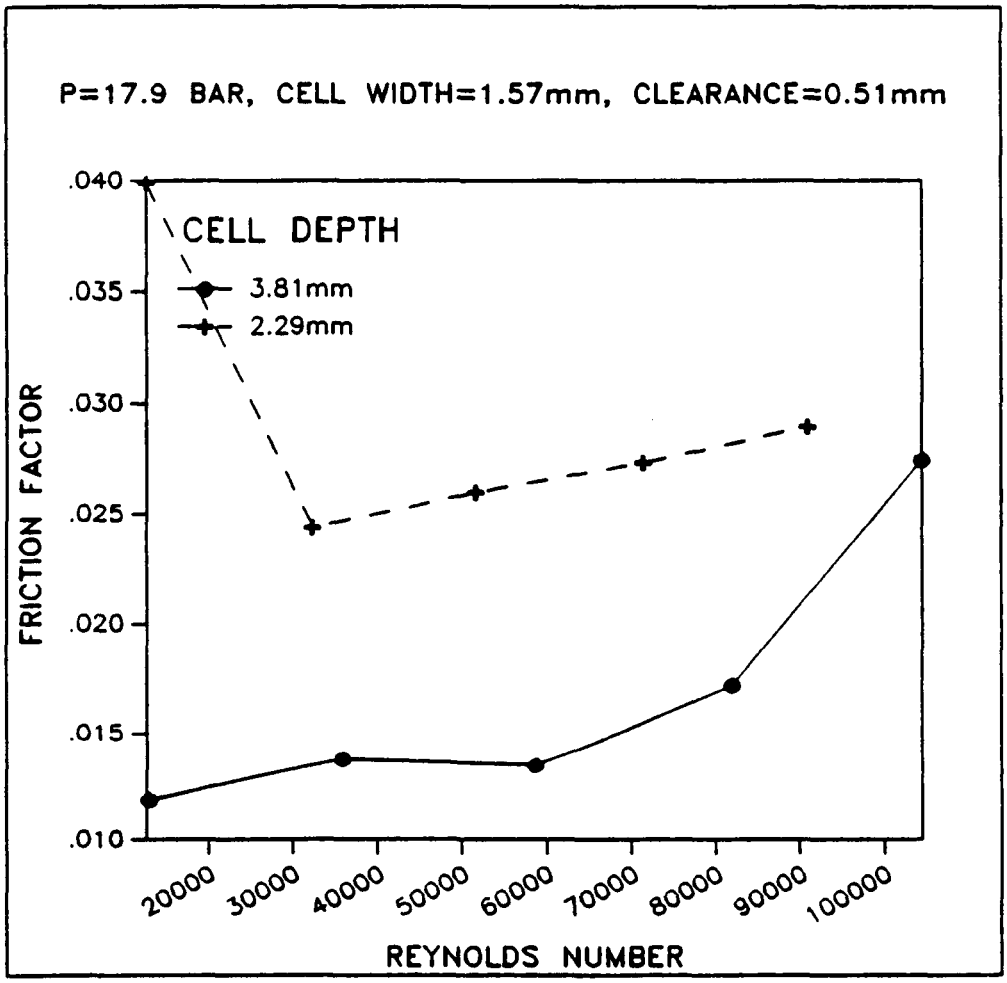

Figure 61. Friction factor versus Reynolds number for tests 6 and 9 of table 1 with inlet pressure 17.9 bar.

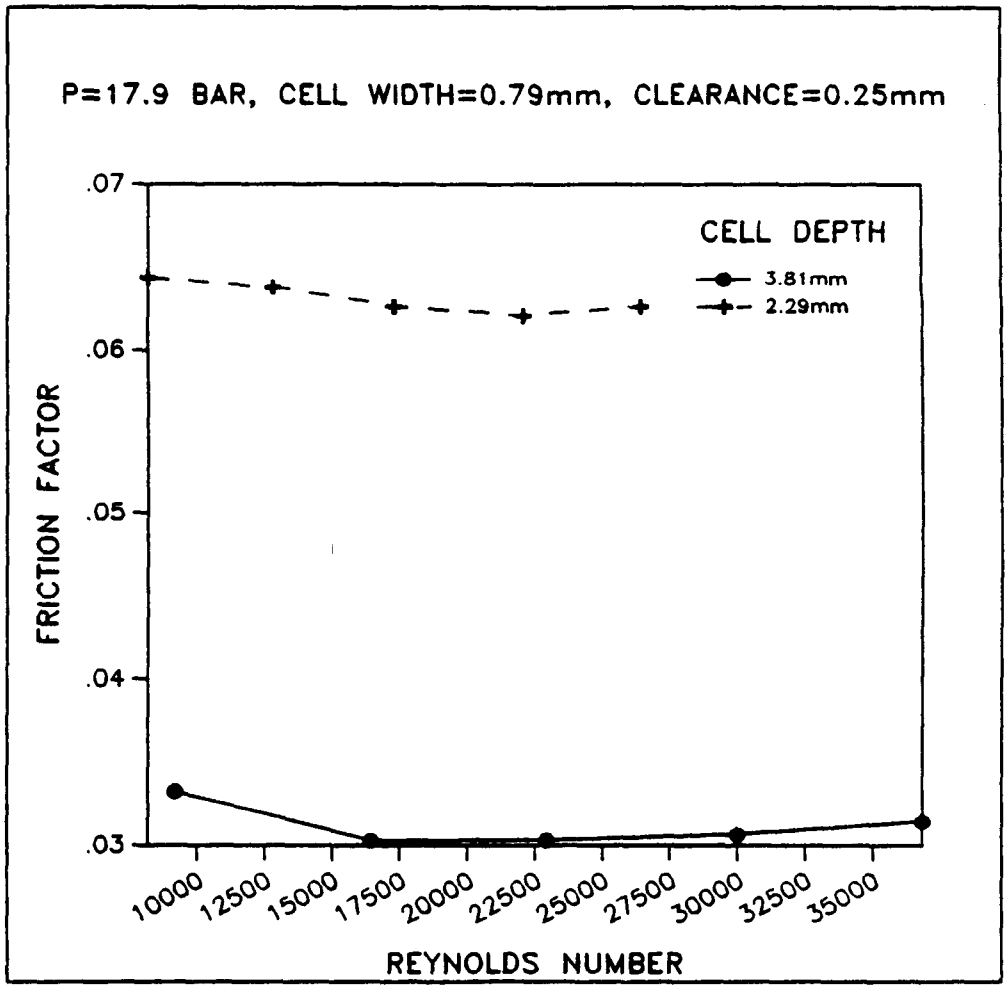

Figure 62. Friction factor versus Reynolds number for tests 10 and 13 of table 1 with inlet pressure 17.9 bar.

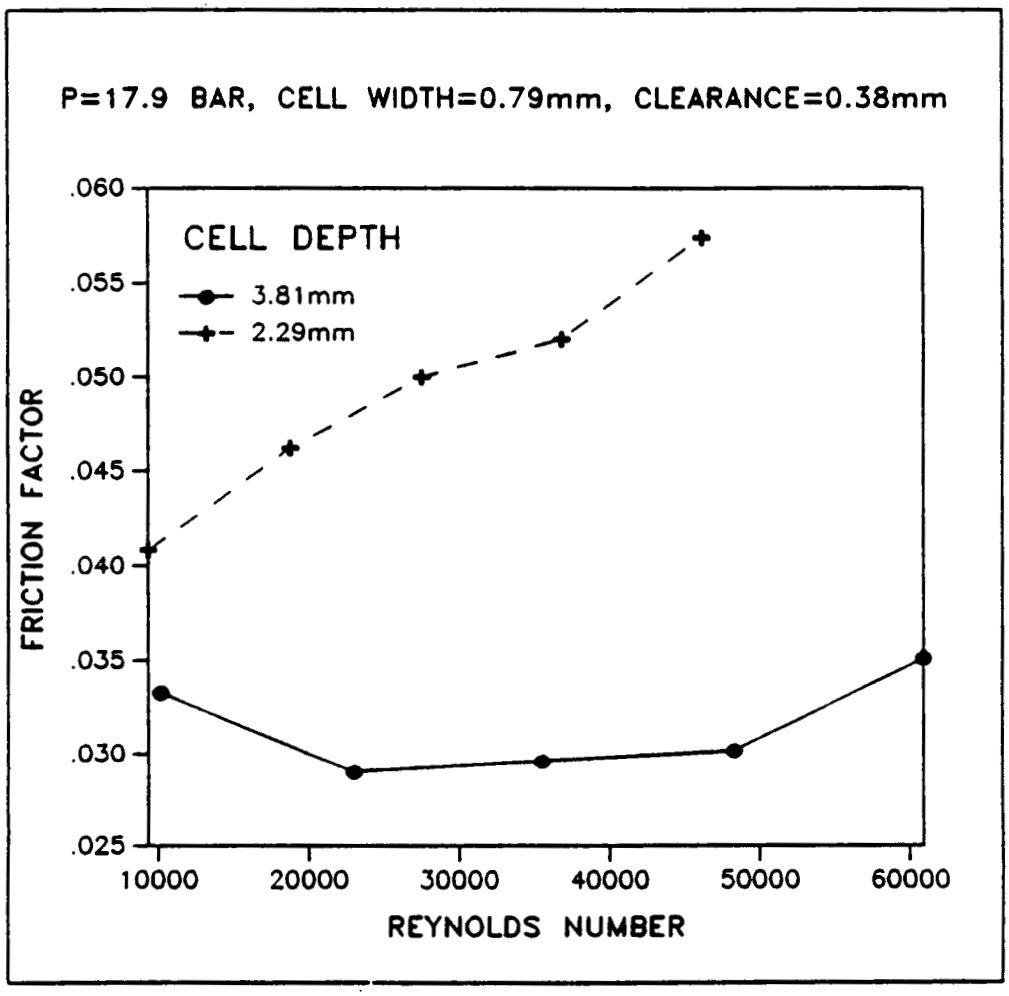

Figure 63. Friction factor versus Reynolds number for tests 11 and 14 of table 1 with inlet pressure 17.9 bar.

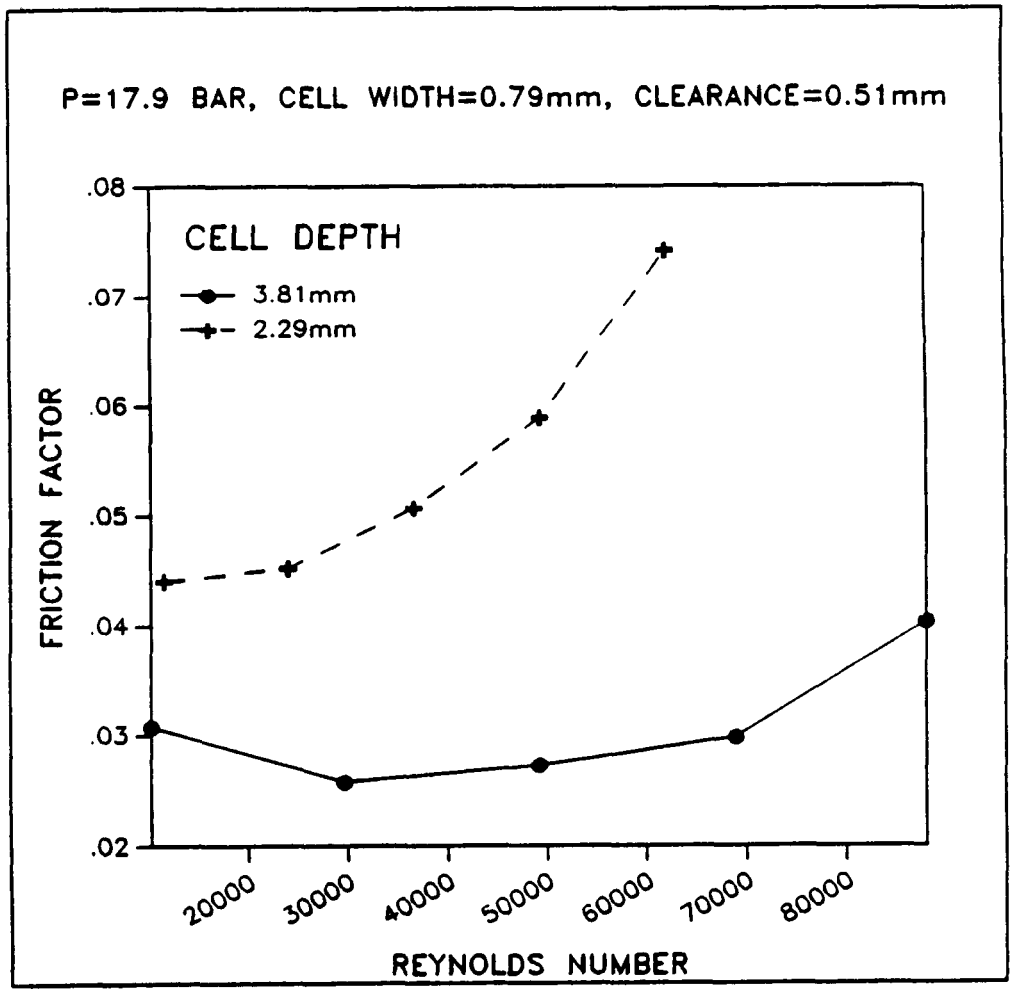

Figure 64. Friction factor versus Reynolds number for tests 12 and 15 of table 1 with inlet pressure 17.9 bar.

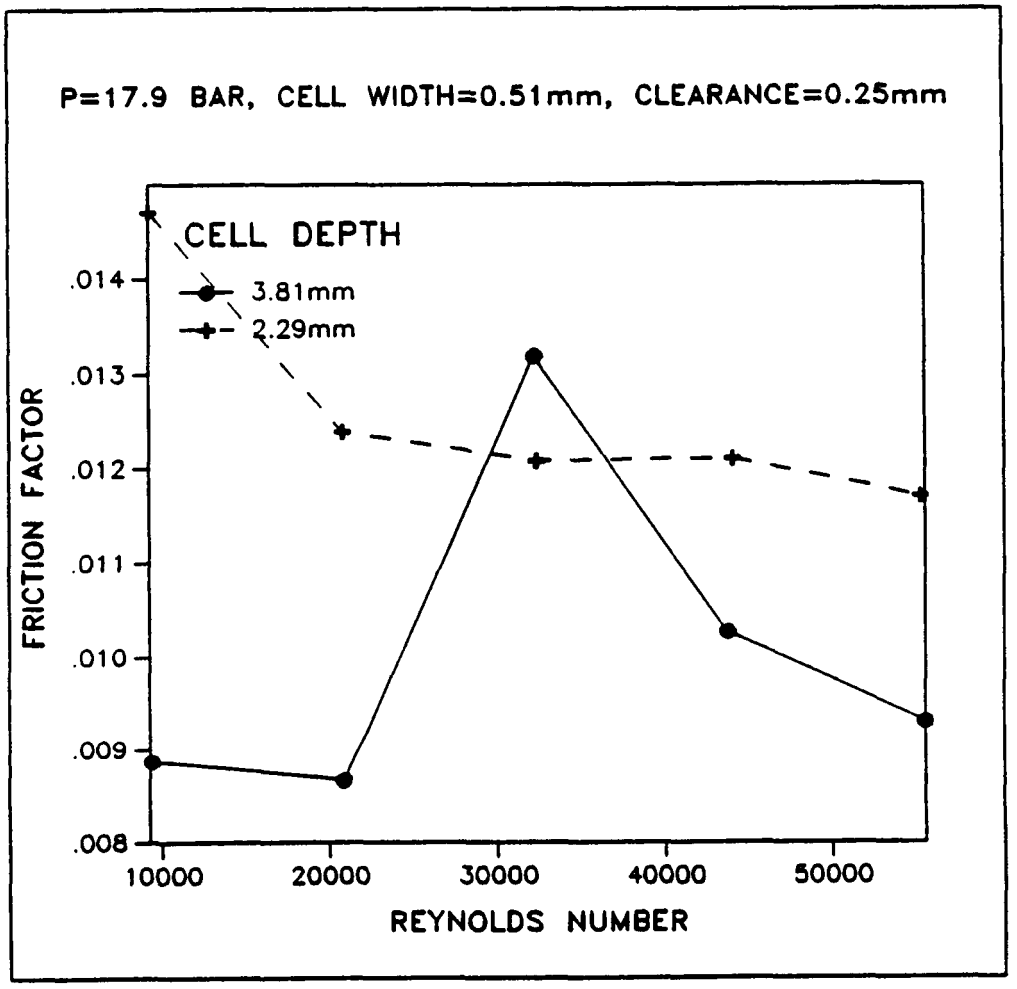

Figure 65. Friction factor versus Reynolds number for tests 16 and 19 of table 1 with inlet pressure 17.9 bar.

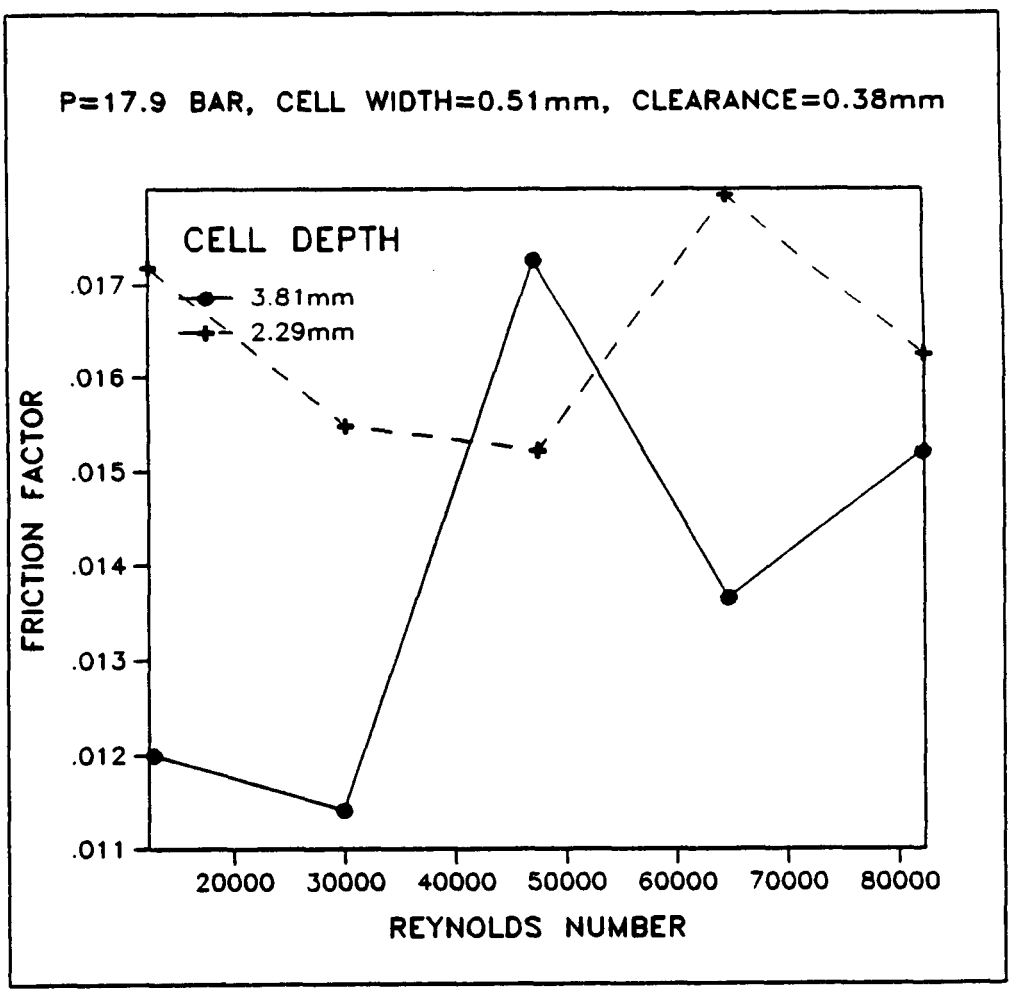

Figure 66. Friction factor versus Reynolds number for tests 17 and 20 of table 1 with inlet pressure 17.9 bar..

c - 2

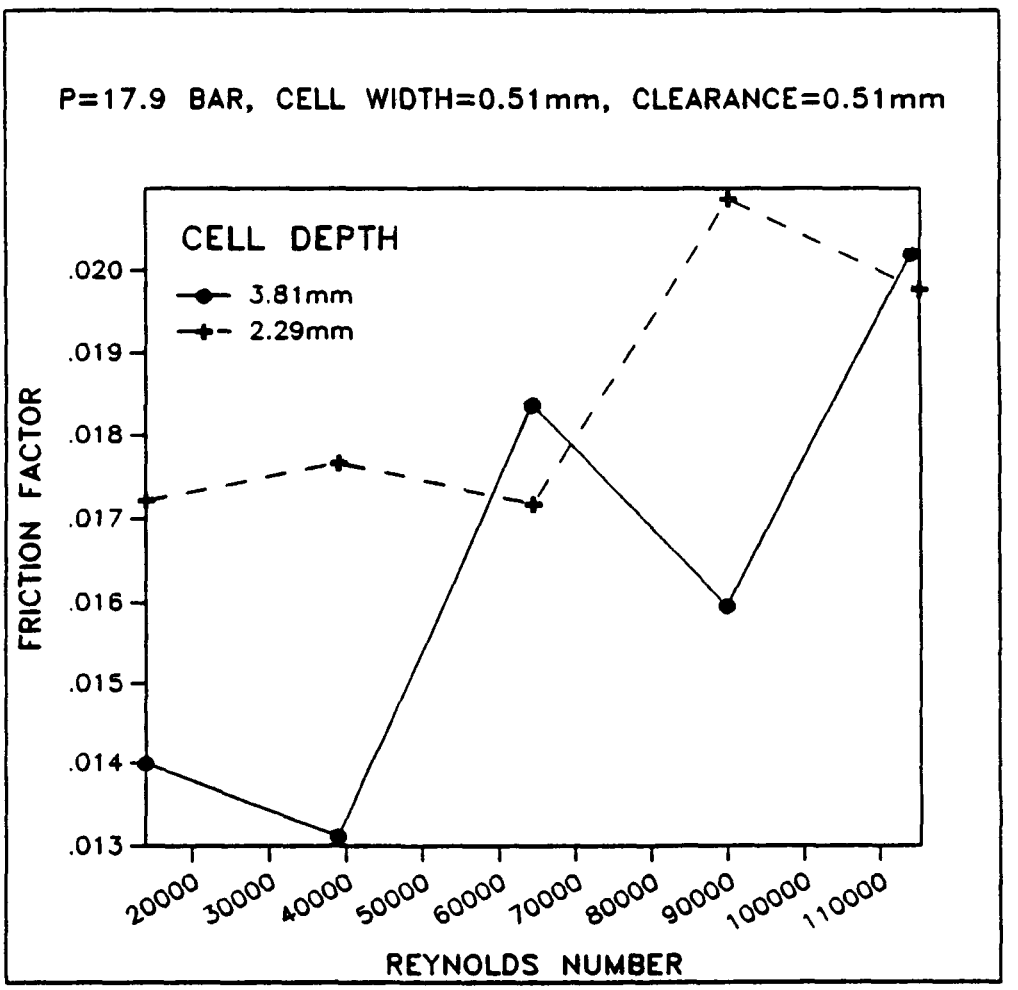

Figure 67. Friction factor versus Reynolds number for tests 18 and 21 of table 1 with inlet pressure 17.9 bar.